Study of the interactions of Neptunium with humic substances and the clay mineral montmorillonite by direct and non direct speciation methods

Dissertation

zur Erlangung des Grades

„Doktor der Naturwissenschaften"

im Promotionsfach Chemie

am Fachbereich Chemie, Pharmazie und Geowissenschaften

der Johannes Gutenberg-Universität Mainz

Víctor Vicente Vilas

geboren in Oviedo (Spanien)

Mainz, 2008

"Siempre que enseñes, enseña a la vez a dudar de lo que enseñas."
[Whenever you teach, teach at the same time to doubt your teaching]
José Ortega y Gasset

To My Family

Index

Abstract

For the safety assessment of radioactive waste, the possibility of radionuclide migration has to be considered. Since Np (and also Th due to the long-lived ^{232}Th) will be responsible for the greatest amount of radioactivity one million years after discharge from the reactor, its (im)-mobilization in the geosphere is of great importance. Furthermore, the chemistry of Np(V) is quite similar (but not identical) to the chemistry of Pu(V).

Three species of neptunium may be found in the near field of the waste disposal, but pentavalent neptunium is the most abundant species under a wide range of natural conditions. Within this work, the interaction of Np(V) with the clay mineral montmorillonite and melanodins (as model substances for humic acids) was studied. The sorption of neptunium onto gibbsite, a model clay for montmorillonite, was also investigated. The sorption of neptunium onto γ-alumina and montmorillonite was studied in a parallel doctoral work by S. Dierking.

Neptunium is only found in ultra trace amounts in the environment. Therefore, sensitive and specific methods are needed for its determination. The sorption was determined by γ spectroscopy and LSC for the whole concentration range studied. In addition the combination of these techniques with ultrafiltration allowed the study of Np(V) complexation with melanoidins. Regrettably, the available speciation methods (e.g. CE-ICP-MS and EXAFS) are not capable to detect the environmentally relevant neptunium concentrations. Therefore, a combination of batch experiments and speciation analyses was performed.

Further, the preparation of hybrid clay-based materials (HCM) montmorillonite-melanoidins for sorption studies was achieved. The formation of hybrid materials begins in the interlayers of the montmorillonite, and then the organic material spreads over the surface of the mineral. The sorption of Np onto HCM was studied at the environmentally relevant concentrations and the results obtained were compared with those predicted by the linear additive model by Samadfam.

The sorption of neptunium onto gibbsite was studied in batch experiments and the sorption maximum determined at pH~8.5. The sorption isotherm pointed to the presence of strong and weak sorption sites in gibbsite. The Np speciation was studied by using EXAFS, which showed that the sorbed species was Np(V).

The influence of M42 type melanodins on the sorption of Np(V) onto montmorillonite was also investigated at pH~7. The sorption of the melanoidins was affected by the order in which the components were added and by ionic strength. The sorption of Np was affected by ionic strength, pointing to outer sphere sorption, whereas the presence of increasing amounts of melanoidins had little influence on Np sorption.

Zusammenfassung

Für die Sicherheitsbeurteilung eines radioaktiven Endlagers muss die Migration von Radinukliden betrachtet werden. Da Np (und auch Th wegen den langlebigen ^{232}Th) den Großteil der Radioaktivität eine Million Jahre nach der Entnahme der Brennelemente aus dem Reaktor ausmacht, ist die Mobilisierung/Immobilisierung von Np in der Geosphäre sehr wichtig. Außerdem ist die Chemie von Np(V) der Chemie von Pu(V) ähnlich (aber nicht gleich).

Man kann drei Neptunium Spezies in der näheren Umgebung eines Endlagers finden, aber fünfwertiges Neptunium ist die häufigste Spezies unter umweltrelevanten Bedingungen. In dieser Arbeit wurde die Wechselwirkung von Np(V) mit dem Tonmineral Montmorillonit und mit Melanoidinen (als Modelsubtanzen für Huminstoffe) untersucht. Die Sorption von Neptunium an Gibbsit, der als Modell für Montmorillonit diente, wurde auch studiert. Die Sorption von Neptunium an γ-Al_2O_3 und Montmorillonit wurde in einer parallelen Doktorarbeit von S. Dierking untersucht.

Neptunium wird nur im Ultraspurenbereich in der Umwelt gefunden, weswegen empfindliche und spezifische Methoden für dessen Bestimmung erforderlich sind. Die Sorption kann mit γ-Spektroskopie und LSC über den ganzen Konzentrationsbereich bestimmt werden; außerdem macht die Kombination dieser Methoden mit Ultrafiltration die Untersuchung der Komplexierung mit Melanoidinen möglich. Bedauerlicherweise kann man mit den verfügbaren Speziationsmethoden (z.B. CE-ICP-MS und EXAFS) den umweltrelevanten Np-Konzentrationsbereich nicht untersuchen, weswegen Batchversuche mit Speziationsanalysen zusammen durchgeführt wurden.

Darüber hinaus wurde die Synthese von tonhaltigen Hybridmaterialien (HCM) Montmorillonit-Melanoidin, für Sorptionsversuche durchgeführt. Die Bildung der Hybridmaterialien beginnt in den Zwischenschichten des Montmorillonits, dann breitet sich das organische Material auf der Oberfläche des Minerals aus. Auch die Sorption von Np an HCM wurde im umweltrelevanten Konzentrationsbereich untersucht, und die Ergebnisse wurden mit den nach dem Linearen Additiven Modell von Samadfam vorausberechneten Daten verglichen.

Die Sorption von Np an Gibbsit wurde in Batchversuchen untersucht, und das Maximum wurde bei pH~8,5 festgestellt. Die Sorptionsisotherme deutet auf die Existenz starker und schwacher Sorptionsplätze hin. Die Speziation wurde mit EXAFS untersucht, und als sorbierte Spezies wurde Np(V) bestimmt.

Der Einfluss von M42 Melanoidinen auf die Sorption von Np an Montmorillonit bei pH~7 wurde auch untersucht. Die Sorption der Melanoidine wird von der Ionenstärke und der Zugabereihenfolge beeinflusst. Die Sorption von Np dagegen wird nur von der Ionenstärke beeinflusst (Hinweis auf außersphärische Komplexe).

Resúmen

Para la seguridad del almacenamiento geológico profundo de residuos radiactivos, hay que considerar, entre otras, la posibilidad de la migración de los radionúclidos. Debido a que el Np será el responsable, junto al Th, de la mayor parte de la radioactividad un millón de años tras la descarga del reactor, su movilización/inmovilización en la geosfera es de gran importancia, además la química del Np(V) es muy similar (aunque no idéntica) a la química del Pu(V).

Es posible encontrar tres especies de neptunio en las cercanías del depósito de residuos, pero, sin duda, es el neptunio pentavalente el más abundante en condiciones naturales. En este trabajo se estudia la interacción de Np(V) con el mineral montmorillonita y melanoidinas (como modelo de los ácidos húmicos), también se estudia la adsorción de neptunio sobre gibbsita, como sustancia modelo de la montmorillonita. La adsorción de neptunio sobre γ-alúmina y montmorillonita es parte de un trabajo de doctorado paralelo realizado por S. Dierking.

El neptunio sólo se puede encontrar en el medio ambiente como ultra traza, por ello se necesitan métodos específicos y sensibles para su determinación. La adsorción puede ser estudiada mediante espectroscopia γ y LSC, estos métodos junto a la ultra filtración hacen también posible el estudio de la complejación con las melanoidinas en todo el rango de concentraciones de interés. Lamentablemente los métodos disponibles de especiación (CE-ICP-MS y EXAFS) no son capaces de alcanzar las concentraciones medioambientalmente relevantes, por lo tanto se llevó a cabo una combinación de análisis de especiación en el rango alto de concentraciones y experimentos en laboratorio a bajas concentraciones.

Además se prepararon materiales híbridos (HCM) basados en arcillas montmorillonita-melanoidinas para estudios posteriores de adsorción. La formación de estos materiales híbridos comienza en los espacios interlaminares de la montmorillonita, expandiéndose después el material orgánico sobre la superficie del mineral. La adsorción de Np sobre estos materiales fue estudiada en concentraciones medioambientalmente relevantes, y los resultados obtenidos fueron comparados con el modelo aditivo linear.

La adsorción de neptunio sobre gibbsita fue estudiada en el laboratorio y se encontró el máximo de adsorción a pH~8,5. La isoterma de adsorción indica la presencia de lugares fuertes y débiles de adsorción. La especiación se estudió usando EXAFS y se determinó que la especie adsorbida era Np(V).

La influencia de melanoidinas del tipo M42 en la adsorción de Np(V) a pH alrededor de 7 también fue investigada. La adsorción de las melanoidinas se ve afectada por el orden en el que se añaden los componentes y por la fuerza iónica. La adsorción de Np solo se ve afectada por la fuerza iónica, indicando complejos de esfera externa, mientras que la presencia de la melanoidina tiene muy poca influencia en la adsorción. Las mediciones con CE-ICP-MS mostraron que en todos los casos el ión neptunilo era la especie dominante.

After years of investigations, the deep geological disposal is up to now the best choice and the most internationally accepted solution for radioactive waste, since the geosphere is stable and secure in a long time scale [Cohen 1977, ENRESA 2004, Omel'yanenko 2007]. The partitioning and transmutation [Madic 2002] of the radionuclides may be of interest in order to reduce the amount of nuclear waste, but there will be still high-level waste (HLW) which has to be considered. The International Atomic Energy Agency (IAEA), defines radioactive waste as "any material for which no use is foreseen and that contains radionuclides at concentrations greater than the values deemed admissible by the competent authority in materials suitable for use not subject to control" [IAEA 1995]. For this work, only the HLW is considered. It contains fission products and minor actinides, it bears over 95% of radioactivity and the heat release remains significant on a scale of several centuries. The deep geological disposal of HLW is not an urgent necessity for any nation, therefore a better understanding of the conditions in those disposals is possible, and also necessary. The composition of the HLW may depend on the initial fuel composition, and on the irradiation conditions. It is widely accepted that Pu, Np, Am, and Cm are the main contributors to the radio toxicity of the spent fuel [Lecomte 2002], and therefore, a study of their behavior in the waste disposal, e.g., sorption, migration, redox behavior and interaction with the organic matter is necessary. Since the migration properties of the actinides from the disposal to the environment are controlled by their interaction with the components of the geological formations and complexation during the migration path [El-Naggar 2000], natural analogues in laboratory research, underground laboratories, and computer modeling are the best tools for the research.

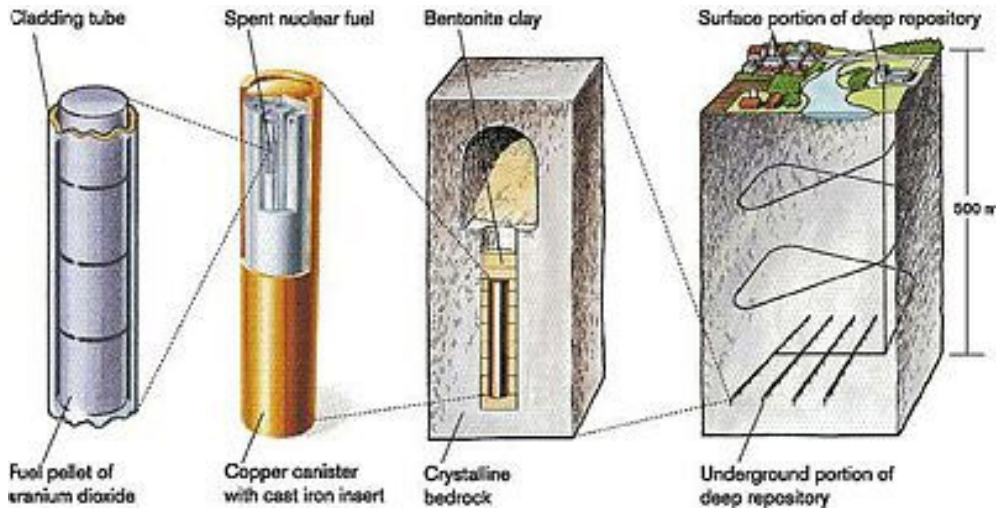

Fig. 1.1. Multiple barriers prevent the radionuclides in the fuel from escaping into the environment (skb.se).

A complete study would have been nearly impossible due to the high amount of variables in the system, so we focused on one system: Np, which will be responsible together with Th, due to the long-lived nuclides ^{237}Np and ^{232}Th, for the greatest amount of radioactivity one million years after discharge from the reactor, in the presence of montmorillonite, an important component of the bentonites, and humic substances, which are naturally occurring complexing agents. The properties of the three components will be discussed in detail in section 2, nevertheless a brief introduction was considered of interest for this section.

Np belongs to the actinide family, which comprises the elements with atomic number between 90 (Thorium) and 103 (Lawrencium). In the environment, it is found mainly due to its release in nuclear weapons tests, and in nuclear fuel reprocessing plants as the isotope ^{237}Np [Holm 1987]. It might exist in aqueous solution in the oxidation states from +3 to +7 but not all the species are stable under geogenic conditions. For the conditions in an underground nuclear waste disposal, the +3 state may not be formed [Lundén 1997]. The +4 state dominates under strongly reducing conditions and forms strong complexes with most anions [Burney 1974]. The +5 state is the most stable species under oxic conditions [Lundén 1997]. It is a large and low charged ion, therefore it is generally only weakly complexed by ligands. In a highly oxidizing ambient, the +6 state might be found. An understanding of the redox behavior of Np under environmentally relevant conditions is of interest, and is required for the investigation of the chemical and physical processes which may occur in the disposal, e.g., redox reactions, complexation and sorption onto mineral surfaces. Although it should be possible to find the three species of neptunium in the near field of the waste disposal, pentavalent neptunium is the more abundant species under natural conditions. Moreover, the chemistry of Np(V) is quite similar (but not identical) to the chemistry of Pu(V). In environmentally relevant neptunium concentrations (10^{-8} to 10^{-12} M), only a few speciation methods are applicable. Therefore, a combination of batch experiments to investigate the sorption mechanism and complexation with the humic substances at low Np concentrations is used, even though these allow only for an indirect speciation. Direct speciation techniques, like the on line coupling CE-DAD-ICP MS [Buda 2006] and EXAFS measurements, at higher neptunium concentrations may be useful in addition. A detailed description of the methods used can be found in section three.

Bentonite clays are widely considered for the engineered barriers in radioactive waste disposals. The main component in bentonites is montmorillonite with a concentration of up to 50 to 80% depending on the bentonite chosen [POSIVA 2004 and Sabodina 2006].

Montmorillonite is a 2:1 layered silicate, where the octahedral and tetrahedral layers contain Si, Al, Mg, and Fe atoms; Na, K, Ca, and also Mg are located in the interlayer spaces. For the sorption, two main processes can be considered; at low pH (below 5), the main process is ion-exchange with the cations located in the interlaminar spaces. Above pH 5, the hydroxy groups may participate in the sorption binding the nuclides on the surface. In this work, STx-1 montmorillonite (Clay Minerals Society) was used as a model montmorillonite. The properties of this special kind of montmorillonite will be discussed in section 2.4. Besides STx-1, gibbsite (α-$Al(OH)_3$) was also used as model substance, in order to gain a better understanding of the role of the octahedral layers of [AlO_6] in the sorption. The sorption of actinides onto minerals has been investigated in the last decades, e.g., sorption of plutonium and neptunium onto kaolinite [Buda 2006 and Banik 2007] and [Jermolayev 2005] respectively, sorption of neptunium onto montmorillonite, quartz, and α-alumina [Bertetti 1998], onto SWy-1 (together with Am (III) and Pa(V)) [Bradbury 2006] and on STx-1 montmorillonite and γ-alumina [Dierking 2008]. In any case, neptunium sorption seems to be weak on most geologic media in the pentavalent state [Allard 1984].

Humic substances play an important role in the geosphere; they affect the mobilization or immobilization of metal ions in the environment. Due to their tendency towards the formation of complexes and their ability to generate colloids, humic substances can enhance the mobility of radionuclides [Choppin 1988]. Furthermore, the presence of clay minerals may affect the formation of humic substances in the environment [Theng 1979, Taguchi 1986, and Ziechmann 1993]. Humic substances do not have a unique structural composition, and have different functional groups depending on their origin. Therefore, the use of model humic substances for understanding the general complexing and sorption properties is needed before determining the particular properties of the humic substances at the disposal site. The sorption of humic substances on minerals was first investigated in 1959 by Evans and Russell [Evans 1959]; subsequently investigations carried out in the 70's on montmorillonite [Theng 1975] found out the way in which melanoidins sorb to montmorillonite. In our days, the sorption of humic substances and melanoidins on minerals has been also studied [Buda 2006, Křepelová 2006 and Banik 2007]. In all cases, a similar tendency was determined independent on the mineral surface.

The complexation of neptunium by humic substances has been investigated using direct and indirect methods. The studies done in the environmentally relevant range of concentrations using ultrafiltration at neutral and alkali pH's by Seibert et al. determined a stability constant for the complexation of neptunium by humic substances at low Np

concentrations (10^{-15} – 10^{-8} M) of log ß= 5.1 ± 0.3 using the charge neutralization model, which includes a correction for different loading capacities making the comparison of results at different experimental conditions possible [Seibert 2001]. EXAFS measurements pointed to a inner-sphere complexes at pH=1 with Np(IV) [Schmeide 2005 a] and a monodentate carboxylate complexation with Np(V) [Sachs 2005 a]. For the complexation of neptunium with melanoidins at high Np concentrations (10^{-5} – 10^{-3} M) a log β of 3.5 ± 0.15 was obtained, which was also in good agreement with the data for the Aldrich humic substances (log β of 3.87 ± 0.19) [Sachs 2005 b].

Within this work, the following binary systems were investigated: montmorillonite - melanoidin (in situ polymerisation of melanoidins in the presence of mineral) and gibbsite – neptunium. The results obtained for the binary systems are discussed in section 4.1. and 4.2., respectively. Since the ternary system is not well understood, two approaches were made to study this system in order to understand and predict the speciation and migration of neptunium under geogenic conditions: the sorption onto the obtained hybrid materials (section 4.3.) and the ternary system Np, melanoidins and montmorillonite at a fixed pH (section 4.4.). For the ternary systems, the linear additive model by Samadfam et al. [Samadfam 2000] was applied. Because the pH of the most natural waters is controlled by the carbonate system [Drever 1982], the experiments with montmorillonite were done in the presence of carbonate to better understand the role of the carbonato complexes in the sorption of neptunium on clay minerals.

2.1. Radioactive Waste Disposals

As said in section 1, the deep geological disposal (DGD) is up to now the best choice and the most internationally accepted solution for radioactive waste, other considered options like the disposal in the oceanic fosses near the subduction zones or sending the HLW to the space were due to the associated dangers dismissed. Together with the radioactivity, HLW emits also heat which is also a variable to be considered in the disposal, in order to reduce the heat emission in the DGD from the HLW, the use of temporal disposal up to 100 years is recommended. After this cooling period, the HLW should be transferred to the DGD.

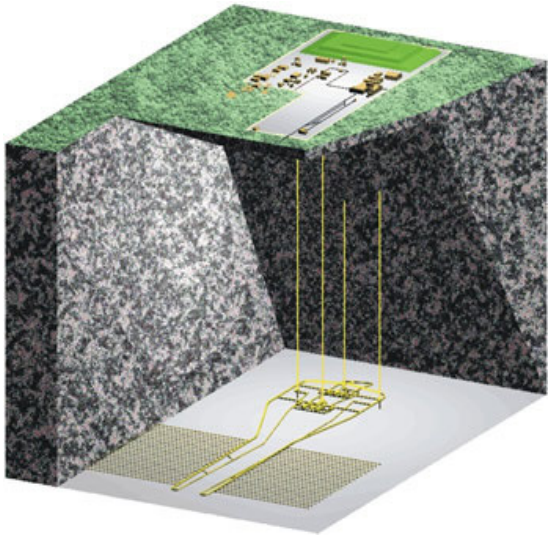

Fig. 2.1. Illustration of the deep-geological radioactive waste disposal concept in Spain (csn.es).

Fig. 2.2. Picture of a canister hole (posiva.fi).

The composition of the HLW may depend on the initial fuel composition, and the irradiation conditions. It is widely accepted that Pu, Np, Am, and Cm are the main contributors to the radiotoxicity of the spent fuel [Lecomte 2002], and due to its long half-life, ^{237}Np is of major importance on a long time scale. Those radionuclides are confined in the UO_2 matrix or enclosed in the glass in the concepts where the HLW is vitrified; the matrix is the first engineered barrier in the DGD. If the DGD site is well selected, the amount of water which can be in closer contact with the HLW is very low, and the time needed for the solution of both matrixes (glass or UO_2) at the expected conditions is up to some millions of years [ENRESA 2004].

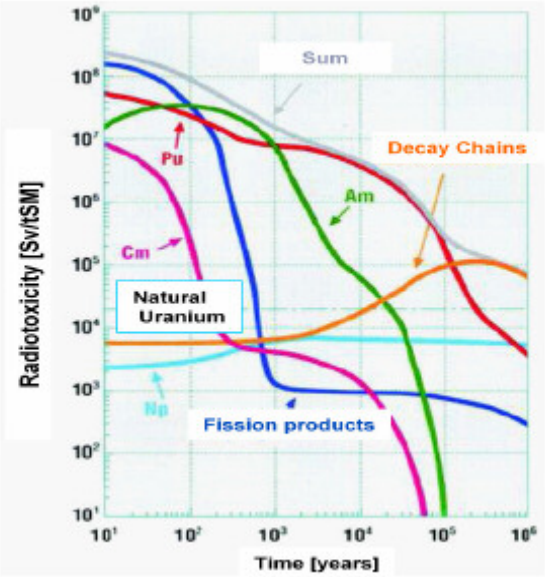

Fig 2.3. Chronological sequence of the radiotoxicity of spent nuclear fuel from a modern pressurized-water reactor (in Sievert Sv per ton heavy metal). Primary enrichment in ^{235}U of the fuel elements 4%, burnout: 40GWd/t, radiotoxicity relating to ingestion [Gomper 2001].

Depending of the selected site for the disposal, there are different geological conditions and the interactions between the actinides and the rock formations has to be studied. There are developed models and concepts for disposals in salt, granite, and clay. Anyway, the interaction with the waste containers, the buffer and the backfill material has also to be considered.

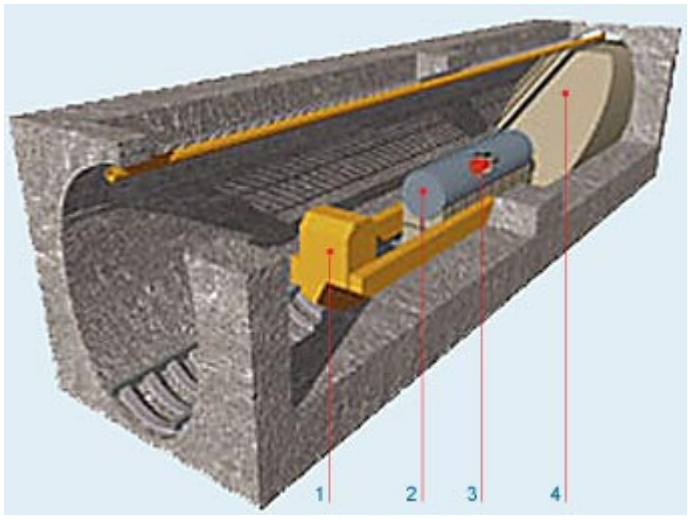

Fig. 2.4. Radioactive waste disposal concept in Switzerland, where 1 is the transport trolley, 2 the container, 3 the residues, and 4 the backfill material (nagra.ch).

The security of the radioactive waste disposal is supposed to depend on the addition of the properties of all the individual components of the multibarrier system. The bedrock shall isolate the disposal from the environment, it has defined and predictable geochemical, mechanical and geological conditions. The tunnel backfill material shall keep the buffer and the canisters in the holes, it contributes to keep the tunnel mechanically stable, and should be also chemically stable. The buffer shall keep the canister in the hole; it isolates the canister from potential rock displacements. It should be chemically and mechanically stable, and it should be able to conduct heat from the canister to the rock. The canister should be stable over periods of 100,000 years, shall conduct the heat to the buffer and attenuate the radiation [POSIVA 2006].

Once the radioactive waste is disposed into the underground site some considerations have to be taken into account. The existence of fractures where the adsorption is less effective than in unfractured media, may give unrealistic estimations. Furthermore, in radioactive waste are many anionic species present, which are not adsorbed significantly, and also ligands, that may complex cations in solution [Drever 1982].

Fig. 2.5. Canister construction (posiva.fi).

For the security assessment in the DGD, underground laboratories, natural and analog systems and modeling (process model, component functional model, system functional model and global models) may be used. The data obtained is fundamental to reach scientific decisions involving the HLW.

Country	DGD
USA	Military radioactive waste in saline rocks, operative. Nuclear plant waste in volcanic turf, operative.
Canada	Granite, planning phase.
Germany	Waste is placed in the nuclear plants until a decision is made. Saline formation proposed in the 70's, nowadays clay is considered alternatively.
Belgium	Clay, researching.
Finland	Granite, characterizing the emplacement, which will be operative in 2020.
France	Transmutation is being developed, for the DGD, clay is considered, researching.
Sweden	Granite, characterizing the selected emplacement.
Switzerland	Compacted clay, researching.
Spain	Granite, researching.
China	Granite, emplacement selected.

Table 2.1. Radioactive disposal international situation [ENRESA 2004].

2.2. The Actinides

The actinide elements constitute the elements with atomic numbers 90 – 103 and are members of a internal transition series following actinium (A = 89). This series is analogous to the lanthanide transition series, where the 4f electrons are added whereas in the actinides fourteen 5f electrons are added. There are important differences between the actinides and the lanthanides due to the lower binding energies and the less effective shielding of the 5f electrons in comparison to the 4f electrons. But there are also remarkable similarities between the two transition series, for example the magnetic, optical and chemical properties of the half-filled shell elements gadolinium and curium.

Actinide	Electronic configuration	Lanthanide	Electronic configuration
Ac	$[Rn]6d^1 7s^2$	La	$[Xe]5d^1 6s^2$
Th	$[Rn]6d^2 7s^2$	Ce	$[Xe]4f^1 5d^1 6s^2$
Pa	$[Rn]5f^2 6d^1 7s^2$	Pr	$[Xe]4f^3 6s^2$
U	$[Rn]5f^3 6d^1 7s^2$	Nd	$[Xe]4f^4 6s^2$
Np	$[Rn]5f^4 6d^1 7s^2$	Pm	$[Xe]4f^5 6s^2$
Pu	$[Rn]5f^6 7s^2$	Sm	$[Xe]4f^6 6s^2$
Am	$[Rn]5f^7 7s^2$	Eu	$[Xe]4f^7 6s^2$
Cm	$[Rn]5f^7 6d^1 7s^2$	Gd	$[Xe]4f^7 5d^1 6s^2$
Bk	$[Rn]5f^9 7s^2$	Tb	$[Xe]4f^9 6s^2$
Cf	$[Rn]5f^{10} 7s^2$	Dy	$[Xe]4f^{10} 6s^2$
Es	$[Rn]5f^{11} 7s^2$	Ho	$[Xe]4f^{11} 6s^2$
Fm	$[Rn]5f^{12} 7s^2$	Er	$[Xe]4f^{12} 6s^2$
Md	$[Rn]5f^{13} 7s^2$	Tm	$[Xe]4f^{13} 6s^2$
No	$[Rn]5f^{14} 7s^2$	Yb	$[Xe]4f^{14} 6s^2$
Lr	$[Rn]5f^{14} 6d^1 7s^2$	Lu	$[Xe]4f^{14} 5d^1 6s^2$

Table 2.2. Electronic configuration of the actinides and lanthanides [Holleman 1995]

As table 2.2. shows, there are, for the actinide ground state electron configurations remarkable differences to the corresponding lanthanides for the early actinides up to and including Np. This is the occurrence of 6d electrons replacing the less bound 5f electrons making the early actinides pseudo “d-elements”. This is remarkably visible in the trend of their atomic volumina which, as a function of the atomic number, follow the typical d-element behavior with a sudden jump to a typical f-element behavior between Pu and Am. This sudden jump is attributed in a rapid transition from delocalized 5f electrons in the early

actinides to localized 5f electrons in Am and beyond. In a recent NATURE article by R.C. Albers [Albers 2001], it is pointed out that this sudden jump even occurs in Pu metal when the room-temperature α-phase of metallic Pu which has delocalized 5f electrons is heated up to 600K (the δ-phase) which is accompanied by a 25% increase in volume. Theoretical calculations show that the f electrons in the δ-phase are half-localized, suggesting that Pu has been "arrested midway though the transition from metal (delocalized f electrons) to insulator (atomic like f electrons)."

Uranium is the longest known element of the actinide series, it was isolated in 1789 (Klaproth), thorium, actinium and protactinium are also naturally occurring elements and where discovered in 1828 (Berzelius), 1899 (Debierne), and 1913 (Fajans and Göhring) respectively. The elements uranium and thorium may be found in relatively high concentrations in the environment and gained by normal mining operations. The transuranium elements which don't occur in nature or appear in very low concentrations were produced using different reactions. So was neptunium discovered in 1940 (McMillan and Abelson), plutonium (Seaborg et al.) in the same year and over the following decades the heavier actinides americium and curium (1944, Seaborg et al.), berkelium (1949, Thomson et al.), californium (1950, Thomson et al.), einsteinium and fermium (1952), mendelevium (1955, Ghiorso et al.), nobelium (1958, Ghiorso et al.) and lawrencium (1961, Ghiorso et al.).

Nuclear power reactors and weapons need the actinides ^{235}U and ^{239}Pu. Am and Cm, major contributors to the radiotoxicity of spent nuclear for time of several thousand years, may be formed by multiple neutron capture which complicates the environmental situation. ^{237}Np and ^{229}Th will be responsible for the greatest amount of radioactivity one million years after discharge from the reactor; therefore an understanding of the chemical and physical properties of these elements is needed in order to determine the dispersion of the radioactivity introduced in the environment.

2.2.1. Actinides' Chemistry

The free actinides have a high chemical activity. Metallic actinides react with oxygen and burn if they are exposed to as powder. Under heating, the actinides react with the most non-metals. Water and bases don't react with the actinides, but under boiling water, the formation of the oxide at the actinide surface is observed. The actinides dissolve in acidic media forming the An-ions, whose oxidation states, due to the 5f-electrons and the little energy differences between the 5f, 6d, and 7s orbitals, may vary between +2 to +7.

Ac	Th	Pa	U	Np	Pu	Am	Cm	Bk	Cf	Es	Fm	Md	No	Lr
						(2)			(2)	(2)	2	2	**2**	
3	(3)	(3)	3	3	3	**3**	**3**	**3**	**3**	**3**	**3**	**3**	3	**3**
	4	4	4	4	**4**	4	4	4	(4)	*4*				
		5	5	**5**	5	5	*5*		*5*					
			6	6	6	6	*6*							
				7	(7)	*7*								

Table 2.3. Oxidation states for the actinides italics indicates not clear states, bold the most stable and parentheses the unstable states [Katz 1986].

As already mentioned light actinides show a more metallic character than the heavy actinides, due the localization (heavy actinides) or delocalization (light actinides) of the f electrons [Albers 2001]. Actinide ions with oxidation states +3 or +4 have strong tendencies to complexation, hydrolysis, and polymerization. The actinides in higher oxidation states have a lower effective charge due to the formation of the actinyl ions (AnO_2^+ and AnO_2^{+2}). These actinyl ions remain as a stable unit during many chemical reactions. Due to the polarization in the An=O bound, the effective charge in the actinide doesn't correspond to the total actinyl charge. For UO_2^{+2}, an effective charge of 3.3 ± 0.1 was found and 2.3 ± 0.2 for NpO_2^+ [Choppin 1983].

The 4f and 5f elements show little polarization, and are therefore hard Pearson acids, which interact strongly with very electronegative ligands like F^- and OH^-.

2.2.2. Neptunium Chemistry

Neptunium was the first transuranium element to be discovered [McMillan 1940], McMillan and Abelson found that neutron activation of uranium in Berkeley led to the formation of the 2.3-d ^{239}Np via

$$^{238}U\,(n,\gamma)\,^{239}U \xrightarrow{\beta^-,\,23\,\mathrm{min}} ^{239}Np \qquad 2.1$$

In their chemical experiments, McMillan and Abelson found that the 2.3-d activity did not precipitate with cerium fluoride in the presence of an oxidizing agent (bromate in strong acid). In the presence of a reducing agent (SO_2) it was quantitatively coprecipitated with cerium fluoride. The proof that the 2.3-d substance is the daughter of 23-min ^{239}U was the demonstration of its genetic link to the latter in a milking experiment. Metallic neptunium has a silvery appearance and passivizes when it is exposed to air at room temperature. It has the highest density of the actinides (19.38 $cm^3 \cdot g^{-1}$) [Holleman 1995 , Lemire 2001] its melting

point, after undergoing three crystal modifications, is about 912 K [Lemire 2001] and an approximate boiling point of about 4447 K was obtained by Eick and Mulford [Eick 1964]. There are many known isotopes of neptunium from the mass number 226 to 244 [Yoshida 2006], which have different nuclear properties, e.g., ^{237}Np is an α emitter, whereas ^{239}Np decays emitting β^- and γ radiation, but all the known isotopes of neptunium are radioactive. The most environmentally relevant isotope of neptunium is ^{237}Np (half-life $2.144 \cdot 10^6$ years), which is produced by irradiating uranium with neutrons.

$$^{238}U\,(n,2n)\,^{237}U \xrightarrow{\beta^-,\,6.75d} {}^{237}Np \qquad 2.2$$

$$^{235}U\,(n,\gamma)\,^{236}U\,(n,\gamma)\,^{237}U \xrightarrow{\beta^-} {}^{237}Np \qquad 2.3$$

$$^{238}U\,(n,\gamma)\,^{239}U \xrightarrow{\beta^-} {}^{239}Np \xrightarrow{\beta^-} {}^{239}Pu\,(n,\gamma)\,^{240}Pu \xrightarrow{\beta^-} {}^{240}Am\,(n,\gamma)\,^{241}Am \xrightarrow{\alpha} {}^{237}Np \qquad 2.4$$

^{237}Np can be found in the biosphere mainly due to its release in nuclear weapons tests and from nuclear fuel reprocessing plants. It was calculated that about 2500 kg of ^{237}Np had been generated [Holm 1987].

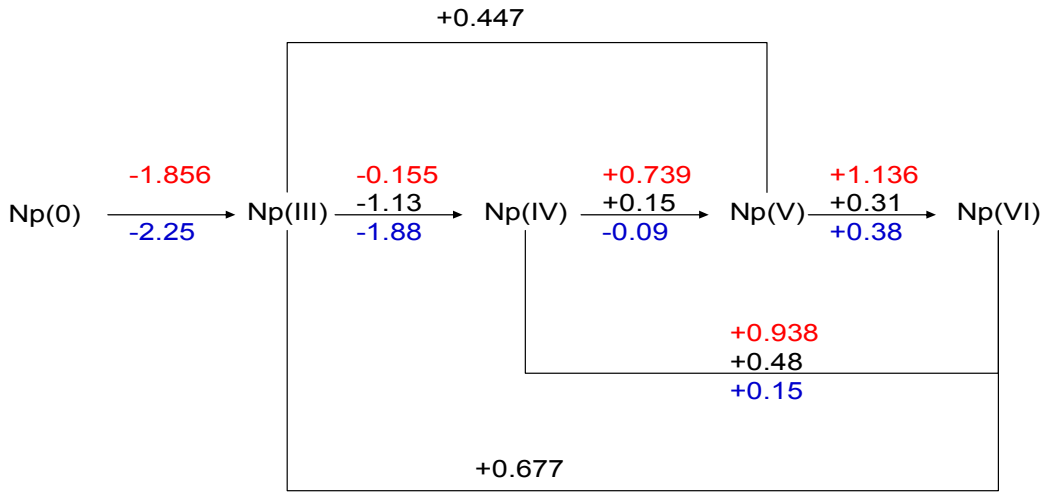

Fig. 2.6. Redox potentials for Np, pH~0, pH~8, pH~14. [Kim 1986].

Neptunium may exist in aqueous solution as Np(III), Np(IV), Np(V), Np(VI), and Np(VII) (Tab. 2.3.), but it is Np(V) which is the most stable form, this is demonstrated in Fig. 2.7. This species may disproportionate in acidic solutions or suffer redox reactions as we can see in Fig. 2.6. [Lieser 1988]. Those redox and disproportionation reactions are influenced by the acid concentration, complexation of the products, light, temperature, and the concentration

of the reactants. Np(V) shows a great range of stability unlike U(V) and Pu(V). Under strongly reducing conditions representative of the bedrock or on the surfaces of mineral containing Fe (low Eh), neptunium may be found as the tretavalent state, whereas the hexavalent state may occur only under strongly oxidizing conditions, representative of the conditions near the spent nuclear fuel [Lundén 1997].

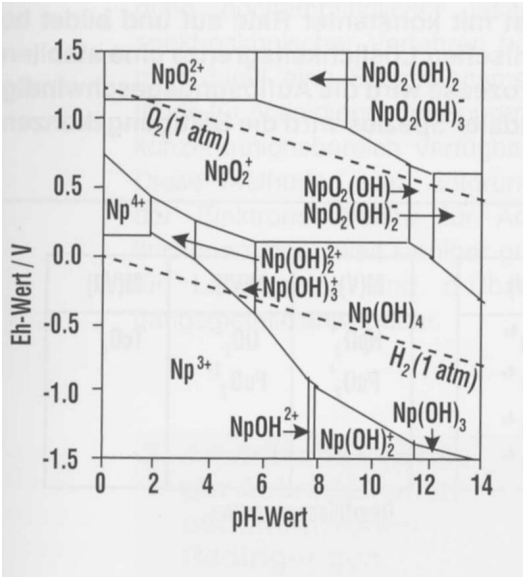

Fig. 2.7. Stability zones for different Np-Species [Klenze 1998].

The actinides are hard acids, and prefer the complexation with hard bases like oxygen-containing compounds (carbonate, phosphate, humic acids, fulvic acids, silicate and sulfate) or the ions fluoride and chloride. Due to its availability in the geosphere and its high concentrations, carbonate is expected to be the most important ligand for the actinides in general [Lieser 1988, Clark 1996, Seibert 1999 and Vitorge 2003].

2.2.3. Neptunium Chemistry at the Waste Disposal

As said previously, carbonates (and bicarbonates) play an important role in the migration of the actinides from a deep geological disposal or in an accidental contamination [Clark 1996]. The main complication of the carbonate-actinide system is the simultaneous presence of hydroxides, which may also complex the actinides. Another process which may appear in the radioactive waste disposals is radiolysis. Radiation is responsible for the formation of ·OH radicals (and O^- radical ions) [Pikaev 2001]. The produced carbonate and bicarbonate radicals are oxidizing agents and may oxidize the neptunium species to Np(V) and Np(VI), which are stable to radiation.

Reducing conditions are expected to be predominant in the near field of the container, which is normally made of steel, but due to its stability against corrosion, copper containers

will be used for the radioactive waste disposals in Finland (POSIVA) and Sweden (SKB). Other materials like Ti, which are mechanically stable against a uniform corrosion are not considered due to its fragility in the presence of hydrogen, and the possibility of a non-uniform corrosion, which is not quantifiable.

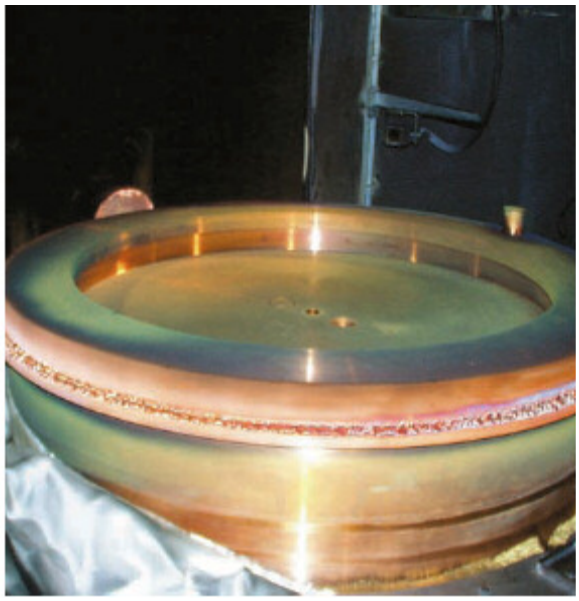

Fig. 2.8. Swedish copper canister (skb.se).

Due to their abundance the metal ions released from the canister (Fe or Cu dependent on the concept chosen), play an important role. They may form complexes with the inorganic anions present in the groundwater, reduce the actinides to not-mobile species, or complex with the humic and fulvic acids. Fig 2.9. summarises the possible near-field processes of spent nuclear fuel.

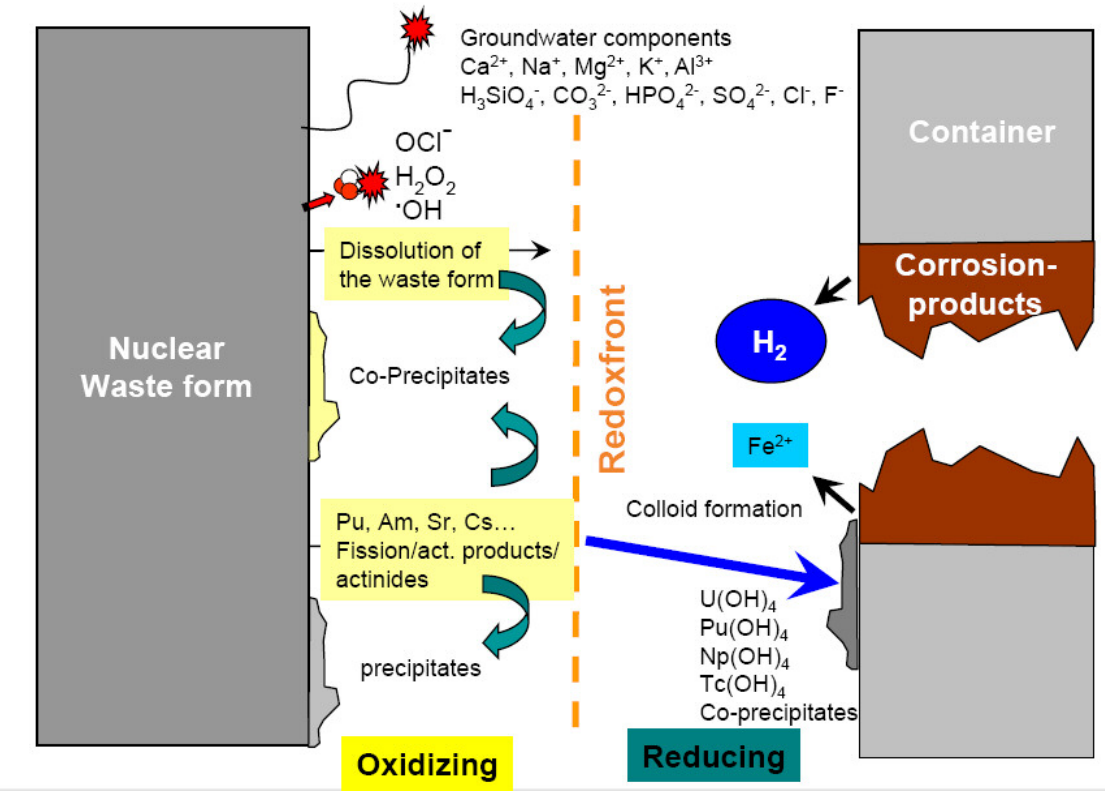

Fig. 2.9. Near field processes of the spent fuel in the disposal [Klenze 1998].

Under reducing conditions, Np(IV) should be the dominant species in the near field of the nuclear waste. In this case, NpO_2 is the solubility limiting phase, and the total concentrations are not above 10^{-9} – 10^{-10} M [Allard 1984]. Following equilibrium has been reported in freshly prepared Np(IV) solutions [Yuov 2004]. For the reaction

$$Np^{4+} + H_2O \longrightarrow NpOH^{3+} + H^{+} \qquad 2.5$$

one finds a log K (recalculated to I=0) = -1.23 ± 0.06. However, other studies consider the [Np(IV)] to be very high and over the solubility limit of the hydrous oxides [Neck 2001]. Therefore, the formation of colloids has to be taken into account [Neck 2001], and two equilibria are proposed [Duplessis 1977], the formation of the 1:1 (equation 2.5) species and the 1:2 species, equation 2.6.

$$Np^{4+} + 2H_2O \longrightarrow Np(OH)_2^{2+} + 2H^{+} \qquad 2.6$$

The equilibrium constants calculated with the previous considerations, were log K^0_1 (I=0) = 0.50 ± 0.2 for the 1:1 and log K^0_2 (I=0) = 0.3 ± 0.3 for the 1:2 species [Neck 2001].

The influence of reducing agents and carbonates on the hydrolysis of Np(IV) was studied by Rai and Ryan [Rai 1985] finding no absolute hydrolysis constant. Rai et al. found an increase in the Np(IV) solubility by increasing the amount of $KHCO_3$ [Rai 1999]:

$$NpO_2(am,hyd) + 4CO_3^{2-} + 2H_2O \longrightarrow Np(CO_3)_4^{4-} + 4OH^- \qquad 2.7$$

For the interaction of Np(IV) with humic substances, Schmeide et al. [Schmeide 2005 a], determined by using EXAFS the formation of inner-sphere complexes at pH = 1, in which the Np(IV) atom is surrounded by 10 oxygen atoms at a distance of 2.36 ± 0.02 Å.

The most stable form of neptunium is anyway Np(V), which is found normally as NpO_2^+. NpO_2OH (am) may be found at pH less or equal to 10; above this value, traces of CO_2 lead to the formation of carbonates [Lemire 2001]. Considering the sodium content in most environments, the maximum solubility of Np(V) is less than 10^{-5} M [Allard 1984].

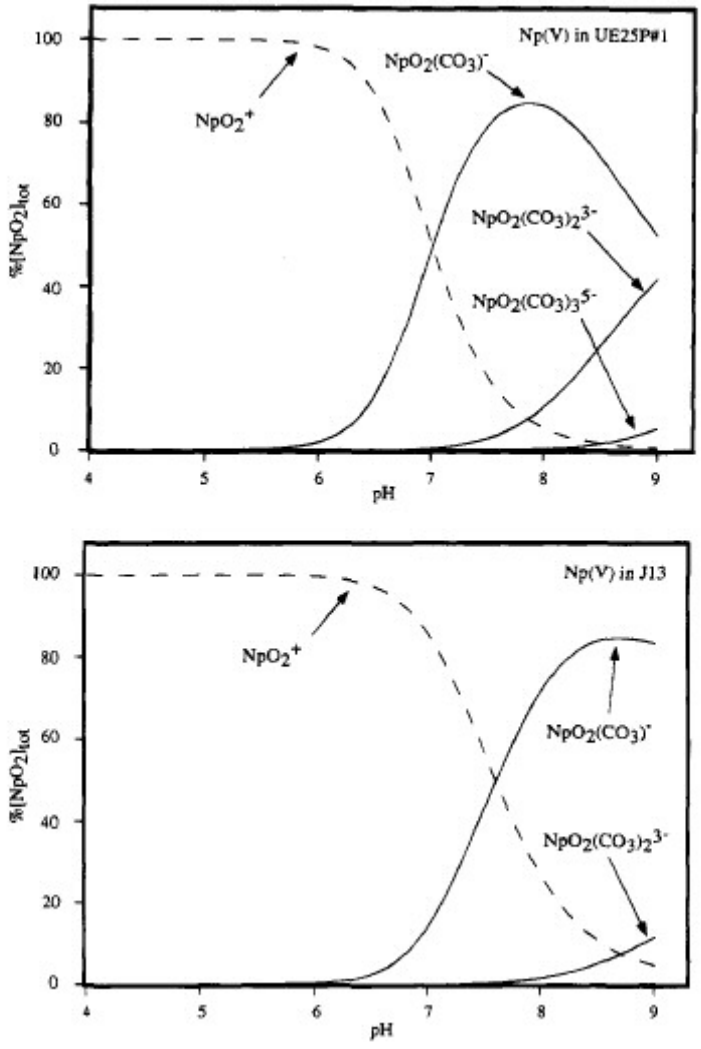

Fig. 2.10. Calculated neptunyl species distributions in carbonate solutions modeling Yucca Mountain UE25P#1 (top) and 5-13 (bottom) groundwaters at 25°C [Clark 1995].

Obviously, in the absence of CO_2, the hydrolysis reactions are very important. There has been an interesting discussion about the equilibrium constants for the hydrolysis of Np(V) between Linfeng Rao [Rao 2004 and Rao 2006] and Volker Neck [Neck 2006].

$$NpO_2^+ + H_2O \longrightarrow NpO_2(OH)(am) + H^+ \quad 2.8$$

$$NpO_2^+ + 2H_2O \longrightarrow NpO_2(OH)_2^- + 2H^+ \quad 2.9$$

In the presence of CO_2 or dissolved carbonates, the carbonato complexes are the most important species found in solution (Fig. 2.10.). There are many published data for the formation and solubility of neptunium (V) carbonates. For our calculations, we used the data of Volker Neck [Neck 1994]. The redox stability of Np(V) in the presence of humic acids was investigated by Schmeide et al. [Schmeide 2005 b]. They concluded that the higher the phenolic content in the humic acids the stronger the reduction Np(V) / Np(IV) and the subsequent stabilization of the tretavalent state. The EXAFS data for the interaction of Np(V) with humic substances point to a monodentate carboxylate complexation [Sachs 2005 a].

Due to the stability of Np(V) in solution, it is more likely that this species will be present in case of a release from the deep geological nuclear waste disposal. Therefore, many sorption studies have been carried out in order to determine if Np(V) would be immobilized by different materials or not. The macroscopic sorption of Np(V) on montmorillonite has been studied by Bertetti et al. (whose data are shown in Fig. 2.11.) [Bertetti 1998] and Mike Bradbury [Bradbury 2006], and previously there are published data in a review article written by Allard et al. [Allard 1984]. They found the same trends in the sorption of neptunium on the different materials.

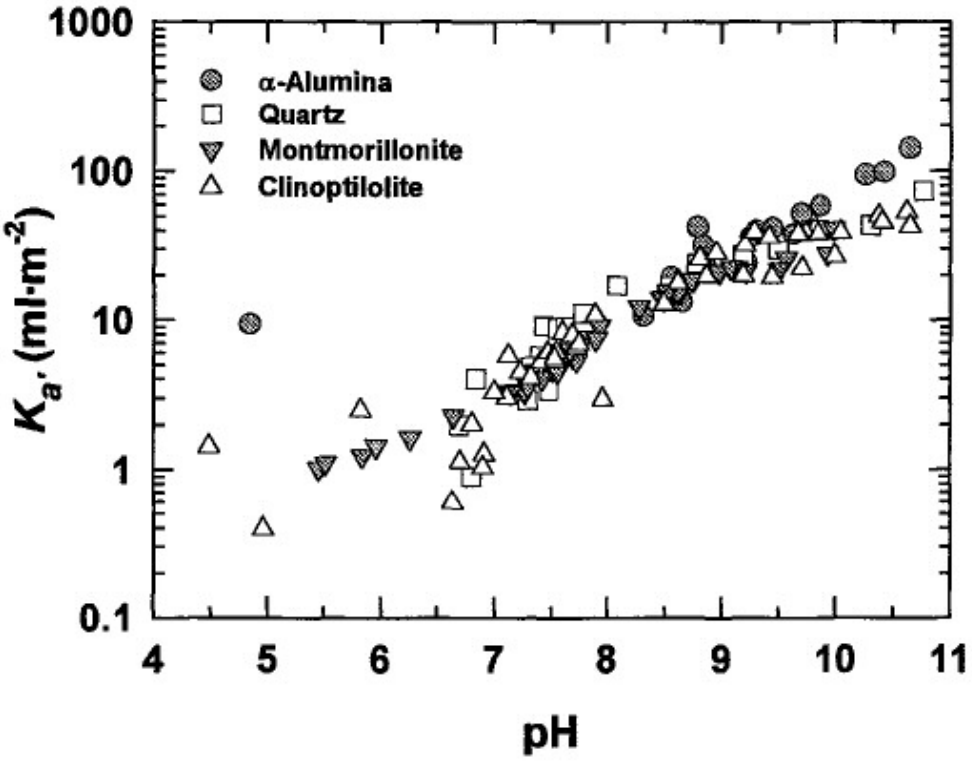

Fig. 2.11. Sorption of Np(V) on different materials Ka' = Kd/S_{EA} (for the Arizona montmorillonite and clinoptilolite was 10% of the N_2-BET, for alumina and quartz $S_{EA} = S_A$) [Bertetti 1998].

Mike Bradbury and Bart Baeyens modeled the sorption of Np(V) on Wyoming montmorillonite using the 2 Site Protolyisis Non-Electrostatic Surface Complexation and Cation Exchange Model (2SPNE SC/CE).

A molecular approach can be achieved by using spectroscopic techniques like EXAFS [Denecke 2006]. Different experiments have been published concerning EXAFS studies of the sorption of Np(V) on different materials like kaolinite [Reich 2007], gibbsite [Vicente Vilas 2007] and γ-alumina [Dierking 2007], the obtained structural parameters are shown in Table 2.4. Thus the axial index (ax) designates the oxygen atoms placed in the perpendicular axis to the carbonate anion plane, hence the equatorial index (eq) designates the oxygen atoms placed in the plane and distal (dis) the oxygen atoms which are in the same axis as the carbon atoms, but farther than the equatorial atoms.

Mineral	Np-O_{ax}	Np-O_{eq}	Np-C	Np-O_{dis}
Kaolinite	2 x 1.84	4 x 2.56	2 x 2.98	2 x 4.26
Gibbsite	2 x 1.82	4 x 2.45	-	-
γ-Alumina	2 x 1.84	5 x 2.49	-	-

Table 2.4. Structural parameters, distances ± 0.02 Å, coordination numbers were held constant, the [Np] was 8µM. Measurements for gibbsite and γ-alumina were done at ANKA (Karlsruhe, Germany), the spectra for kaolinite were taken at the European Synchrotron Radiation Facility (ESRF) in Grenoble (France).

As said before the $CO_3^{-\bullet}$ and $HCO_3^{\bullet}$, which may be produced by the reaction of $^{\bullet}OH$ with CO_3^{-2}, are oxidizing agents able to oxidize the Np(V) to Np(VI) [Pikaev 2001].

$$Np(V) + CO_3^{-\bullet}(HCO_3^{\bullet}) \longrightarrow Np(VI) + CO_3^{2-}(HCO_3^{-}) \qquad 2.10$$

The oxidized neptunium is then found as a carbonato complex in the form of $NpO_2(CO_3)_3^{4-}$. The stability constants for this complex are summarized in the NEA thermodynamic review [Lemire 2001]. Further oxidation to Np(VII) is prevented by the carbonate and bicarbonate ligands [Pikaev 2001].

Carboxylic and amino acids are also found in the geosphere and show stability constants lower than the constants for the carbonato complexes. We can find also in groundwater different complicated organic and inorganic components, like polynuclear iron hydroxide, silica, metal oxides, and clays (see section 2.4.), as well as polysaccharides, peptides, lipids, and mainly humic substances (see section 2.3.). Moulin and Moulin described the composition of representative waters of granitic and sedimentary formations (Boom clay), where the pH range between 7 and 9 (pH of Boom clay waters ~8.5), the pCO_2 between 10^{-5} and 10^{-2} atm and the humic acid concentration between 1 and 10 mg/L for granitic waters and about 150 mg/L for the Boom clay formations. They also found carbonato complexes to be the dominant neptunium species in the clay formations [Moulin 1995].

2.3. Humic Substances

At about 50% of the soil dead organic matter are humic substances (HS) [Theng 2006]. Despite its wide distribution there are still many open questions concerning size, shape, and chemical behavior of the HS. HS must be defined operationally as high molecular weight naturally occurring organic polyelectrolytes, they are heterogeneous, and can be generally described as being yellow to black in color [Aiken 1985]. The HS are normally divided into fulvic acid (soluble in alkali and acidic media), humic acid (soluble only in alkali), and humin (insoluble). Humin can be considered as a naturally occurring hybrid material which is formed preferentially *in statu nascendi* of the HS [Ziechmann 1993 and Theng 2006].

The postulated relationships are depicted in Figure 2.12. in which it can be seen that carbon and oxygen contents, acidity, and degree of polymerization all change systematically with increasing molecular weight. The low-molecular-weight fulvic acids have higher oxygen but lower carbon contents than the high-molecular-weight humic acids. Fulvic acids contain more functional groups of an acidic nature, particularly carboxylic groups. The total acidities of fulvic acids (9 – 14 meq/g) are considerably higher than for humic acids (4 – 8.7 meq/g) [Stevenson 1982].

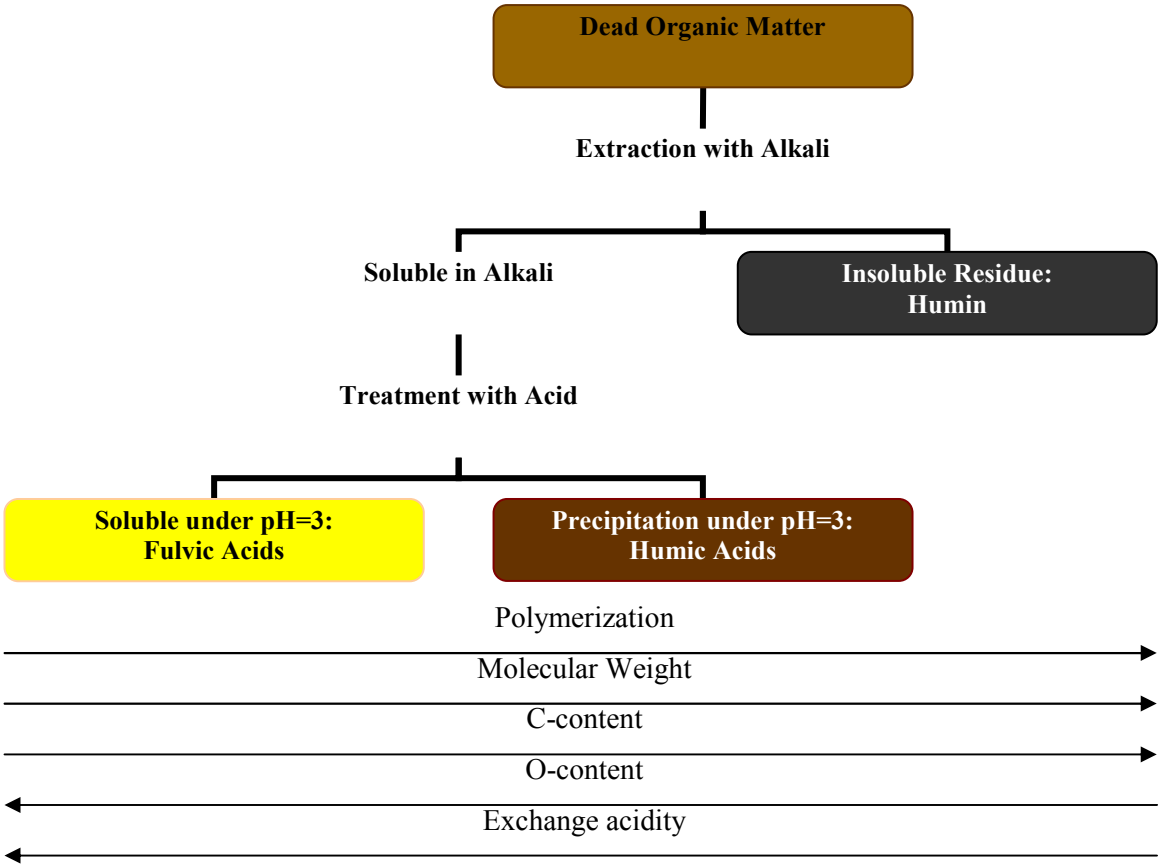

Fig. 2.12. Extraction, classification and chemical properties of humic substances [Stevenson 1982].

Many structures have been proposed in the last years, in order to understand the functionality and the formation pathways of the HS and some examples are shown in the Figures below.

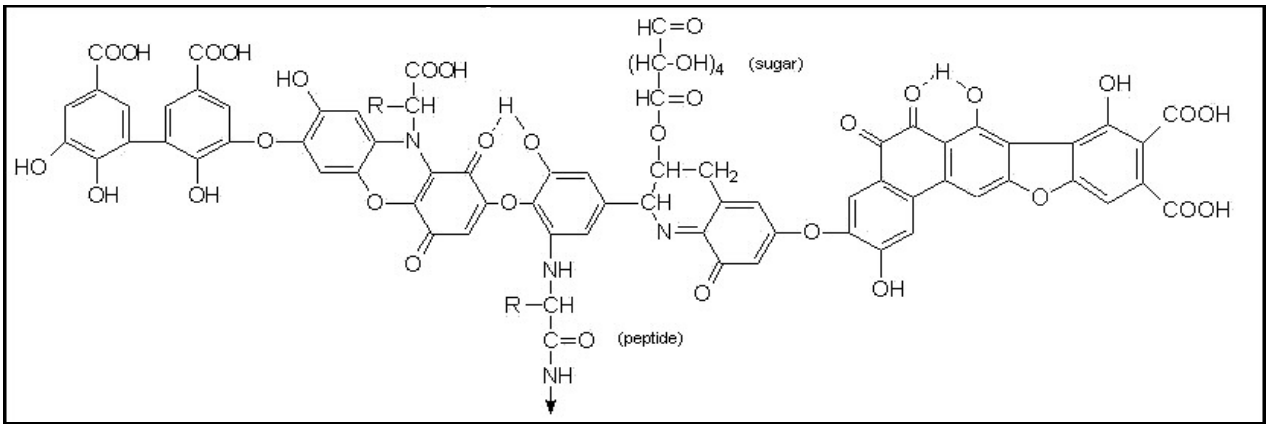

Fig. 2.13. Model structure of humic acid, containing free and bound phenolic OH groups, quinone structures, nitrogen, and oxygen as bridge units and COOH groups variously placed on aromatic rings [Stevenson 1982].

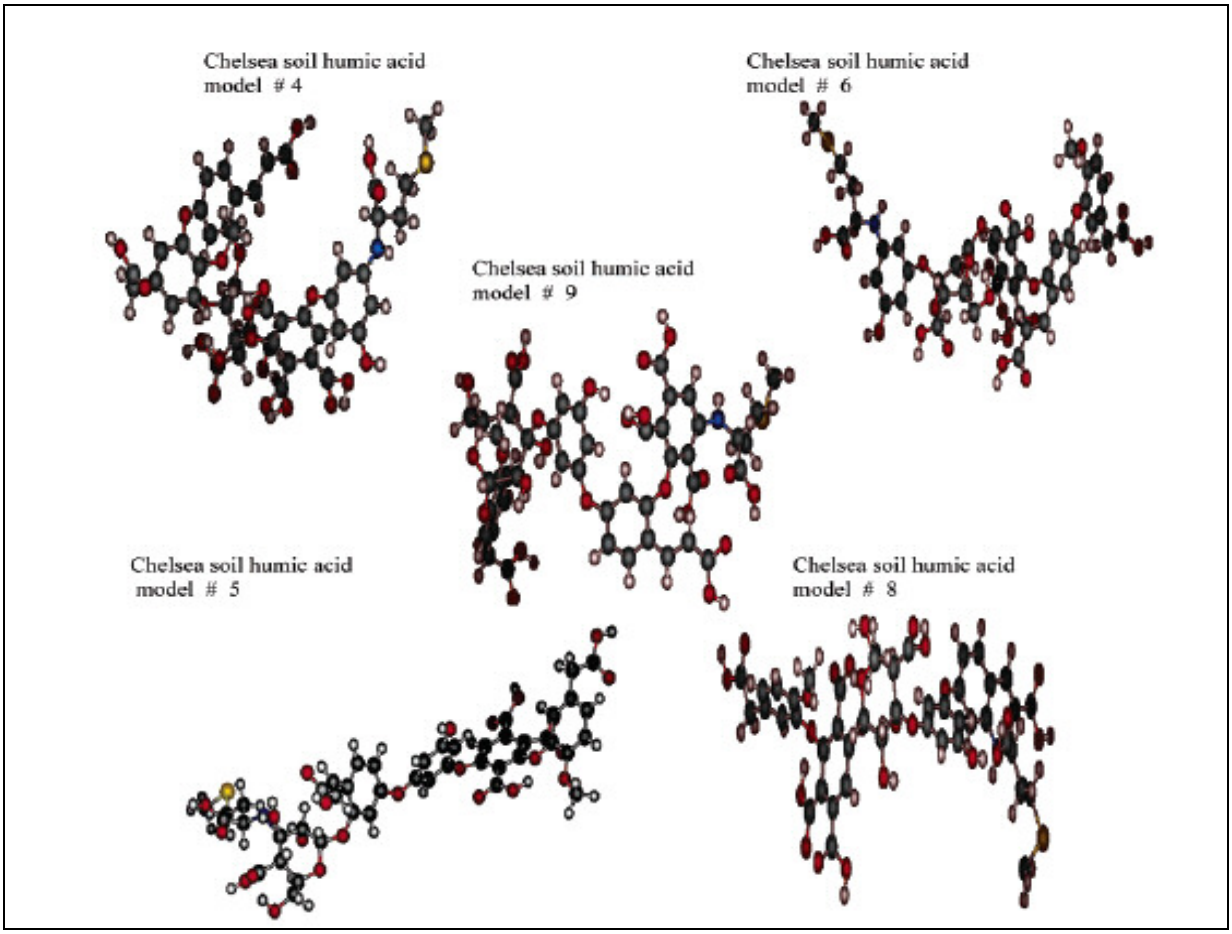

Fig. 2.14. 3-D model structures for Chelsea humic acid (HA). C atoms are in black, O atoms are in red, N atoms are in blue, S atoms are in yellow, and the remaining atoms are H atoms [Diallo 2003].

Several theories have been proposed for the formation of the HS, the lignin theory, the polyphenol theory, and the sugar-amine condensation theory. In the lignin theory (lignin is a complex organic polymer, which is an integral part of plants cell walls), popularised by Waksman [Waksman 1932], lignin is incompletely utilized by microorganism and the residuum becomes part of the soil humus. The nitrogen source for this theory was the condensation of modified lignin with proteins. According to this theory, the formation of humic substances would follow the order humin-humic acid-fulvic acid. Although modifications have been made in order to adapt it to the new discoveries, the ligning-protein theory is now considered obsolete.

Nowadays quinones, which come from lignin decomposition products or from nonlignin C sources (e.g., celulose), are supposed to play an important role in the formation of the humic substances. The polyphenols are then enzymatically oxidized to quinones and converted to humic substances. According to this theory, the formation of humic substances would follow the order fulvic acid-humic acid-humin.

The notion that humus is formed from sugars dates back to the early days of humus chemistry. According to this concept, reducing sugars and amino acids, formed as by-products of microbial metabolism, undergo nonenzymatic polymerization to form brown nitrogenous polymers [Stevenson 1982]. The polyphenol theory is nowadays the most accepted theory, but all the paths have to be considered for a complete understanding of humic substances' formation. Due to the diversity of environments, a particular path may predominate over the others, e.g., sugar-amine condensation in soils under a harsh continental climate or lignin path in wet sediments [Aiken 1985]. Anyway, proteins play a special role in soils, they can bind stably to mineral surfaces. The structural rearrangements of the protein molecule may increase the active sites for further organic sorption to the mineral and, furthermore, the N enrichment of mineral associated organic matter indicates that nitrogen containing compounds are favoured in the sorption onto minerals in soils [Kleber 2007]. Experiments showed that nitrogen in highly decomposed detritus was derived from bacteria rather than plants [Tremblay 2006]. Therefore within this work only the sugar-amine condensation path was considered by using melanoidins as model substances (see section 2.3.2.).

2.3.1. Interactions between humic substances and metals

The complexation of metals by humic substances is influenced by the different groups of the humics, which may play a role, and simultaneously by the different spatial position of the groups, and therefore different electrical environments [Seibert 1999]. In the case of neptunium, we have seen in section 2.2.3. that the complexation takes place with the

carboxylate groups of humic acids, normally as monodentate complexes [Sachs 2005 and Schmeide 2005 a]. The correlation between the acidic groups of the humic and metal bound was already known since the 50's and widely studied, e.g., the bonding of copper by peat humic acid [Lees 1950].

Wolfgang Hummel proposed a formalism for the study of the interaction between metal and humic substances [Hummel 1997]. He did some assumptions in order to simplify the model; those assumptions are listed in table 2.5.

Assumption	Description
1	The metal ion forms only 1:1 complexes with ligand sites L of the humic molecule. This molecule consists of S functional groups (S is not specified but assumed to be fixed by pH and metal concentration).
2	For each metal M, only one kind of ligand L predominates.
3	The complexing strength of the ligand site L is constant, and doesn't vary with the location within the humic molecule.
4	Chemical changes of the humic molecule have no influence on the number of active ligand sites available.
5	The complexing functional groups S do not undergo any proton exchange reactions in the pH of interest.
6	There are no interactions between the different functional groups of the molecule.

Table 2.5. Assumptions inherent in the binding model of humic substances [Hummel 1997].

Considering all the assumptions we obtain the single site model, where the humic is considered as an unknown organic ligand. The constant ${}^{c}K$, usually given in L/g, can be obtained from the equation 2.11.

$$ {}^{c}K = \frac{[MHS]}{[M]\cdot(HS)_{Total}} \qquad 2.11. $$

The total concentration of humic substances can be related to the total concentration of sites by

$$ (HS)_{Total}\cdot SCC = [L]_{Total} \qquad 2.12. $$

where SCC is the Site Complexation Capacity.

$$^{c}K = \frac{K}{1 + K \cdot [M]} \cdot SCC \qquad 2.13.$$

Here are ^{c}K and [M] measurable and K and SCC adjustable. This single site model predicts a ^{c}K constant in the range of trace metal concentrations. It is in this trace level range, which is moreover our range of interest, where this model seems no to be consistent.

By skipping the first assumption, we obtain the so called mixed-ligand model. Here the metal bound to the ligand sites of the humic substances exchanges water from the coordination shell for low molecular weight ligands (X), like carbonate, oxalate, and others. The constant for this equilibrium is

$$K_{mix} = \frac{[MLX]}{[ML] \cdot [X]} \qquad 2.14.$$

The relation between ^{c}K and [M] (measured data) and the adjustable parameters K, K_{mix}, and SCC is

$$^{c}K = \frac{K \cdot (1 + K_{mix} \cdot [X])}{1 + K \cdot (1 + K_{mix} \cdot [X]) \cdot [M]} \cdot SCC \qquad 2.15.$$

In the region of very low metal loading, this equation can be simplified to

$$^{c}K = K \cdot (1 + K_{mix} \cdot [X]) \cdot SCC \qquad 2.16.$$

Glaus et al. showed that mixed complexes are rather weak in comparison to the complexes formed by the low molecular weight ligands and the metal alone [Glaus 1995].

Experiments done at the trace metal concentrations level and higher pH performed by Glaus et al. using the equilibrium dialysis-ligand exchange (EDLE) technique [Glaus 2000], showed very consistent data which were fitted starting from the equation 2.11. with a polynomial in the form

$$^{c}K = a \cdot pH^{2} + b \cdot pH + c \qquad 2.17.$$

The fitting parameters are a function of the ionic strength, but its influence for the metals studied was not as important as the influence of the pH. The constants didn't show a dependence on the humic substance type.

A good estimation for the metal-humate interaction is the "conservative roof" approach applied for performance assessments, which is described in detail by Hummel [Hummel 1997 and Hummel 2000]. The basis of this approach is the overestimation of the parameters taken no consideration if the binding models are right or wrong. For these purpose only main parameters like pH, metal concentration and ionic strength may be considered.

The equations proposed by Hummel et al. [Hummel 2000] for the interactions of humic substances and Np at trace concentrations for the conservative roof approach are specified below, being K_{exch} the equilibrium constant for the metal complexation with organics, [H] the proton concentration and [M] the metal concentration.

$$^{c}K = \frac{SCC}{[M]} \qquad 2.18.$$

$$^{c}K = \frac{K_{exch} \cdot [H]^{-x}}{1 + K_{exch} \cdot [M]/[H]^{x}} \cdot SCC \qquad 2.19.$$

$$\log {}^{c}K = \log K_{exch} + \log SCC + x \cdot pH \qquad 2.20.$$

They found the value of 0.19 ± 0.02 for the adjustable parameter x by studying the interaction of Np(V) with humics [Hummel 2000].

Another formalism was proposed by Tipping and Hurley [Tipping 1992], where the complexation of metals by the humic substances were described as occurring at a number of chemically distinct discrete binding sites. Tipping and Hurley considered only the major proton dissociating groups (e.g. carboxylic and phenolic). The combination of the Humic Ion – Binding Model V [Tipping 1992] with a simple inorganic speciation code for aqueous solutions, results in the WHAM (Windermere Humic Aqueous Model) speciation program [Tipping 1994]. For the calculations, the humic substances are considered as size-homogeneous, rigid molecules, which carry proton-dissociating groups that can bind metal ions either singly or as bidentate pairs [Tipping 1994]. Tipping improved his model proposing the Humic Ion – Binding Model VI [Tipping 1998]. Here, strong sites (carboxylic) and weak sites (e.g. phenolic) are considered.

A more user friendly model is the Stockholm Humic Model (SHM) [Gustafsson 2001], which has been incorporated to the Visual MINTEQ speciation software. Similar to the Humic Ion – Binding Model V [Tipping 1992], the SHM considers a discrete-site approach, but with a different electrostatic submodel based on the Basic Stern concept. The fitting power of the SHM has been probed for soil samples by Gustafsson et al., with good results [Gustafsson 2003].

For low metal concentrations, as for radionuclides, the metal ion charge neutralization model proposed by Kim and Czerwinski [Kim 1996] can be applied. This model supposes that metal cations are surrounded by same amount of negative charges from the humic acid as needed for its electrical neutralization. Within this model the complexation reaction between

the metal cation M^{+z} and the amount of complexing sites needed for the neutralization HA(z), to form the humate complex MHA(z) is described by the equation 2.21.

$$M^{+z} + HA(z) \longleftrightarrow MHA(z) \qquad 2.21.$$

Hence the complexation constant (β) can be described with the equation

$$\beta = \frac{[MHA(z)]}{[M^{+z}]_f \cdot [HA(z)]_f} \qquad 2.22.$$

where the subindex *f*, means free. With the known proton exchange capacity (PEC) of the humic acid, the operational concentration of the humic acid $[HA(z)]_t$ can be obtained.

$$[HA(z)]_t = \frac{(HA)PEC}{z} \qquad 2.23.$$

Thus the loading capacity (LC), which is specific for the reaction conditions, can be then calculated.

$$LC = \frac{z \cdot [M^{+z}]^*}{PEC(HA)} \qquad 2.24.$$

where $[M^{+z}]^*$ is the maximal disposable metal concentration for the complexation with a given humic acid at the experimental conditions. By knowing LC, the free humic acid concentration can be then defined as:

$$[HA(z)]_f = [HA(z)]_t LC - [MHA(z)] \qquad 2.25.$$

and β can be then determined with:

$$\beta = \frac{[MHA(z)]}{[M^{+z}]_f ([HA(z)]_t LC - [MHA(z)])} \qquad 2.26.$$

The β values are then independent of the metal ion concentration, the pH, and origin of the humic acid. In this work, only this approach has been considered for it was developed for the complexation of radionuclides with humic substances and allows the comparison of results obtained at different experimental conditions. Moreover, literature data for the complexation of Np(V) with Aldrich humic substances [Seibert 2001] and M42 type melanoidins [Sachs 2005 b] are available, which have been evaluated with the charge neutralization model.

2.3.2. Melanoidins

Due to the above mentioned complexity of the humic substances, model substances are needed to better understand their properties under controlled conditions. The best known

model substances since the works of Maillard in 1912 [Maillard 1912] and Enders and Theis in 1938 [Enders 1938], are melanoidins.

Melanoidins are polymers obtained after the condensation and dehydration of amino acids and sugars. Melanoidins were first described by Lois Camille Maillard in 1912 and are the products of a chemical reaction between an amino acid and a reducing sugar, usually requiring the addition of heat. The Maillard reaction is present in our daily lives, it occurs in the dehydration of food products at moderate temperatures (caramel or roasting) and it has been found to occur in the human body, as part of the aging reaction of proteins [Ledl 1990]. Amadori reported in 1925 and 1931 the production of two isomers the stable and the unstable one [Amadori 1931]. The products of the Amadori rearrangement are subject to undergo; **a**. fragmentation, **b**. dehydratation (two water molecules) to form reductones, **c**. dehydratation (three water molecules) to form hydroxymethyl furfural. Those three products are highly reactive towards the formation of brown polymers in the presence of amino compounds [Stevenson 1982].

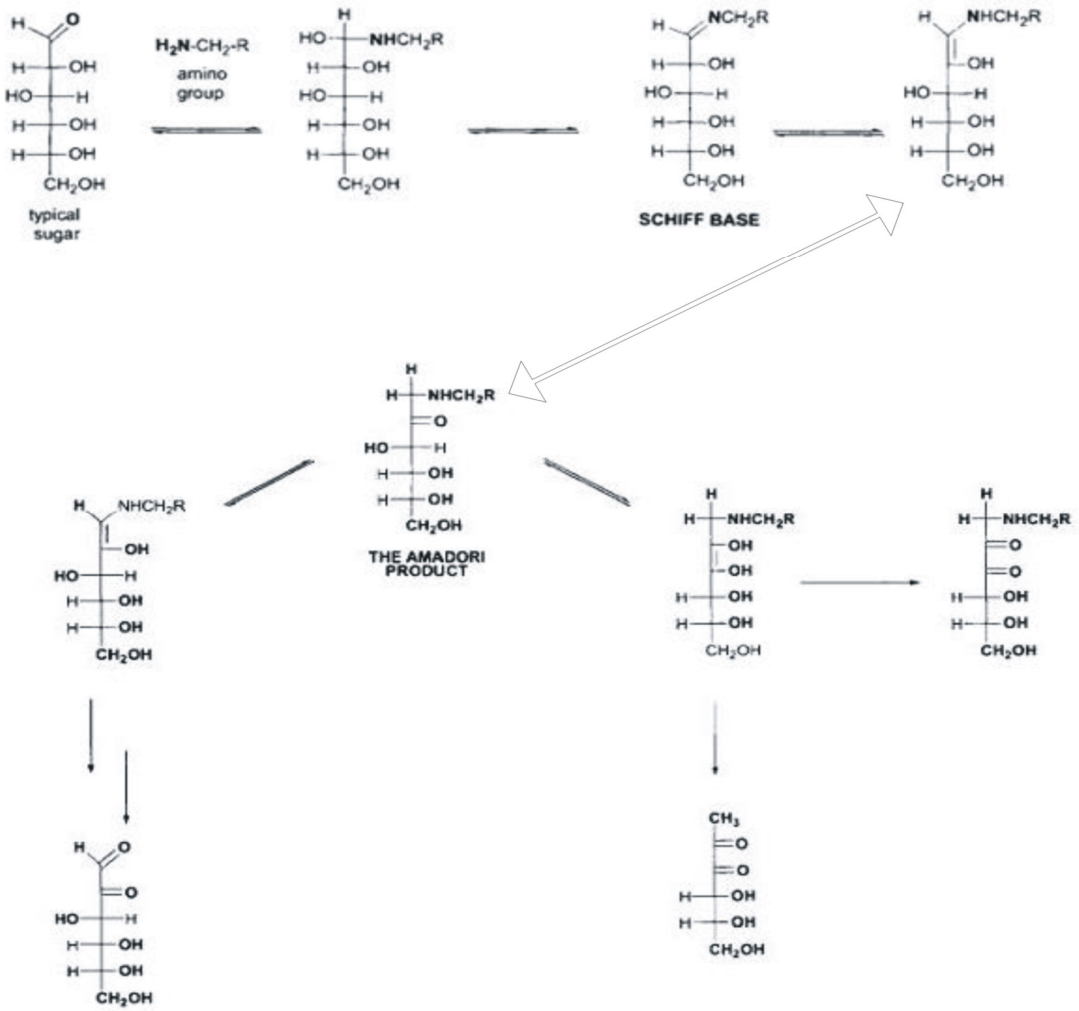

Fig. 2.15. Maillard reaction scheme, from the Royal Society of Chemistry [Ledl 1990].

The use of melanoidins as natural analogues in order to understand the reactions of humic substances with the actinides has been reported in the last years. The most successful approach was the synthesis of the melanoidin M42, which has similar properties as Aldrich Humic Substances [Pompe 1998].

2.3.3. Mineral-Organic interaction

Since the early studies of Greenland [Greenland 1956], it is known that the greatest amount of naturally occurring organic matter in the environment is associated to clay minerals. It was supposed that clay minerals may affect the formation of the humic substances due to their catalytic effect [Ziechmann 1993]. This catalytic effect was studied in the forty's using colour reactions catalyzed by clays; Hendricks and Alexander examined the reaction of aromatic diamines with clays, and found that the minerals of the kaolinite group where not so active as the minerals of the montmorillonite group [Hendricks 1940]. The preparation of kaolinite containing nanocomposites needs the pretreatment of the kaolinite in order to expand the layers [Komori 1998 and 1999]. Other interesting observations were that the amount of iron in different montmorillonites was also important to explain the activity of the minerals as electron exchanger [Solomon 1968]. Furthermore, montmorillonites may affect polymerization reactions, e.g., polymerization of styrene monomers [Theng 1974].

Several ways for the bonding of soil organic material with clays have been proposed [Stevenson 1982 and Aiken 1985]:

- As insoluble polymeric complexes of humic and fulvic acids.
- As macromolecular complexes bound together by di- and trivalent cations.
- In combination with clay minerals by bridging by polyvalent cations, hydrogen bonding, van der Waals forces and other ways [Theng 1979].

In most of the mineral soils, clay and humic occurs as an association, normally as a clay-metal-humus complex (see section below) [Aiken 1985]. Studies on the sorption of humic acids and melanoidins on clay minerals show similar tendencies independent of the mineral surface, while the mineral surface is positively charged (pH < point of zero charge) the negatively charged humic substances may be adsorbed onto the mineral. When pH > point of zero charge, the negative charge of the mineral surface repells the also negatively charged humic substances which can be seen in Fig. 2.16.

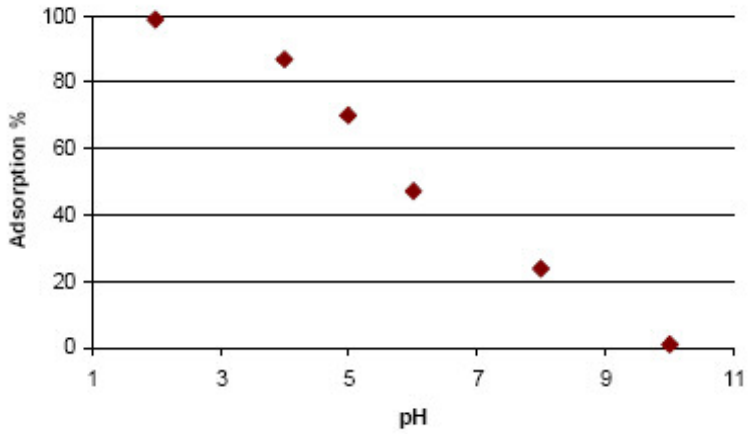

Fig. 2.16. pH dependence of the adsorption of Aldrich humic acid onto kaolinite (reported point of zero net proton charge about 5.0 and 5.4 [Schroth 1997], I = 0.1 M $NaClO_4$ [Buda 2006].

Experimental data show that polyvalent cations may act as a bridge between the functional group of the humate (or fulvate) and the negatively charged clay surface. The uptake by clay minerals rises with an increase in the cation valence [Theng 1979]. Those experiments indicated the formation of a water bridge between the cation and presumably the carboxylate group of the humic acids. The sorption isotherms in Fig. 2.17. show the dependence between cation charge and humic acid sorption.

Another important mechanism for the retention of organic substances by layered clays is through the adsorption on the interlayers. This point will be discussed in the next section.

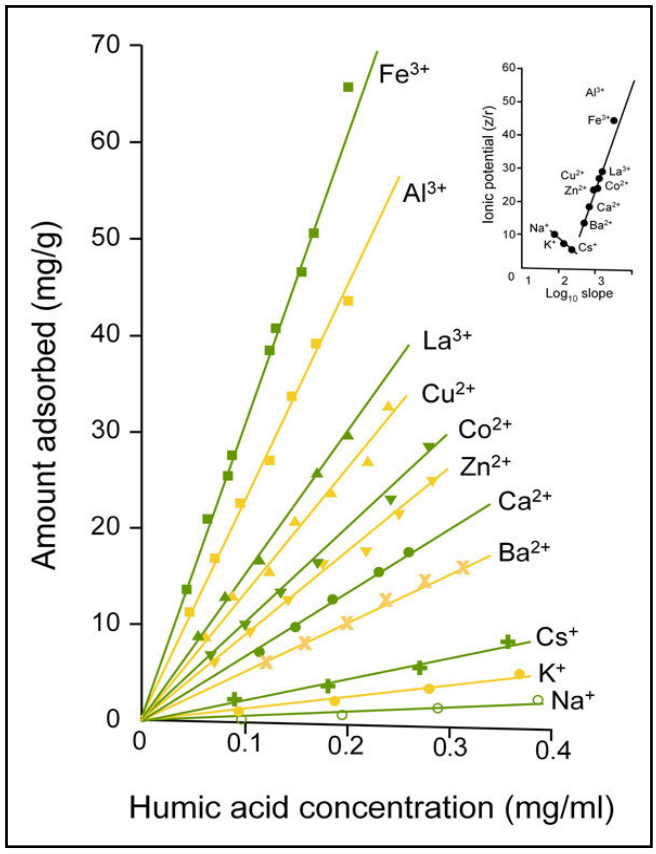

Fig. 2.17. Isotherms for the adsorption at 293 K and pH 7 of humic acid by montmorillonite saturated with different cations [Theng 1975 and 2006].

So far we can conclude that there are different interaction mechanisms for humic substances with clays, which includes cation-bridge interactions and hydrogen binding, the interaction mechanisms are summarized in Fig. 2.18.

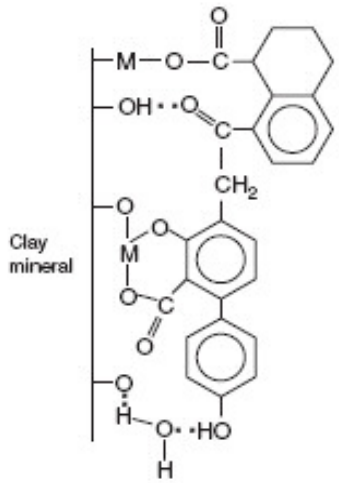

Fig. 2.18. Types of bonding interaction in forming the clay humate-complex [van Loon 2005].

2.4. Clay Minerals

As backfilling materials, clay minerals with swelling or non swelling properties may be used, or in some cases other naturally occurring soils with high contents of fineries (silt and clay). The big advantage of using clay minerals as backfill materials is their low hydraulic conductivity, high specific surface area, and in some cases swelling ability. The possible disadvantages of natural clays as backfilling material are linked, e.g., to compressibility, sensitivity to water content during emplacement, and sensitivity to salt content of the groundwater in the expected repository conditions [POSIVA 2004].

Bentonites are the most widely considered material for backfilling. They are a wide range of commercial clay materials with different definitions [Bates 1987], but all the bentonites are composed dominantly by smectite clay minerals, which give the bentonite swelling properties, when in contact with free water. This is due to the absorption of water molecules into the interlayer space. The smectite content for the most used bentonites varies between 65% and 96% in weight. This holds for Moosburg, Ca-bentonite (Germany) and FEBEX, Ca-bentonite (Spain) respectively [POSIVA 2004]. There are also other concepts with different naturally swelling clays, which involve normally smectite rich clays, and concepts involving non swelling clays like kaolinite and soils with high contents of fineries like basalt tills.

Clay minerals are layered aluminosilicates, where the tetrahedra are corner-linked and the octahedra edge-linked. These sheets may be linked together in two ways, 1:1 and 2:1. The 1:1 layer structure comprises one tetrahedral sheet and one octahedral; this is the structure of kaolinite. The 2:1 layer structure comprises one octahedral sheet between two tetrahedral sheets. Due to the importance of bentonites and therefore of the smectite group of clay minerals, only montmorillonite was considered for this work.

2.4.1. Metal-mineral interactions

The consideration of adsorption and desorption processes is of vital importance in environmental soil science. In the case of DGD, the sorption data are used for radionuclide retardation calculations, which is fundamental for the site adjudication. Several models are used for the interpretation and generalisation of the obtained sorption data, but it is to be kept in mind:

> *"Adherence of data to a proposed equation does not prove that the assumed (or corresponding) adsorption mechanism is actually occurring. It does, however, establish a platform (albeit often temporary) that allows the process of scientific inquiry to proceed."*
>
> [Schulthess 1996]

Due to their dominant relevance, only the Freundlich and the surface complexation model are considered for this section.

The Freundlich (and also Langmuir) sorption equations are early sorption models and are still often used. Freundlich demonstrated the generality of a mathematical relationship obtained by Bemmelen (1878) for the adsorption of metals. The Freundlich equation is usually written as:

$$C_{metal,adsorbed} = K_F \, C_{metal,equilibrium}^{1/n_F} \qquad 2.27.$$

or in the linearized form:

$$Log\, C_{metal,adsorbed} = Log\, K_F + \frac{1}{n_F} Log\, C_{metal,equilibrium} \qquad 2.28.$$

In most cases, $0<n_F<1$, depending on the nature of the sorbent and sorbate. Everett A. Jenne warns against segmenting and fitting the data sheets, due to the high amount of non-investigated variables [Jenne 1998]. The main deficiency in both models (i.e. Freundlich and Langmuir) is the lack in transferability. The latter should be enhanced with surface complexation models. This kind of models considers sorption reactions of pH dependent surfaces to occur in the same way as the reactions in the aqueous phase. Equations 2.29. and 2.30. are then the protonation and deprotonation of neutral surface sites respectively.

$$\equiv SOH^{0} + H^{+} \longleftrightarrow \equiv SOH_2^{+} \qquad 2.29.$$

$$\equiv SOH^{0} \longleftrightarrow \equiv SO^{-} + H^{+} \qquad 2.30.$$

In the same way, metal cation adsorption is described in this model as:

$$\equiv SOH^{0} + M^{+z} \longleftrightarrow \equiv SOM^{+(z-1)} + H^{+} \qquad 2.31.$$

It is difficult to determine the Gibbs free energies needed for the surface reactions and the effect of the neighboring sites, moreover diverse implementations (normally three) concerning the interface area are used in sorption studies, i.e. the constant capacitance complexation model, the diffuse double layer complexation model and the triple layer complexation model. Due to the complexity of this kind of models, their application becomes usually a data-fitting exercise.

Within this work, the Freundlich equation was used to fit the neptunium-gibbsite sorption isotherm (section 4.2.2.) and the sorption parameters published by M.H. Bradbury and B. Baeyens [Bradbury 2006] for the sorption of Np(V) onto SWy-1 montmorillonite were used for comparison purposes.

2.4.2. Smectites and montmorillonite

The negative charge of smectites make this group extremely reactive in soils. They are responsible for most of the swelling properties of soils. The smectites are also responsible for the cation exchange capacity of many soils. They may exchange the cations which are necessary for plant growth and may also adsorb organic compounds. They are 2:1 layer silicates, which are divided into dioctahedral and trioctahedral smectites (see table below). The most important properties of smectites are swelling, cation exchange capacity, and high specific surface area. They are widely distributed throughout the world. Montmorillonites and beidellites are the most commonly found; nontronites occur mainly as hydrothermal alteration products; and saponites may occasionally occur in soils. The distribution of hectorites is very limited, due to their high Li contents.

Smectites	Species	Ideal Formula
Dioctahedral	Montmorillonite	$Ca_{(y/2)}Si_4(Al_{(2-y)}Mg_y)O_{10}(OH)_2$
	Beidellite	$Ca_{(x/2)}(Si_{(4-x)}Al_x)Al_2O_{10}(OH)_2$
	Nontronite	$Ca_{(x/2)}(Si_{(4-x)}Al_x)Fe^{3+}{}_2O_{10}(OH)_2$
Trioctahedral	Hectorite	$Ca_{(y/2)}Si_4(Mg_{(3-y)}Li_y)O_{10}(OH)_2$
	Saponite	$Ca_{([x-y]/2)}(Si_{(4-x)}Al_x)(Mg_{(3-y)}(Al,Fe^{3+})_y)O_{10}(OH)_2$
	Sauconite	$Na_{0,3}Zn_3(Si,Al)_4O_{10}(OH)_2{\cdot}4(H_2O)$

Table 2.6. Classification of the smectites.

Montmorillonites have a predisposition to little whole charges in comparison to beidellites and nontronites. The charge is mostly originated by the substitution of aluminium cations (Al^{+3}) through magnesium (Mg^{+2}) cations. The Clay Minerals Society has characterized different montmorillonites, e.g., SAz-1, STx-1, and SWy-2 [Constanzo 2001], and selected them as source clays, which shall serve as reference materials among the researchers. The percentage of the major elements is shown in Table 2.7.

Sample	SiO_2	Al_2O_3	Fe_2O_3	MgO
SAz-1	59.65	19.98	1.77	6.73
STx-1	70.03	17.86	1.20	3.79
SWy-2	61.46	22.05	4.37	2.94

Table 2.7. Elemental composition of source montmorillonites selected by the Clay Minerals Society concerning only Al, Si, Fe and Mg as oxides [Mermut 2001].

The little amount of iron, which made the clay not so active for catalysis and redox reactions, combined with the amount of magnesium lead us to the STx-1 montmorillonite. The STx-1 montmorillonite has a cation exchange capacity (CEC) of 89 ± 2 meq/100 g, with this value being between SWy-2 (85 ± 3 meq/100 g) and SAz-1 (123 ± 3 meq/100 g) [Borden 2001]. For the STx-1, a formula has been proposed where χ is the monovalent interlayer cation $(Si_{7.84}\ Al_{0.16})\ (Fe_{0.07}\ Al_{3.53}\ Mg_{0.40})\ O_{20}\ (OH)_4\ \chi^{+}_{0.56}$ [Laboriau 1996].

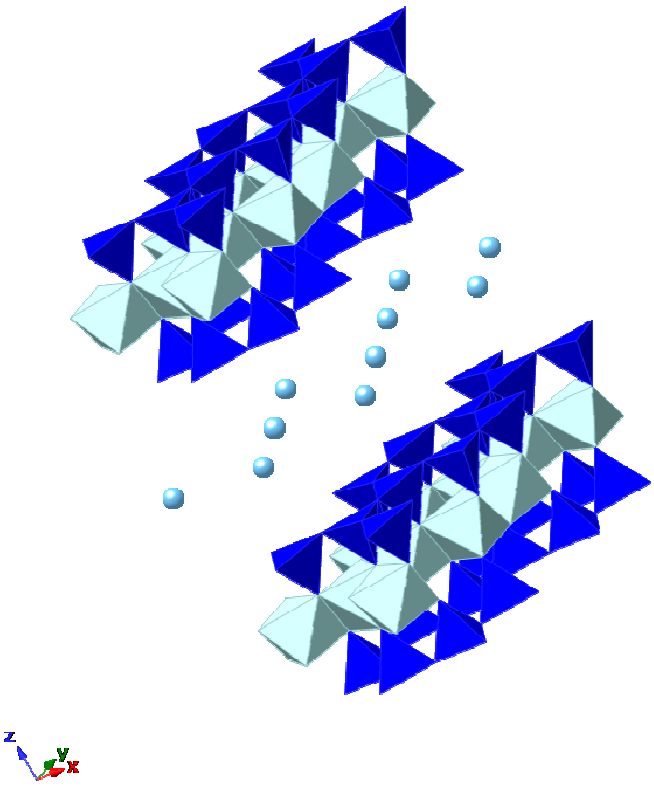

Fig. 2.19. Structure of montmorillonite [Viani 2002]. The dark blue tetrahedra represent the SiO_4 units, the pale blue octahedra the AlO_6 units and the spheres in the interlaminar space the interlayer cation.

2.4.3. Hybrid clay-based materials

As stated before, humic substances may be found in the interlayers of swelling clays [Stevenson 1982]. There are many laboratory evidences of defined organic compounds absorbed into the interlayers of clay minerals, but little is known about the existence of those complexes in natural soils, due to the extraction methods, which are able to destroy the silicates. There is evidence for the interlayer sorption of fulvic acids at pH below 5.0 [Schnitzer 1967], but the higher weight humic acids may be too large to penetrate the interlamellar spaces [Stevenson 1982]. In order to simulate natural conditions, a different approach has to be used, i.e. the preparation of hybrid clay-based materials. This approach may throw new light on the problem as humic-clay-complexes are likely formed *in statu nascendi* of the humic substances [Ziechmann 1993].

In the last years the preparation of hybrid clay-based materials has gained importance due to the possibility of controlling the formation of advanced materials [Brandt 2003]. The formation of those hybrid materials may be achieved by using three different techniques, see Fig. 2.20.

Studies concerning the formation of nanocomposites with layered inorganic solids have been performed in the last years with different goals. In this context, caramel-clay nanocomposites as a precursor of carbon-clay nanocomposites were prepared by Margarita Darder [Darder 2005]. More related to our work, Ziechmann studied the formation of humic like substances emerging from hydroquinone in the presence of clay (bentonite) [Ziechmann 1993]. He concluded that:

1. Only low molecular precursors of the humic acids may react forming interlayer complexes or nanocomposites
2. The reaction is catalyzed by the clay mineral, which acts as an e^--acceptor.
3. Humification proceeds then in two different directions:
    a. Inwards into the interlayer space
    b. Outwards into the solution
4. Three main types of complexes:
    a. The structure similar to a cork on a bottle.
    b. The structure where the organics are held in the interlayer.
    c. Fixed on the edges

- Melt intercalation

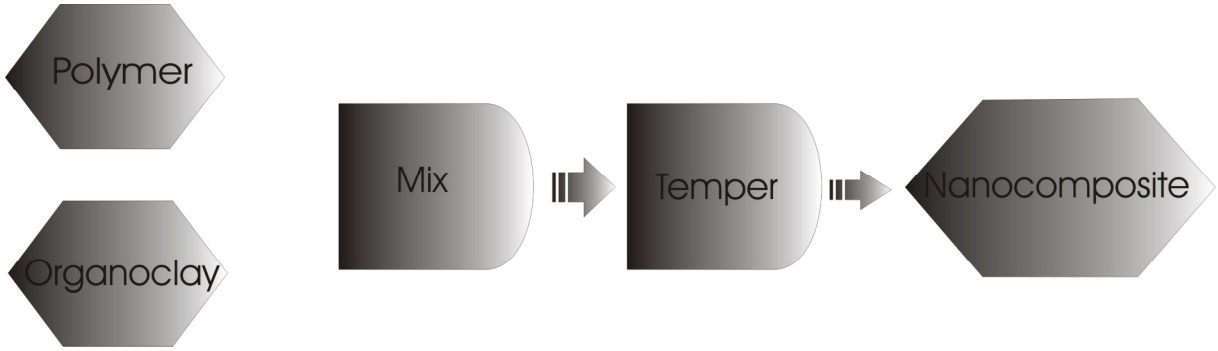

- Direct intercalation

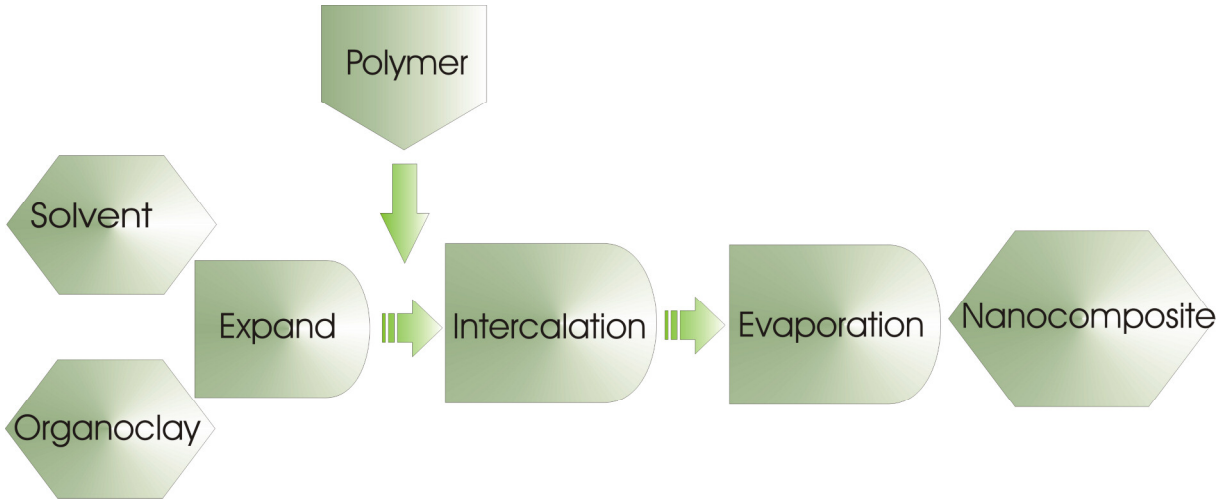

- In situ polymerization

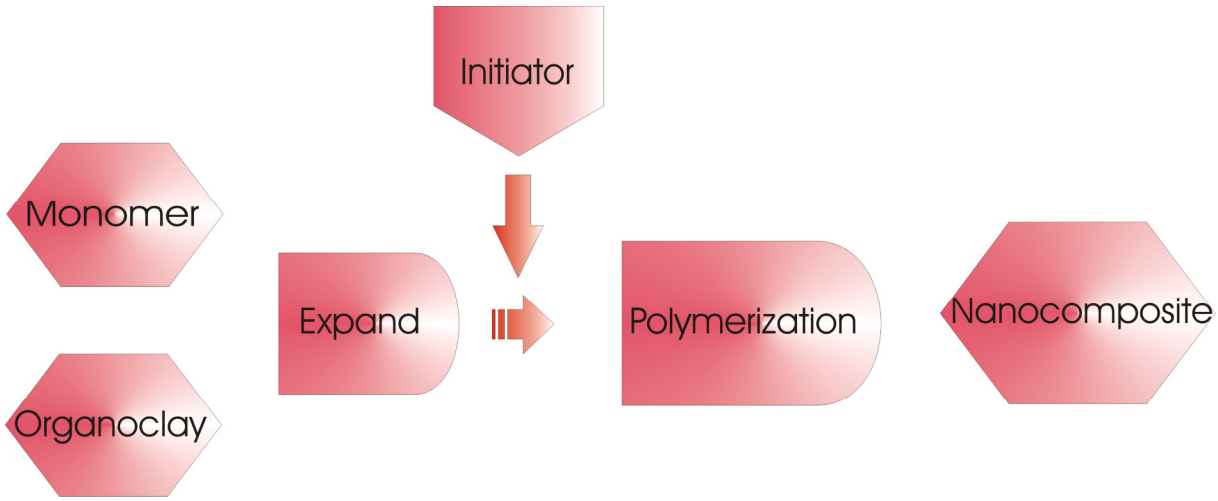

Fig. 2.20. Different methods for the preparation of nanocomposites [Schleidt 2006].

Attempts to study the formation of melanoidins in the presence of kaolinite (KGa-1b) were done by Sachs and Bernhard in 2004. They didn't observe any differences in the melanoidins formed in the presence of kaolinite and those which were synthesized without kaolinite. In addition, the sorption of U(VI) was also investigated on this materials [Sachs

2004]. In the pH range below 5.5 the sorption is comparable to the sorption of U(VI) on kaolinite if melanoidins are present, above 6.5 the sorption is reduced in comparison to the sorption on pure kaolinite and on kaolinite in the presence of melanoidins. Above 8.5, the sorption is similar to the sorption on pure kaolinite [Sachs 2004].

3.1. Preparation of the reactants

The preparation and purification of the used materials is discussed in this section.

3.1.1. Synthesis of the hybrid clay-based material (HCM)

L-glutamic acid, L-tyrosine, and D(+)-xylose (Merck, Darmstadt, Germany), were used in the synthesis of the composites. The composites were synthesized in a batch experiment starting from 16.5 g xylose, 13.5 g L-tyrosine or 11 g glutamic acid, 3.2 g Na-montmorillonite STx-1, and 150 mL water. After reflux boiling (100°C, 90 h) for L-tyrosine and (80°C, 90 h) for glutamic acid [Pompe 1998] a brown solid was formed. A higher temperature was selected for the synthesis with L-tyrosine due to its lower reaction velocity [Maillard 1912]. After centrifugation, the solid product, containing both melanoidins and HCM, was ground with ethanol and ether (Acros Organics), and again centrifuged. This solid was stirred with 150 mL 2 M NaOH (Merck) 8 hours under N_2. After centrifugation, the solid was again stirred with 100 mL 2 M NaOH (Merck). From both supernatants, melanoidins can be recovered. After centrifugation, the HCM were isolated, dialyzed, in order to desalt the products, using dialysis tubes (Spectrum Laboratories Inc., exclusion limit MWCO <1000) against purified water and then lyophilized (Steris Corporation). Fig. 3.1. illustrates the synthesis, unfortunately one synthesis run didn't work properly, hence the high weight errors in both HCM and related melanoidin.

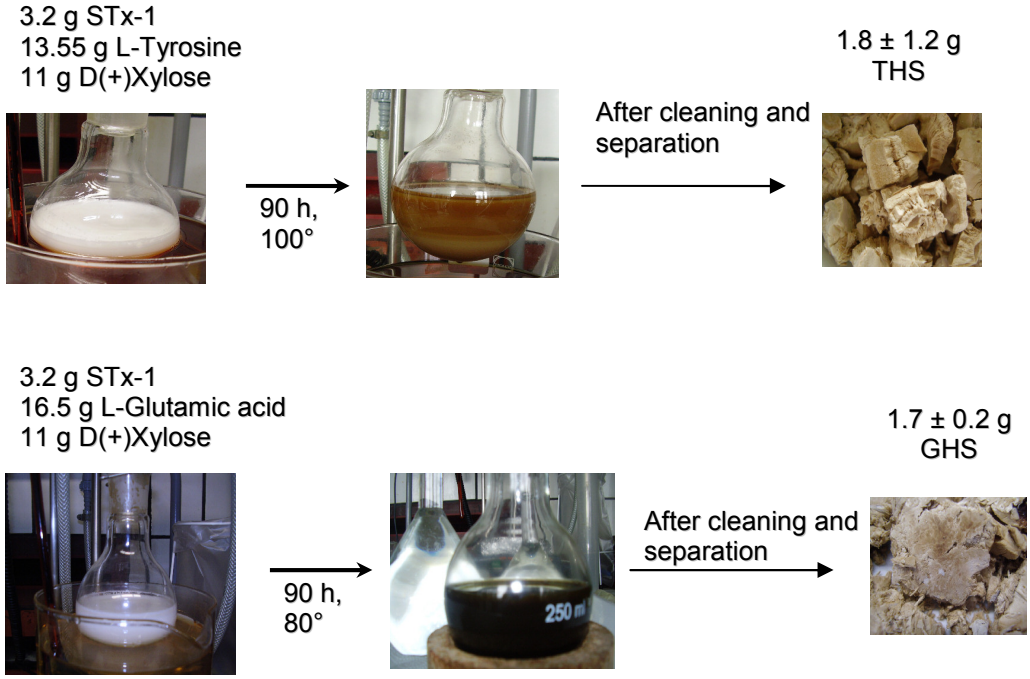

Fig. 3.1.Synthesis of HCM and yields for the reaction.

Two products were obtained, the tyrosine hybrid material solid (THS), and the glutamic acid hybrid material solid (GHS). In the same synthesis, the extraction of the related melanoidins from the solution was also possible.

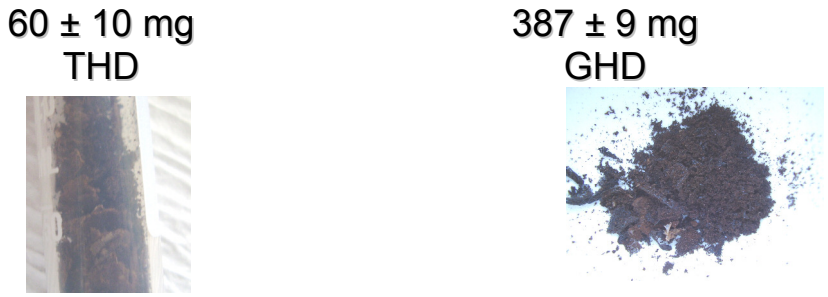

Fig. 3.2.Yields obtained for the melanoidins tyrosine humic like dark solid (THD) and the glutamic acid humic like dark solid (GHD).

3.1.2. Preparation of the STx-1

Following the method proposed for Wyoming montmorillonite (SWy-1) by Baeyens & Bradbury [Baeyens 1995], the Texas montmorillonite (STx-1) was prepared. First of all, the sodium perchlorate electrolyte solutions, which were prepared using Fluka "pro analysis" chemicals, were purified using the sorption properties of Aldrich 99.99% Al_2O_3. This purification procedure should avoid the presence of heavy metals impurities which. At the same time, Millipore water was equilibrated with montmorillonite (1 mL montmorillonite suspension in dialysis bag, Spectrum Laboratories Inc. exclusion limit MWCO <12,000 – 14,000, in 1 L Millipore water).

Preparation of the STx-1:

- In order to convert the clay to the homo-ionic Na-form, 2 L of the purified 1 M sodium perchlorate solution is added to 60 g montmorillonite, the suspension is then allowed to flocculate (1 h) and the supernatant is sucked off. New sodium perchlorate is then added. The process is repeated 3 times.

- 2 L of the purified 1 M sodium perchlorate is put in a 20 L container. The clay suspension is divided in twelve 250 mL centrifuge bottles (Beckmann Coulter), filled up with equilibrated Millipore water, and centrifuged 7 min. at 614 g (2000 rpm). The supernatant is sucked off the container. The process is repeated 10 times. This step allows the separation of the <0.5 µm clay fraction.

- The container is filled up with 1 M sodium perchlorate, and the suspension is allowed to flocculate over night.

- The supernatant is sucked off, and the suspension is reduced to 5 L. More 1 M sodium perchlorate is then added to force the flocculation.

- Due to the washing process, clay may hydrolyze. Therefore, the half of the suspension is acidified to pH 3.5 for 1 h, and centrifuged 7 min. at 5524 g (6000 rpm). The deposit is then adjusted to pH 7, and can be conditioned to any ionic strength by using dialysis (Spectrum Laboratories Inc. exclusion limit MWCO <12,000 – 14,000).

The conditioned montmorillonite can be stored in the fridge for six months.

3.1.3. Preparation of ^{237}Np stock solutions

Solid NpO_2 was dissolved using freshly prepared aqua regia, and heating the solution. The ^{237}Np solution was then evaporated to dryness and the residue was dissolved in 8 M HCl. The impure ^{237}Np solution (^{239}Pu, ^{240}Pu and ^{241}Am impurities) was cleaned in a temperate (55°) anion exchange column (Dowex AG 1 x 8, BioRad). The lanthanides and americium elute by using 8 M HCl (Fischer Scientific, Germany). For the elution of Pu, as Pu(III), NH_4I (750 mg in 25 mL HCl 8 M) was added, and the elution of Np is achieved with 4 M HCl (Fischer Scientific, Germany)/ 0.05 M HF (Merck, Germany). The Np solution is heated and the total volume is reduced to 1 mL.

That 1 mL is added into a second temperate (55°) column (Dowex AG 1 x 8, BioRad). ^{233}Pa, which is a decay product of ^{237}Np, elutes by using 9 M HCl (Fischer Scientific, Germany). In order to achieve the elution of ^{237}Np, 5 M HCl (Fischer Scientific, Germany) was used. The neptunium solution was dried and then fumed off three times with 10 mL 1 M $HClO_4$ (Merck, Germany) in order to have only Np(V). The Np(V) is then transferred to a bottle with 3 mL 0.1 M $NaClO_4$ (Fluka, Germany), a little amount of $NaNO_2$ (Merck, Germany) is added, and the solution is adjusted to pH about 5. The neptunium solution is stable against disproportioning, but has to be cleaned from decay products every two months. The concentration of the obtained solution can be determined by LSC (see below section 3.2.1.) and γ-spectroscopy (see section 3.2.2.).

3.1.4. Preparation of ^{239}Np stock solutions

For the production of ^{239}Np, about 20 to 30 mg $UO_2(NO_3)_2 \cdot 6H_2O$ (≤ 0.3% ^{235}U) in 1 mL Millipore water were irradiated 6 hours at 100 kW at the TRIGA Mark II – Reactor in Mainz, shown in Fig. 3.3. The neutron flux was about $7 \cdot 10^{11}$ n/s·cm^2.

^{239}Np was obtained by using the reaction which led to the discovery of neptunium (equation 2.1).

$$^{238}U(n,\gamma)^{239}U \xrightarrow{\beta^-,23\,\mathrm{min}} {}^{239}Np \xrightarrow{\beta^-,2.35\,days} {}^{239}Pu \qquad 3.1$$

Fig. 3.3. The TRIGA Mark II – Reactor at the Institute of Nuclear Chemistry, University of Mainz (kernchemie.uni-mainz.de/234.php**).**

After a decay time of 16 hours, the irradiated uranium can be taken out from the reactor. The cleaning method for the ^{239}Np solution was described by U.A. Seibert [Seibert 1999]. One mL 37% HCl (Fischer Scientific, Germany) was added to the turbid solution. These 2 mL solution are then added to a temperate (55°) anion exchange column (Biorad AG 1 x 8, 200 – 400 mesh). The exchange resin is in the chloride form. Neptunium will be held at the column as $[NpCl_6]^{-2}$. The fission products elute by using 8 M HCl (Fischer Scientific, Germany), and the elution of Np can be achieved by using 4 M HCl (Fischer Scientific, Germany)/ 0.05 M HF (Merck, Germany). The neptunium fraction is recovered in a Teflon beaker, and dried. The dried neptunium is redissolved in 5 mL 1 M $HClO_4$ (Merck, Germany), and fumed off three times in order to have only Np(V). The Np(V) is then transferred to a bottle with 3 mL 0.1 M $NaClO_4$ (Fluka, Germany) a little amount of $NaNO_2$ (Merck, Germany) is added and the solution is adjusted to pH about 5. The stock solution is stable against disproportioning, and the concentration can be determined by γ-spectroscopy (see section 3.2.2.).

3.1.5. Preparation of ^{14}C labeled M42 type melanoidins

For the study of the interaction of humic acids and humic acid like substances with minerals, the use of radiolabeled substances provides reliable results if the concentration of the dissolved organic matter (DOM) after centrifugation is very low. Theng and Scharpenseel prepared ^{14}C-humic substances by cultivating grass under $^{14}CO_2$ and extracting the humic

substances from the soil after six months [Theng 1975]. Another, simpler approach was done by Sachs et al. [Sachs 2003]; they proposed the synthesis of ^{14}C labeled M42 type melanoidins. The synthesis of the ^{14}C labeled M42 type melanoidins follows the same scheme as the above described synthesis of the HCM (see section 3.1.1.), with the particularity of adding [U-^{14}C] glutamic acid instead of the inactive glutamic acid added for the inactive synthesis.

3.2. Methods used

During this work, different methods were used for determining the concentration of ^{237}Np, ^{239}Np, ^{14}C, and for the speciation of Np in the presence of montmorillonite and melanoidins. A brief description of the methods used for the characterization of the HCM is also enclosed in this section.

3.2.1. Liquid Scintillation Counting (LSC)

LSC is an analytical technique consisting in the incorporation of a radiolabeled analyte or radionuclide into a chemical medium which is able to convert kinetic energy from nuclear emissions into light. This chemical medium is normally composed of a solvent, a primary scintillator and a secondary scintillator. The emitted particles excite the primary scintillator. In the case of ^{237}Np we handle with α particles and ß particles are emitted in samples with ^{14}C. It is possible to differentiate between the two radionuclides ^{14}C and ^{237}Np via pulse-shape discrimination.

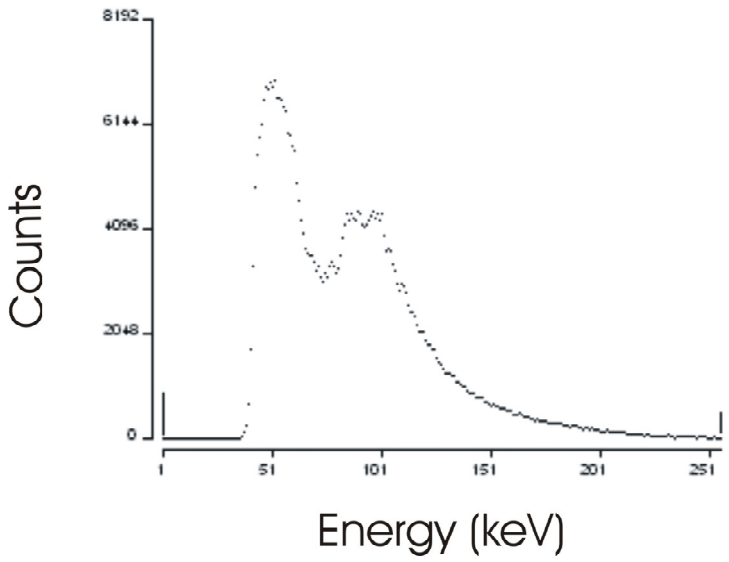

Fig. 3.4. Above pulse form spectrum in energy window of a ^{237}Np / ^{14}C mixture, [Np] = 8µM / $[Melanoidins]_0$ = 0.25 mg/mL.

The excited primary scintillator decays emitting fluorescence. The secondary scintillator is a blue fluorescence emitter, which improves the signal by shifting it to longer wavelengths. The excited scintillator molecules emit light, which decays in form of an exponential function. This light liberates electrons in the cathode of the photomultiplier and as a result of this there is an electricity current pulse in the anode.

The scintillation cocktail Ultima Gold AB (Perking Elmer, Germany) was used, the sample volume relationship was 1:10. The LSC system used for this work was homemade.

3.2.2. γ-Spectroscopy

The nuclear decay is often accompanied by photon emission. The energy of those emitted photons is characteristic for the emitting nuclei. Thus gamma spectra can be used for the specific determination of gamma emitting isotopes. There are mainly two different kinds of gamma detectors [Peerani 2006]:

- Inorganic scintillator, like the NaI detectors.
- Semi conductor detector, mainly high purity Ge or Cadmium-Zinc-Telluride detectors.

For this work, Ge detectors (DSG, Mainz, Germany) were used. Ge detectors have a p-i-n structure, being the intrinsic region (i) sensitive to ionizing radiation [CANBERRA 2003]. The interaction of photons with the detector produces charge carriers, which are, in the case of photo effect; proportional to the energy of the incoming photon. Other interactions of the incoming photons like Compton scattering and pair production are not useful for γ-spectroscopy. Germanium detectors have to be cooled, in order to avoid the thermal production of charge carriers.

For the determination of ^{239}Np and ^{237}Np, γ-spectroscopy uses the photopeaks at 106.12 keV and 103.76 keV for ^{239}Np and the 29.4 keV and 86.5 keV for ^{237}Np.

3.2.3. CE-ICP-MS

The use of the coupling of capillary electrophoresis with inductively coupled plasma mass spectrometry, CE-ICP-MS, for the separation of Np(IV) and Np(V) in groundwaters has been investigated by Kuczewski et al. [Kuczewski 2003]. He demonstrated the possibility of using this method for the separation of different oxidation states of actinides and lanthanides under geogenic conditions.

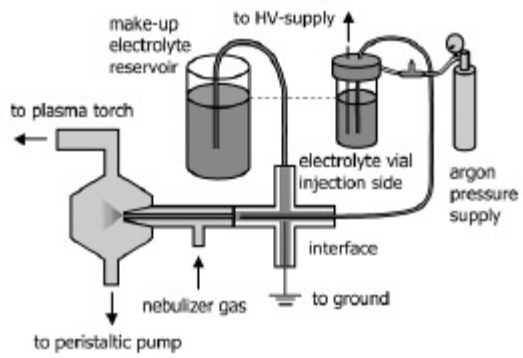

Fig. 3.5. Set up for the coupling between the homemade CE system and the ICP-MS [Kuczewski 2003].

Capillary Electrophoresis

The fundamentals of the technique are widely described [Oda 1997] and the method used was improved and described by Kuczewski et al. [Kuczewski 2003]. Therefore, only a few remarks will be made in this section.

Capillary electrophoresis is a relatively old technique, which was first described by Michaelis [Michaelis 1909]. Its principal advantage is the small amount of sample needed and therefore low costs, duration of the measurement and changes in the sample. This technique uses the differences in the mobility of the analytes, in our case the neptunium ions, in a capillary when applying an external electric field. The main factor which affects the mobility (μ) of the analytes in the capillary is the charge to radius ratio [Buda 2006].

$$\mu_i = \frac{\vec{\upsilon}_i}{\vec{E}} = \frac{z_{ion}}{r_i} \cdot \frac{e}{6\pi\eta} = \frac{L}{t} \cdot \frac{L_t}{V} \qquad 3.2$$

μ_i electrophoretic mobility

υ_i electrophoretic velocity

η dynamic viscosity of the solution

E electrical field

z_{ion} ionic charge

r_i ionic radius

e elemental charge

L distance from the inlet to the detection point

L_t total length of the capillary

t time needed for the species to reach the detection point

V applied voltage on the electrodes

The overall velocity is also dependent on the electroosmotic flow (EOF), which was first described by Helmholtz in the late 1800s [Helmholtz 1879]. It is dependent on the electrical field applied. Therefore we can conclude that the electrical field, proportional to the applied potential, is the decisive parameter. A more comprehensive description of the fundamentals of the electrophoretic process was done by Jorgenson and Lukacs [Jorgenson 1981]. The system we used allowed us changes in the voltage applied and in the polarity at the capillary ends.

For the speciation of neptunium after separation with capillary electrophoresis, one suitable method is the coupling with ICP-MS. This method will be briefly described in the next section. For the interface based on the patent of Schaumlöffel and Prange [Schaumlöffel 1998] the commercially available nebuliser Mira Mist (Burgener Research Inc.) was used.

Inductively Coupled Plasma Mass Spectrometry

The use of inductively coupled plasma (ICP) for the analytical chemistry is very popular due to its robustness and simplicity. The use of a plasma ion source for the mass spectrometry was introduced by Gray only in 1975 [Gray 1975]. The argon ICP is generated by applying RF power (usually 27.12 MHz in frequency and 0.5 – 2.5 kW in RF power) to argon gas. The high temperatures reached in the plasma atomize the sample, which can be then ionized. An overview of the interference effects was published by Ross et al. [Ross 1991].

The most commonly use mass separator is a quadrupole magnet (see Fig. 3.6.). Here a combination of DC and AC electric potentials applied to four parallel metal rods discriminates the different ions based on their mass to charge ratio. The use of the quadrupole provides quick analysis (milliseconds) indeed but it can only determine one mass ion per charge at a time; this can lead to quantification problems when measuring large mass domains.

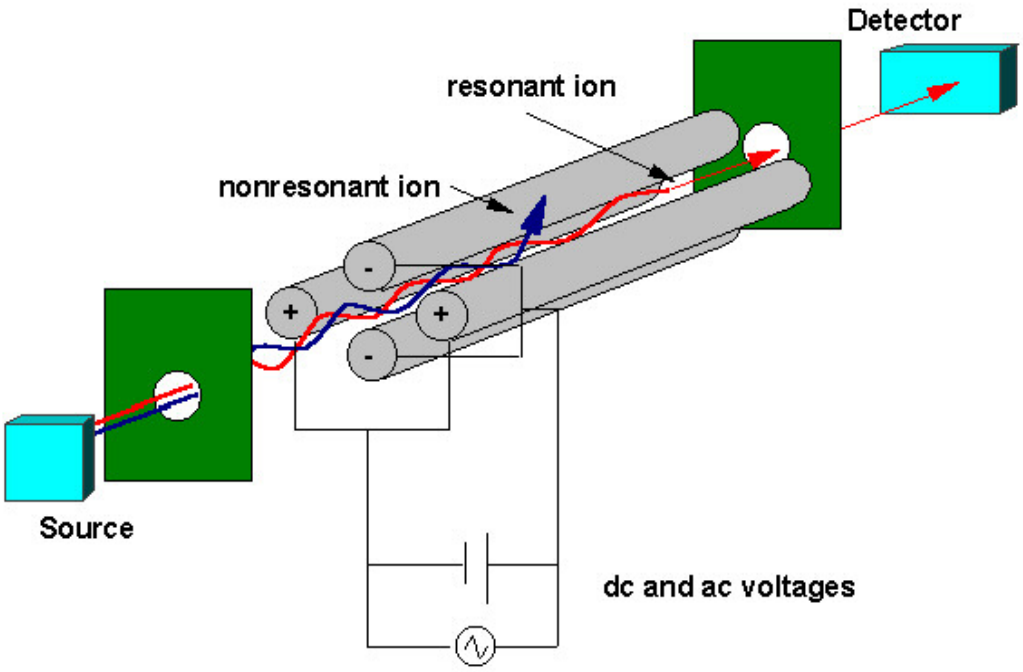

Fig. 3.6. Schematic view of a quadrupole (chem.vt.edu/chem-ed/ms/quadrupo.html**)**

The ICP-MS system used was a HP 7500 (Agilent, Waldbronn, Germany) at the Institute of Nuclear Chemistry Mainz.

The coupling CE-DAD-ICP-MS

For the determination of the humic substances and the radionuclide species (in our case neptunium), Buda [Buda 2006] proposed the coupling of the CE separation to a diode array detection (DAD) system for the detection of the fractions containing humic substances and

the final detection of the radionuclide by ICP-MS in each fraction. A schematic chromatogram is shown in Fig. 3.7.

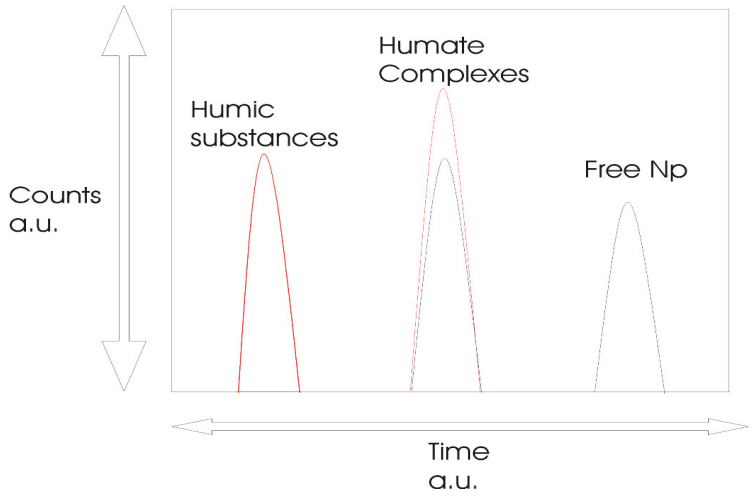

Fig. 3.7. Schematic, idealised chromatogram performed with CE-DAD-ICP-MS for determining the ratio humic substances/humat-neptunium complexes/free neptunium ions.

The system was tested with Aldrich humic substances and iodine species, and improved for the detection of the humic substances and melanoidins, by using a background light blocking adaptor [Buda 2006]. The DAD is based on the same principles as the UV/Vis spectroscopy. Light goes through the solution and the changes in the light absorption are function of the changes in the composition of the solution. The DAD system used in the following experiments was a Knauer DAD K-2800 (Knauer ASI, Germany).

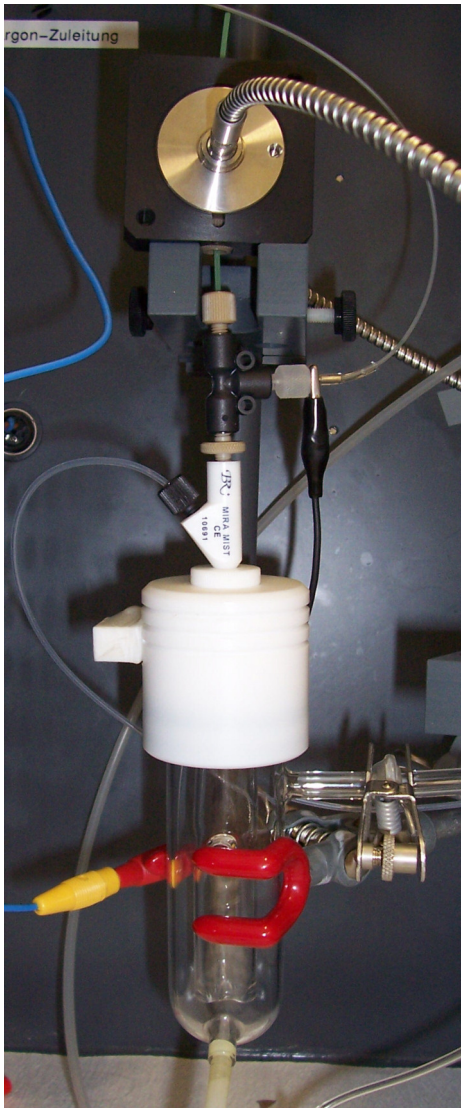

Fig. 3.8. Picture of the CE-DAD-ICP-MS with the Scott-type spray chamber set up.

3.2.4. EXAFS

X-ray absorption fine structure (XAFS) gives information about the chemical state of the selected atom using the absorption of x-rays at energies near and above the core-level binding energies. XAFS is element specific and able to determine an interferogram of the atomic surrounding of the absorber [Mangold 2007]. Furthermore, it is possible to determine the valence of the studied atoms by analyzing the X-ray Absorption Near Edge Structure (XANES) spectrum. Studies for the case of neptunium have been performed at the ANKA Synchrotron by Denecke et al. [Denecke 2005]. Since XAFS is an atomic probe it provides information not being influenced by its physical state and the matrix.

X-ray absorption is a transition between an initial state where an incident beam excites a selected atom with core electrons and a final state where the atom has emitted a photo

electron leaving a core hole. The atom can refill the core hole by dropping an electron from a higher energy shell emitting well defined and element specific fluorescence, or by the Auger effect where a higher electron fills the deeper core hole and a second electron is emitted to the continuum [Newville 2004]. A schematic representation of both processes is shown in Fig. 3.9. For energies of the incident ray above 2 keV, fluorescence is more likely to occur than the Auger effect, therefore as the L_{III} fluorescence line (L shell electron falling into the K level) of Np is about 17610 eV, only fluorescence will be considered.

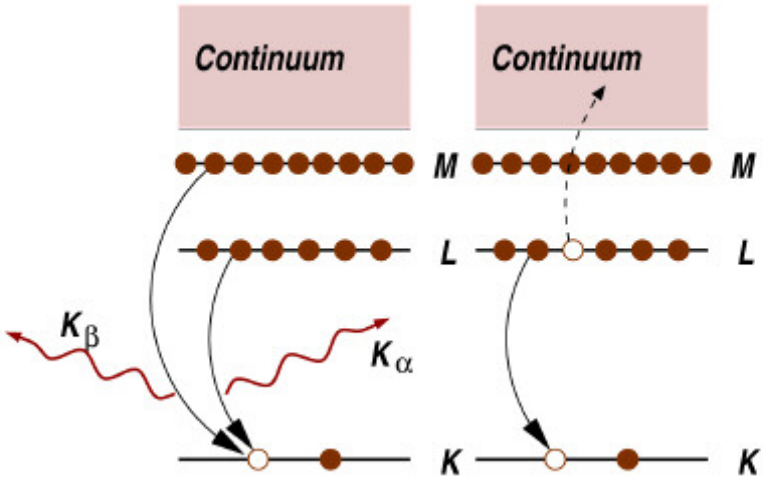

Fig. 3.9. Possibilities for the decay of the exited state, fluorescence (left) and Auger effect (right). [Newville 2004].

For EXAFS we are interested in the oscillations which happen above the absorption edge which are defined with the function:

$$\chi(E) = \frac{\mu(E) - \mu_0(E)}{\Delta\mu_0(E)} \qquad 3.3$$

Here is μ(E) the measured absorption, μ_0(E) is a background function which represents the absorption of an isolated atom, and $\Delta\mu_0$(E) is the jump at the absorption energy E_0. Fig. 3.10. shows an example μ(E) as a function of the x-ray energy.

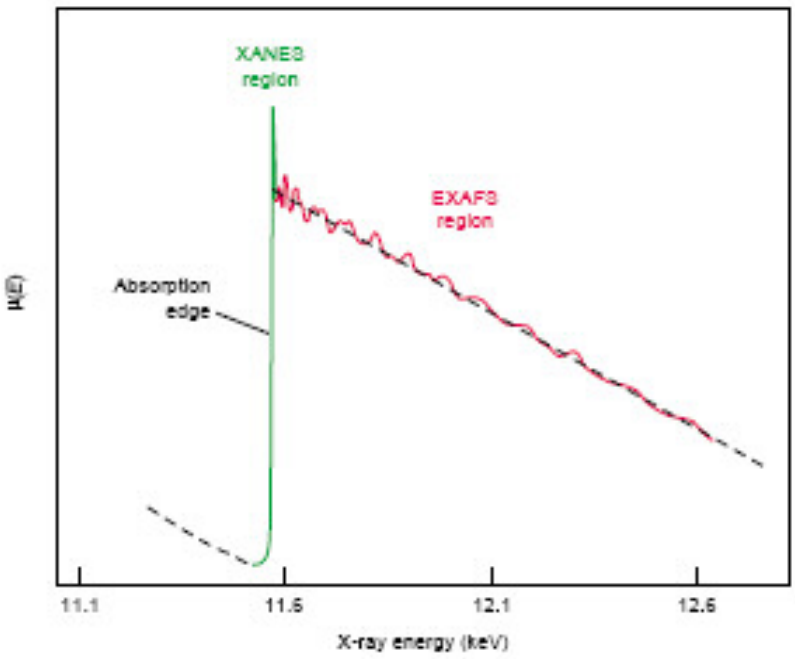

Fig. 3.10. Typical XAFS spectrum [Conradson 2000].

It is also common to see the EXAFS spectra as a function of the wave number of the photo-electron (k), defined as:

$$k = \sqrt{\frac{2m(E - E_0)}{\hbar^2}} \qquad 3.4$$

where E_0 is the absorption edge and m the electron mass. The oscillations as a function of the energy, $\chi(E)$, are then converted into a "new" EXAFS equation as a function of k, $\chi(k)$.

$$\chi(k) = \sum_j \frac{N_j f_j(k) \exp(-2k^2\sigma_j^2)}{kR_j^2} \sin[2kR_j + \delta_j(k)] \qquad 3.5$$

Here are f(k) and δ(k) scattering properties of the neighboring atoms, N is the number of the neighboring atoms, R the distance to the neighbors and σ² the disorder in the neighbor distance.

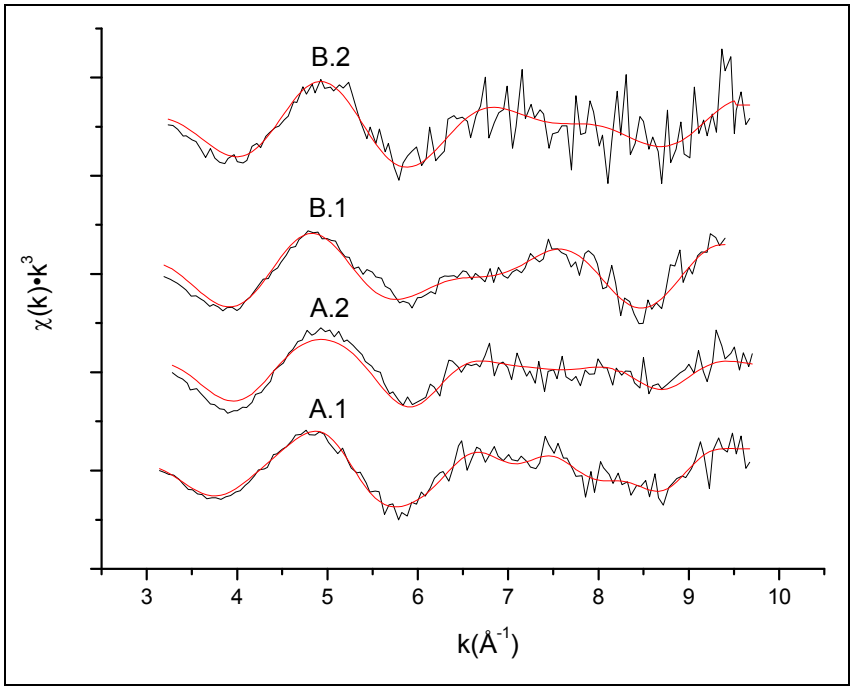

Fig. 3.11. Np L_{III}-edge k^3-weighted EXAFS data for different Np-gibbsite samples [Vicente Vilas 2007].

A comprehensive description of the formalism used to obtain the EXAFS equation can be found in Newville 2004, Tommaseo 2002, and Conradson 2000. At the end, the mathematical description of EXAFS can be achieved by the equation 3.6. [Tommaseo 2002]:

$$\chi(k) = (-1)^l \sum_j S_0^2(k) \frac{N_j}{kR_j^2} \left|F_j(k,\pi)\right| \exp(-2k^2\sigma_j^2) \exp(-2R_j/\lambda(k)) \sin[2kR_j + \phi_{ij}(k)] \quad 3.6$$

l: orbital angular momentum of the photoelectron ground state.

$S_0^2(k)$: amplitude reduction factor as a function of k.

N_j: number of scattering atoms in the shell j.

R_j: distance to the neighbors in the shell j.

$F_j(k,\pi)$: amplitude function, which describes the scatter capacity of the scattering neighbors in the shell j as a function of the scatter angle and k.

σ_j^2: disorder in the neighbor distance.

$\lambda_j(k)$: mean free path of the photo electron.

ϕ_{ij}: sum of the phase displacements.

A Np L_{III}-edge k^3-weighted EXAFS spectrum is shown in Fig. 3.11. To emphasize the oscillations, the $\chi(k)$ are usually multiplied by a power of k. For the measurement, the transmission modus and the fluorescence modus can be chosen. For concentrated,

homogeneous and samples free of pin-holes, transmission is often chosen, but for our diluted and heterogeneous samples, the fluorescence modus was more adequate [Newville 2004].

The fully comprehension of the data treatment may be challenging, but it can be divided in two principal steps:

- Reduction and extraction of the data
- Data modeling

In the data reduction, six steps are normally done [Mangold 2007]:

1. Pre-Edge Subtraction: subtraction of the background.
2. Normalization: estimation of $\Delta\mu_0(E_0)$, and normalization to this value.
3. Post-Edge Background: approximation of $\mu_0(E_0)$ by a spline function.
4. Isolation of the EXAFS $\chi(k)$ and k-weighting.
5. Fourier transformation $\chi(R)$.

The data treatment and modeling was done using Athena /Artemis [Ravel 2005] and EXAFSPACK [George 2000].

The INE Beamline for actinides at ANKA

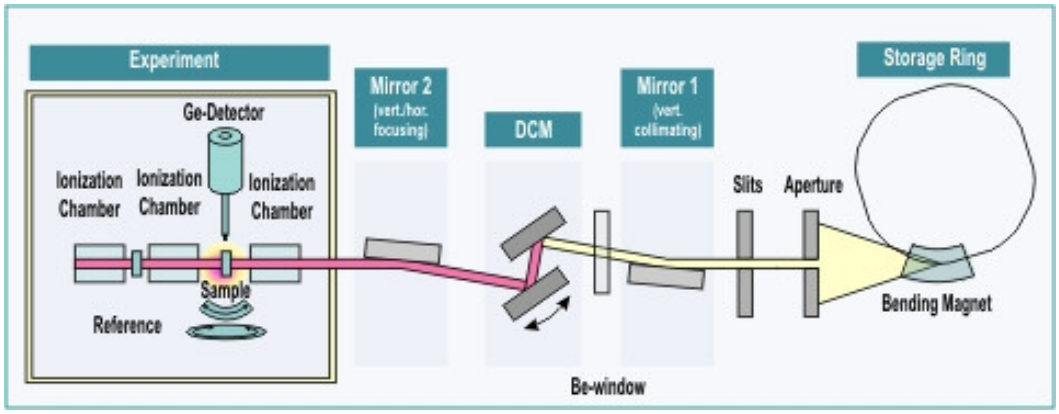

Fig.3.12. Schematic view of the INE Beamline for actinides at ANKA [ANKA 2007].

The INE (Institute for Nuclear Waste Disposal) Beamline (Fig. 3.12.) is dedicated to the actinide research, and provides the necessary infrastructure and equipment for radioactive experiments up to 10^6 times the limit of exemption, in our case more than 25 mg of ^{237}Np.

Energy range	2.1 keV – 25 keV
Flux	~$3.5 \cdot 10^{11}$ photons/sec at Zr K edge
Source	1.5 T Bending magnet
Optics	Double crystal monochromator, water-cooled first crystal, mechanically coupled movement of the second crystal to ensure fixed

	exit, MOSTAB, exchangeable crystal pairs InSb (111), Si (111), Si (311), Ge (220), Ge (422). Rh coated silicon mirrors for a ~500 µm x 500µm beam at the sample SESO x-ray beam position monitor
Experimental set-up / sample positioning	♦ sample holders for radioactive samples ♦ HUBER sample positioning system, goniometer and auxiliary slits for XAFS and surface sensitive grazing incidence techniques ♦ LN_2 cryostat for low temperature measurements ♦ 1.2 x 3 m² breadboard optical table ♦ sealed media feed-through chicanes and separate ventilation/filter system for experimental hutch ♦ access through lock-room with hand/foot-contamination monitor
Experimental set-up / detectors	♦ Ionization chambers ♦ Setup for total electron yield measurements ♦ 5 pixel high purity Ge solid state fluorescence detector (Canberra Ultra-LEGe)

Table 3.1. INE Beamline characteristic parameters [ANKA 2007].

A view of the experimental set-up at the INE-Beamline of ANKA at FZ Karlsruhe is shown in Fig. 3.13.

Sample preparation for the INE Beamline at ANKA

Samples were prepared from $^{237}Np(V)$ stock solution that was purified from traces of ^{239}Pu and ^{233}Pa (see section 3.1.3). The mineral was suspended in MilliQ water (at the chosen ionic strength) and equilibrated with CO_2 over two days; pH was adjusted to the desired value with $HClO_4$ or NaOH. Np(V) was then added and the pH adjusted if necessary. The total Np concentration was in the micro molar range. This is below the solubility limit of any solid phase, e.g., $NaNpO_2CO_3(s)$ [Neck 1994]. After a contact time of two days, the solid and liquid phases were separated by centrifugation. The wet pastes were then loaded into the sample holders. The Np uptake by the mineral phase was determined by LSC and γ–spectroscopy of the supernatant.

Fig. 3.13. Fluorescence set-up in use in the experimental hutch at the INE-Beamline.

3.2.5. Characterization of the HCM

For the characterization of the HCM, different analytical methods were used in collaboration with other institutes at the Johannes Gutenberg-Universität Mainz, the Max Planck Institute for Chemistry, and the Institute for Nuclear Waste Disposal in Karlsruhe. A brief description of the methods used is enclosed in the following section.

Scanning electron microscopy

Scanning electron microscopy (SEM) is a non destructive technique, which allows the study of bigger specimens in comparison to transmission electron microscopy (TEM) and with shorter sample preparation times [Vernon-Parry 2000]. In our case, we used a field emission microscope which provides the brightest beam with very small deviations in electron energy.

In this study, untreated and H_2O_2-treated samples (destruction of the organic material), following the method published by Chahi et al., [Chahi 1996], were analyzed by scanning electron microscopy (SEM) using the high resolution field microscope LEO 1530, shown in Fig. 3.13., (Zeiss, Oberkochen, Germany) located at the Max Planck Institute for Chemistry in Mainz. No ultrasonic treatment was done on the samples in order to maintain the structure of the hybrid materials [Ziechmann 1993]. To maintain the surface structure, no coating was done on the samples. The samples were dried at 50°C and placed on the Al-SEM studs.

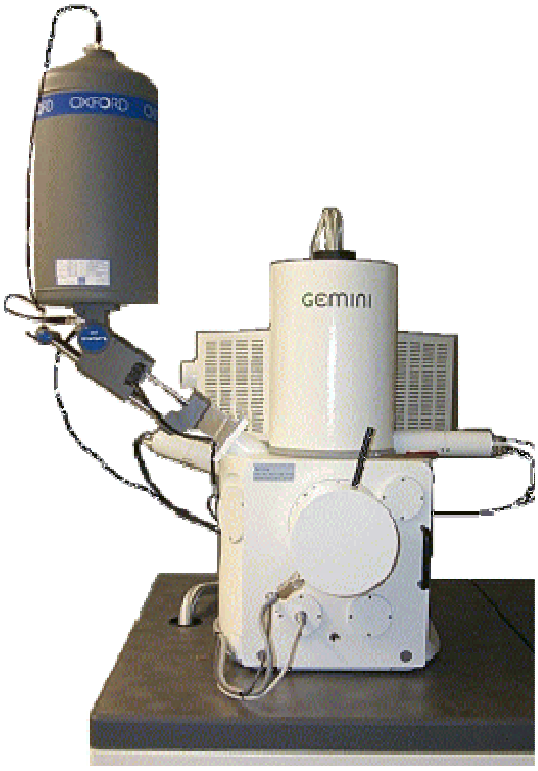

Fig. 3.14. The LEO 1530 high resolution field emission scanning electron microscope, located at the Max Planck Institute for Chemistry in Mainz (Germany) (mpch-mainz.mpg.de/~kosmo/huth/leo.htm**).**

Solid state NMR

Nuclear magnetic resonance is based on the exposition of the sample, immersed in a static magnetic field, to a second oscillating magnetic field. The principles of NMR are widely described in the literature; a pretty modern work using NMR spectroscopy for the study of humic substances functionalities, contains a complete theoretical description of the NMR formalism [Günzl 2000].

For the solid state NMR studies, a DSX400 Spectrometer (Bruker, Rheinstetten, Germany) of the Institute of Inorganic Chemistry and Analytical Chemistry, operating at 100.5 MHz for ^{13}C and 79.4 MHz for ^{29}Si was used. The ^{13}C spectra of GHS and THS needed 40k, 32k, and 20k scans respectively for a satisfying signal to noise ratio. The ^{29}Si spectra needed only 10k to 20k scans however. All samples were measured using CP-MAS with 5kHz spinning rate.

X-ray photoelectron spectroscopy

The X-ray photoelectron spectrometer (SPECS, Berlin, Germany) at the Institute of Nuclear Chemistry, University of Mainz, was used for this study. The principles of this method are described elsewhere [Feuerbacher 1978]. Measurements were done under a

vacuum of 10^{-9} – 10^{-10} mbar. The operation modus of the PHOIBOS 10D energy analyzer lens was small area (SA), and the X-ray source was operated at 100 W. Powder samples were pressed in indium foil, which was fixed on a copper disk.

In order to determine the Auger lines, survey spectra were taken at an analyzer pass energy of Ep = 50 eV with Mg Kα irradiation (hυ = 1253.6 eV, range 0 – 1200 eV) and Al Kα irradiation (hυ = 1486.6 eV, range 0 – 1300 eV). From the Mg Kα survey spectrum, the different energy ranges were determined for the single spectra. Single spectra (ten scans each) were measured using two different analyzer pass energies, Ep = 50 eV, and Ep = 13 eV. The data treatment was done using the computer software CasaXPS [Fairley 2005]. We used a linear background. The XPS line shape was approximated using a product function of a Gaussian and a Lorentzian.

For the determination of atomic ratios n_1/n_2 from relative peak intensities I_1/I_2, the equation described by Wagner et al. [Wagner 1979] and reduced by Briggs and Seah [Briggs 1983] was used, $N_A/N_B = \sigma_B \cdot I_A/\sigma_A \cdot I_B$; the photoionization cross sections (σ) were obtained from Band et al. [Band 1979]. The binding energies were corrected for the C 1s value (289.85 eV) and we used the Al 2p and Si 2p energies (74 and 102.3 eV respectively) to obtain the atomic ratios.

X-ray absorption studies

The Scanning Transmission X-Ray Microscopy (STXM) studies were done at the National Synchrotron Light Source (NSLS) at Brookhaven National Laboratory undulator beamline X1A1, operated by the State University of New York at Stony Brook. Basically, in this method, coherent radiation from the X1 undulator is monochromatized and focused to a spot using a Fresnel zone plate, which are x-ray diffractive lenses, and are circular diffraction gratings with radially decreasing line width. The sample is scanned through the focus pixel by pixel. For each pixel, the transmitted intensity is recorded by a large area detector, resulting in an absorption contrast image of the specimen. The principles of this method are detailed in Jacobsen et al. [Jacobsen 1991]. The experimental set up at the beamline is described in Schäfer et al. [Schäfer 2005], and shown in Fig. 3.14.

Spectra were recorded at the carbon K-edge in the range from 280 eV to 295 eV. The spectra were then baseline corrected and normalized for comparison.

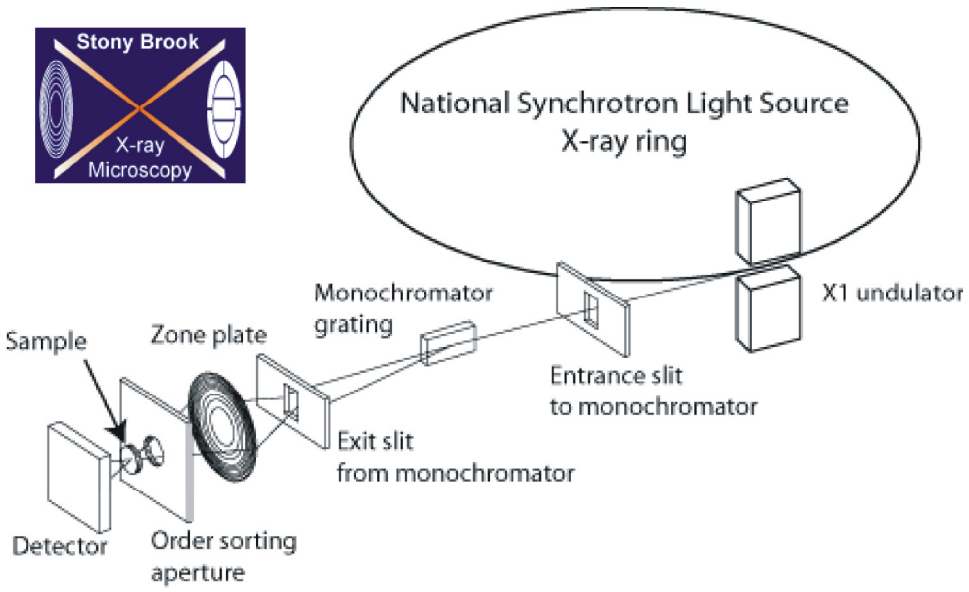

Fig. 3.15. Schematic set up of the STXM Beamline at the NSLS (xray1.physics.sunysb.edu).

Thermal analysis

Differential thermal analysis (DTA) shows the effects of energy changes in the samples in comparison to a standard, and is plotted usually against time or temperature. For clay, endothermic reactions are associated with desorption of surface H_2O and dehydration at low temperatures (below 100°C), dehydration and dehydroxilation at higher temperatures. Exothermic reactions are normally associated with recrystallization at high temperatures. The Thermal Gravimetry (TG) curves show only weight changes during the heating process. The variations in results for clay minerals may be explained by the ambient humidity in the different laboratories and the fugacity of water [Gugenheim 2001]. Kodama and Schnitzer used DTA for the study of the complexation of mineral with fulvic acid [Kodama 1969], further thermal studies on clays have been performed to elucidate organo-clay structures [Yariv 1990]. A further description of their results is found in chapter 4. Anyhow, for the interpretation of the DTA analysis is important to notice whether the studied material releases the energy (exothermic) or absorbs the energy (endothermic).

A NETZSCH STA 429 (Selb, Germany) situated at the Institute of Inorganic and Analytical Chemistry, University of Mainz, was used for the analysis. An Ar flow rate of 100-120 cc/min was used for the DTA and TG. Al_2O_3 crucibles were used for the measurements. A heating rate of 10°/min was maintained for all the experiments. 78.8 mg of STx-1 montmorillonite was used as well as 38.1 mg of THS and 20.8 mg of GHS.

3.2.6. Ultra filtration

Ultra filtration is a quick and physical method for the separation of the humate species and the free ions, in our case neptunium (mainly as neptunyl cation or neptunyl carbonate). The free ions pass through the membrane filter, if no sorption occurs, and the humate complexes remain on the filter. A cut-off of 1kDa has been proposed in the literature for this kind of experiments [Kim 1989].

1kDa Microsep 1kOmega membrane filters (Pall Life Sciences, USA) in combination with centrifugation (Fritz Bayet OHG, Frankfurt M., Germany) at about 2500 rpm for 20 minutes was used for this purpose. The retention of neptunium between pH 6 and 8 and in the concentration range from pico Molar to $1 \cdot 10^{-4}$ M by the membranes was studied by U.A. Seibert [Seibert 1999], and she founded that about 90 to 100% of the initial Np was recovered after filtration. The retention of the humic substances was investigated by S. Bürger [Bürger 2005] finding that about 85 to 95% of the humic substances were retained by the membranes.

After passing the membrane, the free neptunium concentration can be determined by γ-spectroscopy or LSC, and the amount of humic substances by UV/Vis spectroscopy (see below).

3.2.7. UV/Vis

The use of UV/Vis spectroscopy for the quantification and speciation of neptunium samples is possible but the high neptunium concentrations needed [Katz 1986] make this method not suitable for environmentally relevant samples. UV/Vis spectroscopy, however, is a very quick and reliable technique for determining the main species in the ^{237}Np stock solutions.

Nevertheless the use of the UV/Vis spectroscopy is suitable for the determination and quantification of melanoidins and humic substances. For our studies, we used a high resolution spectrometer Cary 50 from Varian (USA). Samples were measured at wavelengths λ=310nm [Buda 2006], using 10mm plastic cuvettes (Brand GmbH, Wertheim, Germany). A set of such spectra is shown in Fig. 3.15.

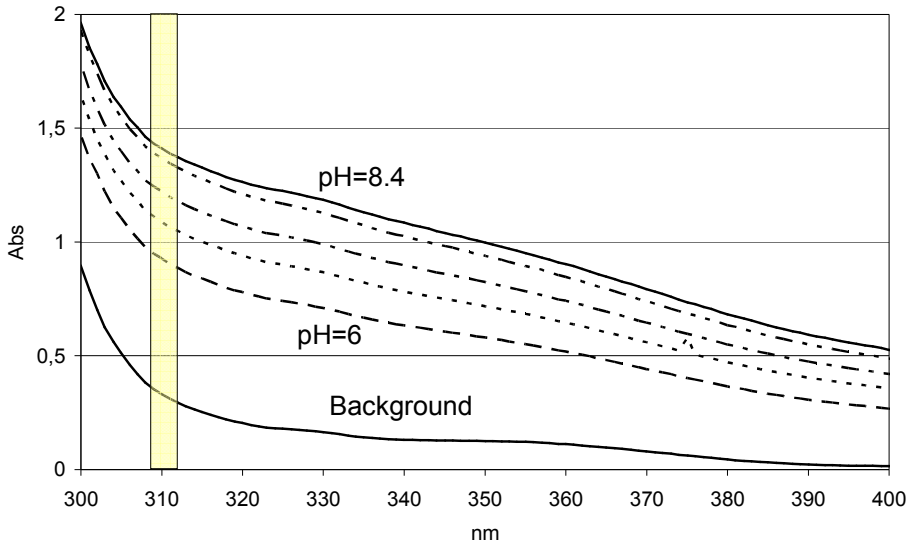

Fig. 3.15. UV/Vis spectra of GHS supernatant samples at different pH's.

4.1. Synthesis and characterization of the hybrid clay-based material montmorillonite-melanoidin

The study of the interactions between metals, minerals, and humic substances is important in order to understand the migration of inorganic pollutants in the geosphere. Furthermore, a considerable amount of organic matter in the environment is associated with clay minerals [Greenland 1956]; in order to understand the role of organic matter in the environment and their association with clay minerals, hybrid clay-based material (HCM) montmorillonite (STx-1)-melanoidin has been prepared starting from L-Tyrosine (THS) and L-Glutamic Acid (GHS). Those HCM were characterized by different analytical methods, e.g., elemental analysis, NMR, XPS, scanning transmission X-ray microscopy (STXM), and thermal analysis. The presence of organic materials on the surface was confirmed by using XPS and STXM. The new STXM results presented in this section show the presence of organic spots on the surface of the STx-1, and we were able to characterize the functional groups present in those spots. The thermal analysis confirmed the existence of organics in the interlayers of montmorillonite pointing to the formation of a composite where the melanoidin is located partially between the layers of montmorillonite and partially on the surface, like a champagne bottle cork confirming former results by W. Ziechmann [Ziechmann 1993].

4.1.1. Yields obtained and elemental composition

Silicon is able to react with electro negative reactants due to its free d states. Therefore, the reaction with L-tyrosine was supposed to be favored, since the reaction of Ca-bentonite with hydroquinone studied by [Ziechmann 1993] takes place in the first phase as a donation of electrons from the hydroquinone to the silicon.

The yields for the reaction (Table 4.1.), concerning only the HCM, are very similar for the synthesis with L-tyrosine and with L-glutamic acid, indicating no preference in the reaction for any reactant, e.g., L-tyrosine or L-glutamic acid: The aromatic ring of the L-tyrosine has no influence or effect on the reaction. The observation by Ziechmann couldn't be confirmed. Similar yields were also obtained while forming a caramel-clay nanocomposite under MW irradiation [Darder 2005].

Sample	Yield (g)	C %	H %	N %
GHS	1.7 ± 0.2	1.7 ± 0.3	1.6 ± 0.3	0.11 ± 0.02
THS	1.8 ± 1.2	1.3 ± 0.2	1.7 ± 0.1	0.06 ± 0.03
STx-1	-	0.03 ± 0.01	1.39 ± 0.02	<0.02

Table 4.1. Yields and C, N, H content for the two composites isolated, and comparison with the contents in STx-1.

The carbon content (Table 4.1.) for the two HCM (GHS and THS) is in the same range and about 40 to 60 times higher than that of the STx-1. The reaction seems to be not complete when using L-tyrosine ($C_9H_{11}NO_3$) which has higher carbon content than L-glutamic acid ($C_5H_9NO_4$).

4.1.2. Sample morphology

The presence of organics in the samples obviously inhibits the conglomeration of the clay particles. The SEM pictures (Figure 4.1.) of the GHS show big spaces between the clay particles, whereas in the H_2O_2-treated hybrid material, the clay particles lay flat together. It may be possible that the treatment of the samples affects their aggregation. However, we think that the method used doesn't affect the morphology of the sample due to the mild conditions used. Ziechmann [Ziechmann 1993] postulated that without ultrasonic treatment, some organic material would remain in the interlaminar spaces of the mineral. The organics on the surface seems to have been removed by the H_2O_2 treatment, thus making possible the conglomeration of the clay particles.

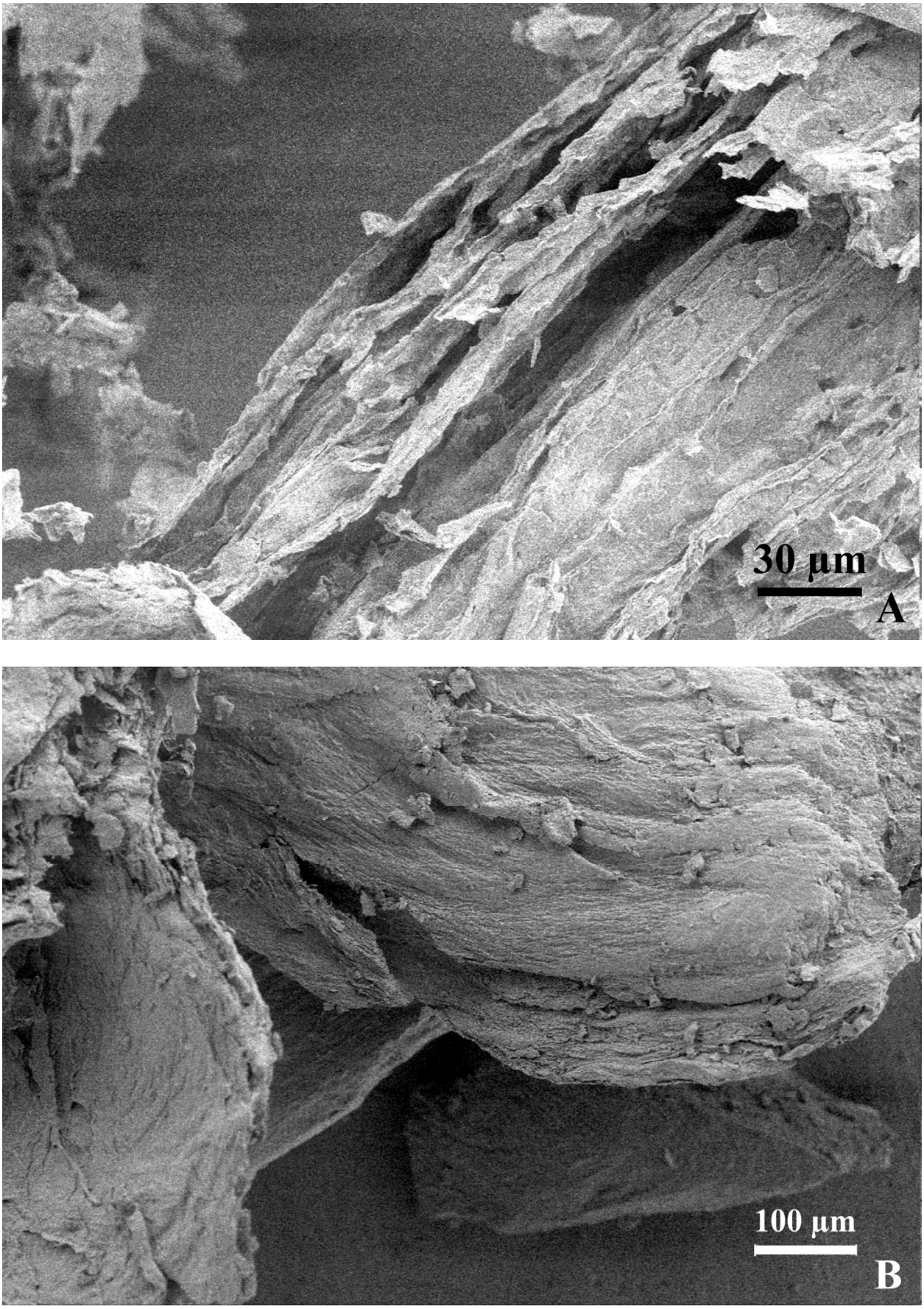

Fig. 4.1. SEM images of the (*A*) GHS melanoidin–STx-1 hybrid material (*B*) the same sample after treatment with H_2O_2.

4.1.3. Functional groups and structural changes

The ^{13}C spectra (Figure 4.2.) show the presence of organics in the two HCM. Those signals were particularly high in the range of chemical shifts typical for aliphatic bonds. The HCM synthesized from L-glutamic acid shows a higher signal than the THS, and a broad peak at about 85 ppm, thus pointing to the presence of aliphatic carbons in the samples.

The signal at higher ppm's, where the aromatic and heteroaromatic compounds shift occurs, are less pronounced.

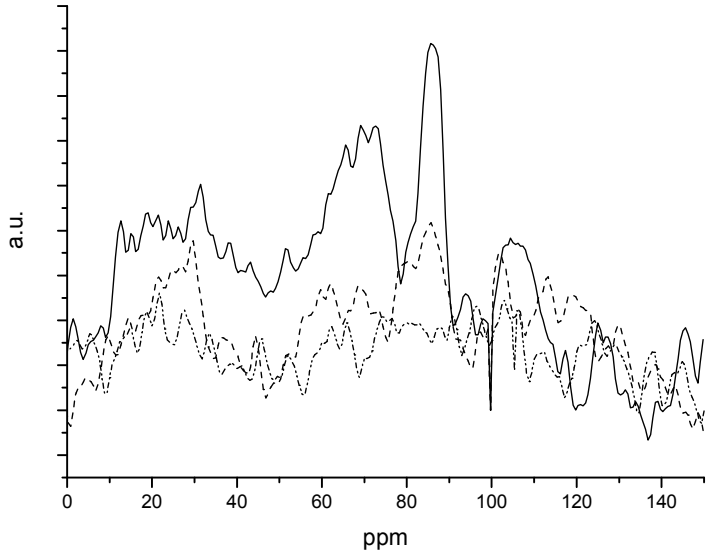

Fig. 4.2. Solid state ^{13}C-NMR spectra of the GHS (solid), THS (dashed), and STx-1 (dotted).

The ^{29}Si spectrum (Figure 4.3.) of the parent montmorillonite contains two resonances. The -93.5 ppm resonance is attributed to T(3Si,1Al) in the clay octahedral layer. The second resonance near -112.3 ppm is attributed to silica impurities present in the parent clay [Occelli 2000]. The two HCM show a big peak about -94.5 ppm. There is also a little shift between the parent clay and the synthesis products.

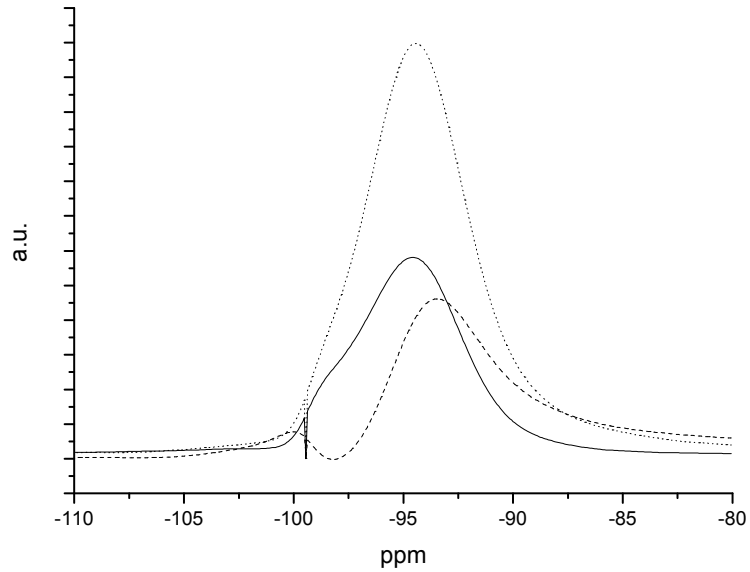

Fig. 4.3. Solid state ^{29}Si-NMR spectra of the GHS (solid), THS (dotted), and STx-1 (dashed).

After the treatment with H_2O_2, no difference in the peak position was observed (Figure 4.4.). The NMR results point to the existence of some organic material in the interlayers of the montmorillonite, i.e. the treatment with H_2O_2 is not able to remove the whole amount of organics from the sample, and some amount remains in the interlayers [Ziechmann 1993].

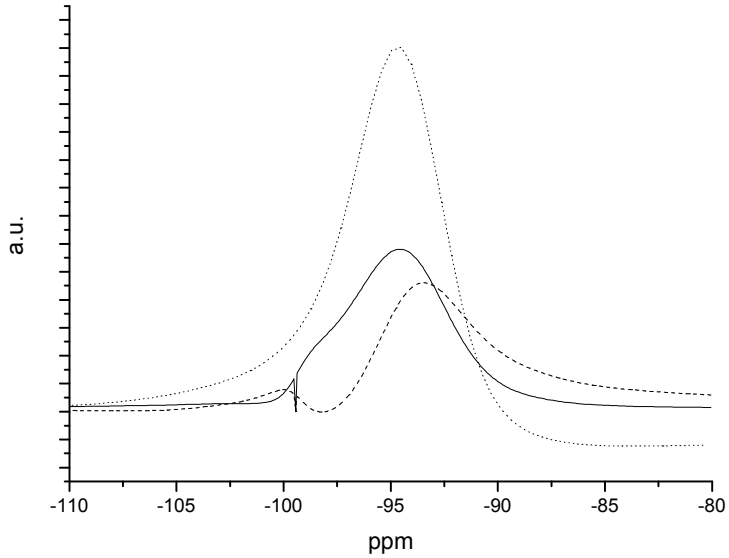

Fig. 4.4. Solid state ^{29}Si-NMR spectra of GHS (solid), the same sample after treatment with H_2O_2 (dotted) and the parent montmorillonite (dashed).

4.1.4. Surface chemical investigation

The XPS experiments (Table 4.2.) show the presence of organics on the surface of both HCM's. Accumulation of the organic substances on the surface of the mineral was demonstrated in both HCM. It seems that GHS has a higher melanoidin accumulation on the surface of the montmorillonite than THS. This is in good agreement with the elemental composition data, where the carbon content for the GHS was higher than the content for THS. The atomic ratio Al/Si measured for STx-1 is in good agreement with the published elemental composition data [Mermut 2001]. The differences in the HCM may be due to the hydroxide treatment which may be able to etch partially the mineral surface or interferences due to the melanoidins. Moreover XRD analysis of the bulk showed no differences in the structure between the HCM's and STx-1 [Rubert de la Rosa 2007].

	n(C)/n(Al)	n(C)/n(Si)	n(Al)/n(Si)
STx-1	0.1	0.03	0.3
GHS	0.59	0.25	0.42
THS	0.42	0.17	0.4

Table 4.2. Atomic ratios obtained from XPS measurements.

4.1.5. Organic functional groups surface distribution

The STXM spectra (Figure 4.6.) show the relationship between the melanoidins and their correspondent HCM. The main difference for THS/THD can be observed in the region around 286 – 288eV, where a higher absorption compared to the reference spectra [Boese 1997] is observed. These results indicate that either additional OH-groups are associated to the aromatic ring through the polymerization process and/or aliphatic structures are generated. The comparison between THS and THD furthermore shows that the reaction products of surface associated organics and the organics in the supernatant are not significantly different from the C(1s) spectra point of view. In contrast, the GHS and GHD carbon edge spectra indicate a build up of C=C bonds and therefore aromatic groups compared to the reference spectra of glutamic acid [Kaznachcheyev 2002]. The spectral region around 286.6 eV shows a strong absorption band which can be interpreted as aromatic ring associated OH- groups. Taking the correlation of Francis and Hitchcock [Francis 1992], an estimation of >2OH groups per aromatic ring can be given. The average spectra of the GHS fraction is very comparable to the spectral features obtained for the humic acid M42 synthesized with the

same starting materials (Figure 4.5.) in the absence of mineral phases provided by the research center Dresden-Rossendorf [Pompe 1998]. Organic hot spots were also identified on the surface of GHS (Figure 4.7.). The spectra extracted from this particular organic hot spot shows in comparison to the average spectra of GHS that the mineral associated organics are highly enriched in aliphatics (287.4eV) and depleted in phenol-type groups (286.6eV). Interestingly, for the GHS, the GHD, and the hot spot extracted spectra, the absorption in the carboxyl-type group energy region (~288.4 eV) is very similar, which points to an independence of these functional groups from the presence/absence on the mineral phase. Further studies are underway to elucidate this process. Both, the NMR and C(1s) STXM results give hint to a preferential formation of aliphatics as reaction products. Natural fulvic acids (e.g., Gorleben system) show significantly higher absorption in the aromatics region of the carbon edge spectra and lower amount of phenol-type groups independent of their origin [Schäfer 2005] compared to the synthesized humic-type material presented in this study (see Figure 4.5.).

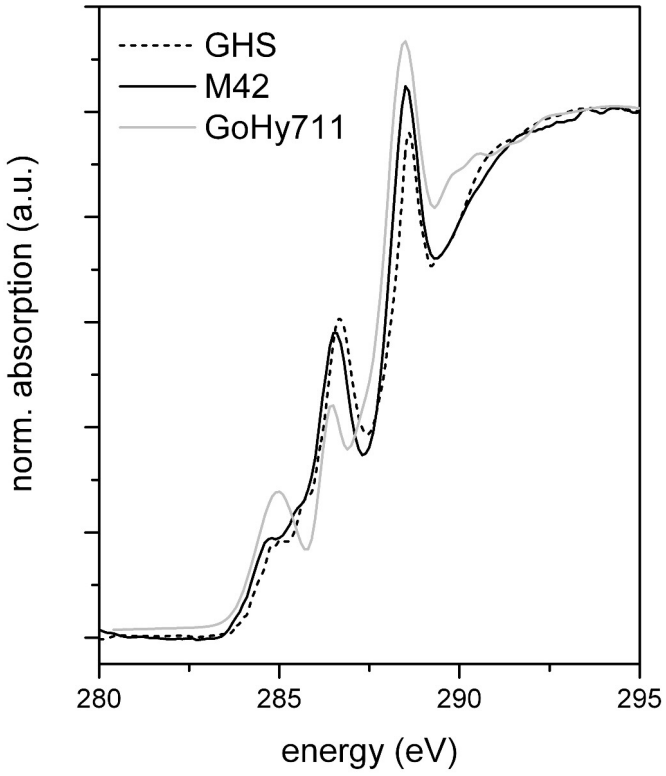

Fig. 4.5. Comparison of STXM spectra taken from the GHS sample, the synthetic humic acid M42 and the natural fulvic acid GoHy-711 originating from recharge dominated groundwater systems of the Gorleben site, having low aromatic content [Schäfer 2005].

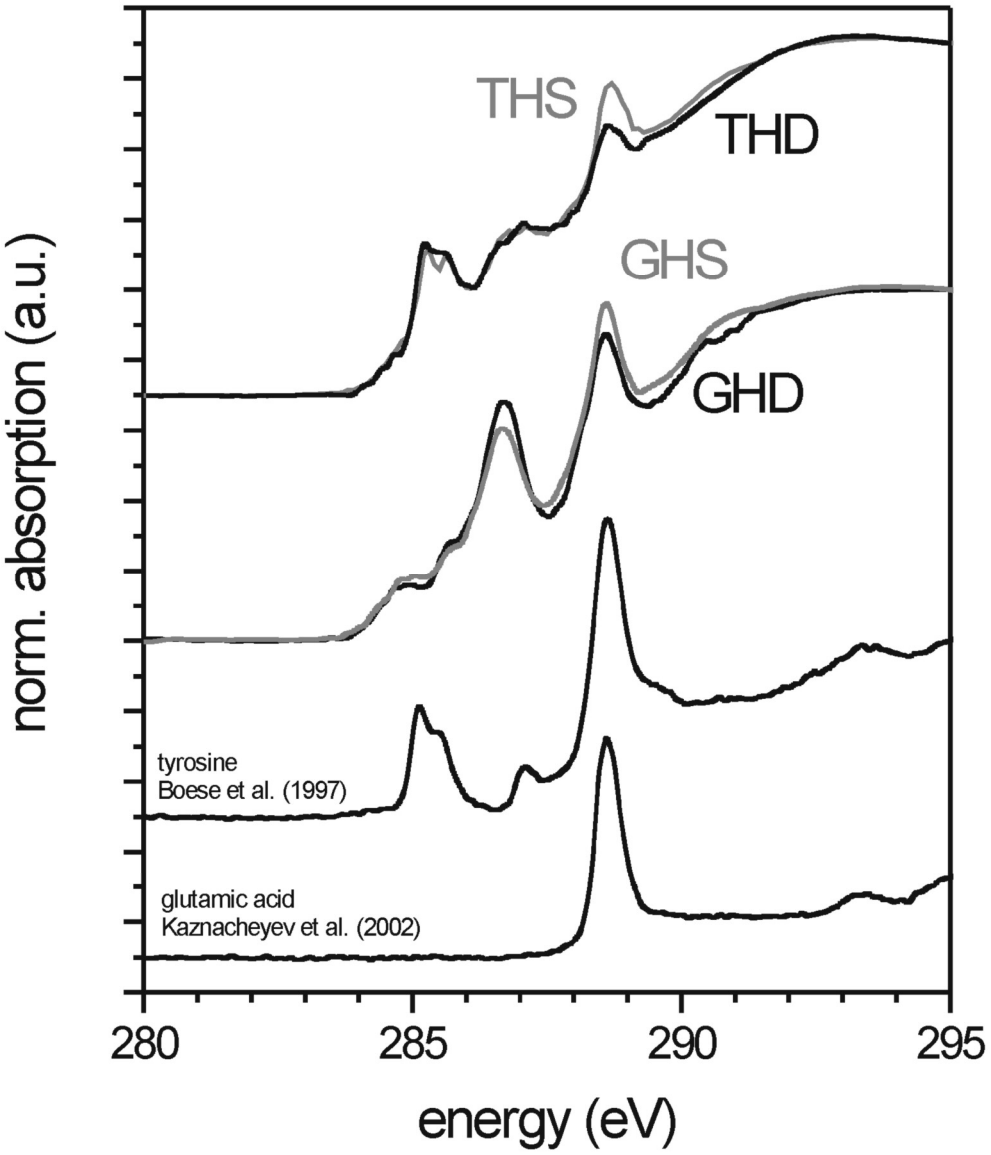

Fig. 4.6. STXM spectra of THS and its associated melanoidin as well as of GHS and its associated melanoidin. Reference spectra of tyrosine and glutamic acid are also shown.

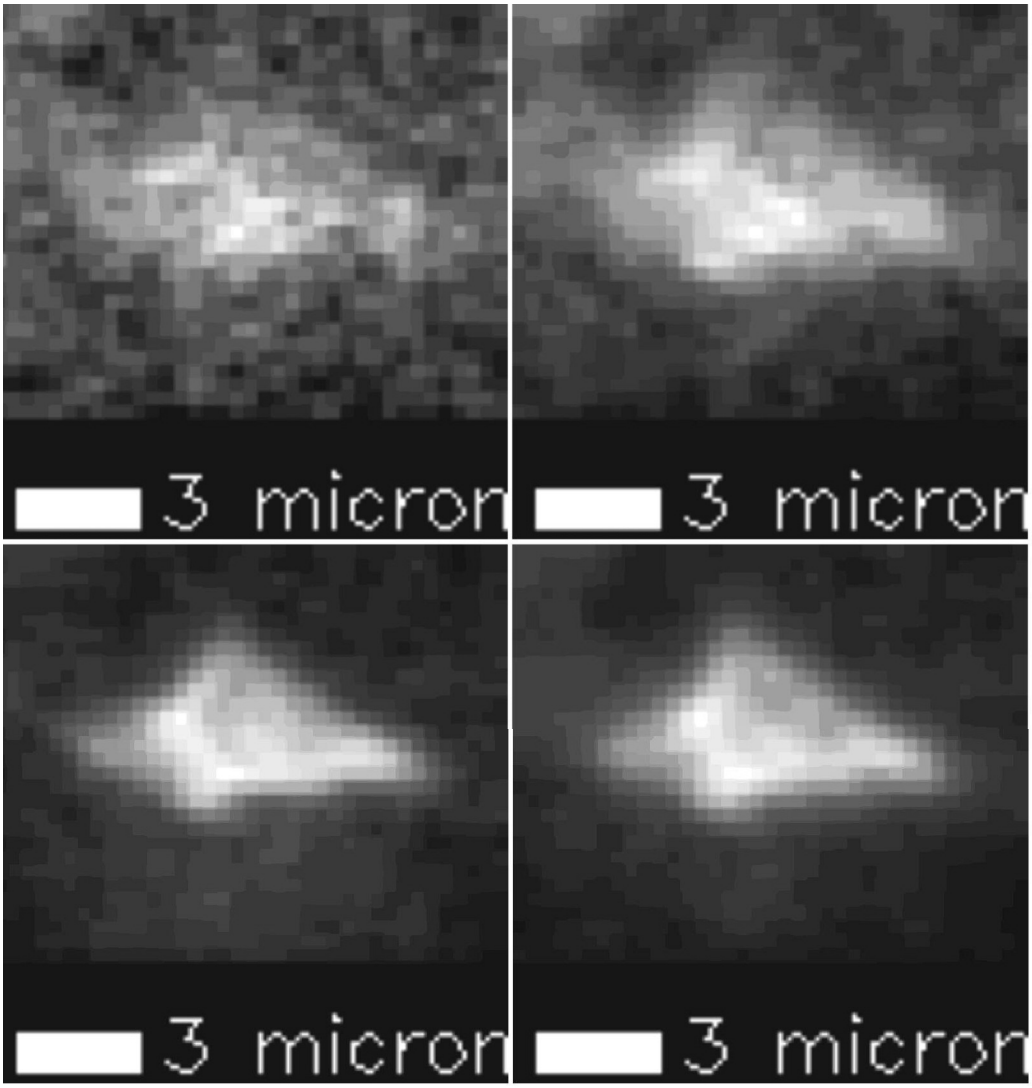

Fig. 4.7. From left to right distribution of aromatics, phenolic-type groups, aliphatics and carboxyl-type groups in sample GHS (light grey values indicate high functional group content).

4.1.6. Structure clarification

Different fulvic acid-montmorillonite complexes were studied by Kodama and Schnitzer [Kodama 1969]. They found that, for the presence of fulvic acid in the interlaminar spaces, the DTA spectra showed the presence of a broad exotherm between 400° and 450°; another broad exotherm appeared centering at 670° instead of the endotherm in the spectrum of montmorillonite. Surface complexes show only an individual peak between 400° and 450° [Kodama 1969].

The two HCM show (Figure 4.8.) also those two broad exotherms at about 450° and 670°; pointing to the existence of organic material in the interlaminar spaces of STx-1 montmorillonite.

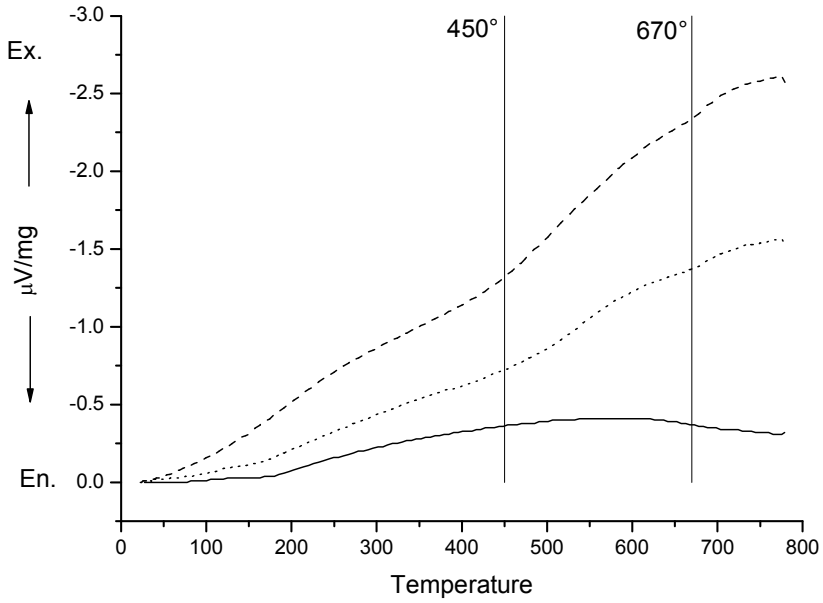

Fig. 4.8. DTA measurements of the STx-1 (straight line) and the two HCM, THS (dotted) and GHS (dashed).

4.1.7. Discussion

The synthesis of hybrid clay-based materials starting from a reducing sugar, an amino acid, and montmorillonite has been achieved. The organic material seems to penetrate partially into the interlayers of montmorillonite but stays also on the surface of the mineral, thus confirming former studies of Ziechmann [Ziechmann 1993]. This result was confirmed by the thermal analysis and comparison with literature data for the incorporation of fulvic acid in the interlaminar spaces of montmorillonite [Kodama 1969]. Ziechmann studied the formation of humic like material using hydroquinone in the presence of bentonite and proposed the formation of composites where the organic material was located partially between the layers of the mineral and partially on the surface, like a champagne bottle cork [Ziechmann 1993]. Presence of organic material on the surface could be confirmed by XPS and STXM. Treatment with H_2O_2 removes only the organic material located on the surface, making possible the agglomeration of the clay particles. The remainder of organics after treatment with H_2O_2 was confirmed by ^{29}Si solid-state NMR. Thus we can conclude that the formation of the melanoidins takes place in a first stage between the layers of the montmorillonite, since the precursors of the melanoidins are able to penetrate into the interlayers. The melanoidins spread out of the interlayers and fill the outer regions being fixed on the surface, with a champagne bottle cork structure [Ziechmann 1993].

4.2. Sorption of Np(V) onto gibbsite (α-$Al(OH)_3$)

Montmorillonite and other clay minerals like kaolinite contain octahedral layers of [AlO_6] as structural units. To better understand the role of these aluminium layers for the sorption of Np(V) onto clays, we investigated the Np(V) sorption on the reference mineral gibbsite (α-$Al(OH)_3$). For montmorillonite and kaolinite, different experimental data for the sorption of Np(V) are available [Jermolayev 2005, Weijuan 2003, Turner 1998, Bertetti 1998], but regarding gibbsite, there are only data for the sorption behaviour of uranium (VI) [Baumann 2005] and nickel [Yamaguchi 2002]. Figure 4.9. shows the three-dimensional structure of gibbsite.

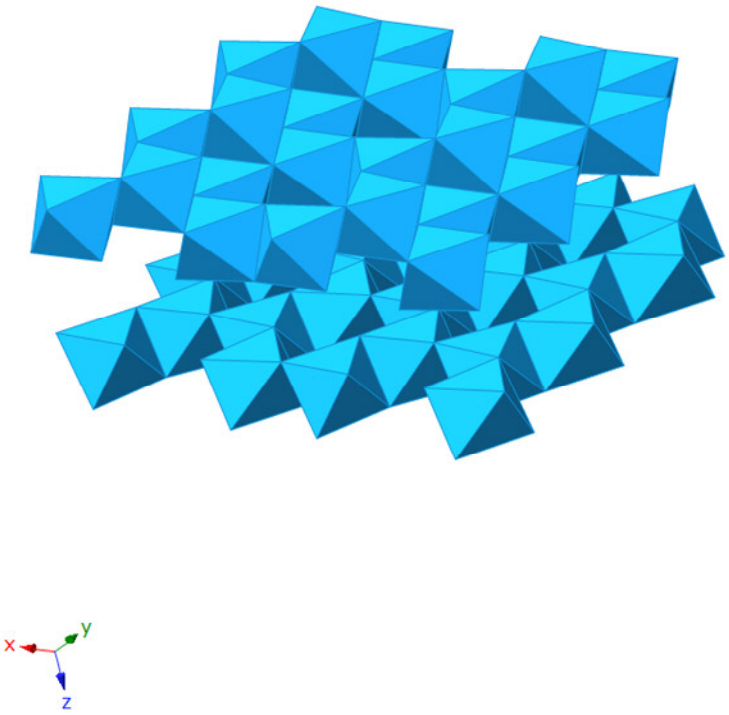

Fig. 4.9. Gibbsite structure, obtained with Crystal Maker and the published data calculated with DFT [Balan 2006].

4.2.1. Procedure

Different experiments were performed, e.g., batch experiments of Np(V) sorption onto gibbsite (Merck, 1.22 m^2/g) as a function of pH (6.5 – 10.5); Np concentration 7.0 pM with a concentration of background electrolyte of 0.1 M $NaClO_4$. A study of the sorption behaviour at the same ionic strength as a function of the Np concentration ($1 \cdot 10^{-13}$ M – $1 \cdot 10^{-4}$ M) was performed too, as well as batch experiments with two different concentrations of background electrolyte (0.1 M and 0.01 M $NaClO_4$). The samples were pre-equilibrated at least 3 days; the equilibrium with CO_2 was accelerated by adding $NaHCO_3$ and Na_2CO_3 (Merck). The pH was

daily controlled and if necessary readjusted with $HClO_4$, or NaOH (Merck). The contact time with Np was 3 days. After that, the final pH of the suspensions were measured and the phases were separated using a Sigma 3K30 centrifuge. $^{239}Np(V)$ stock solution was produced by irradiation of ^{238}U (see section 3.1.4.). The neptunium concentration in the supernatant was determined by using γ-spectroscopy (section 3.2.2.).

4.2.2. Batch experiments

Figure 4.10. demonstrates the influence of CO_2 on the sorption of Np(V). The gibbsite concentration here was 4 g/L. In the air-equilibrated system, the formation of neptunium-carbonato complexes above pH 8.5 reduces the amount of Np sorbed onto the mineral surface. In the CO_2-free system, the Np uptake by gibbsite increases continuously from pH 6.5 to 9.5.

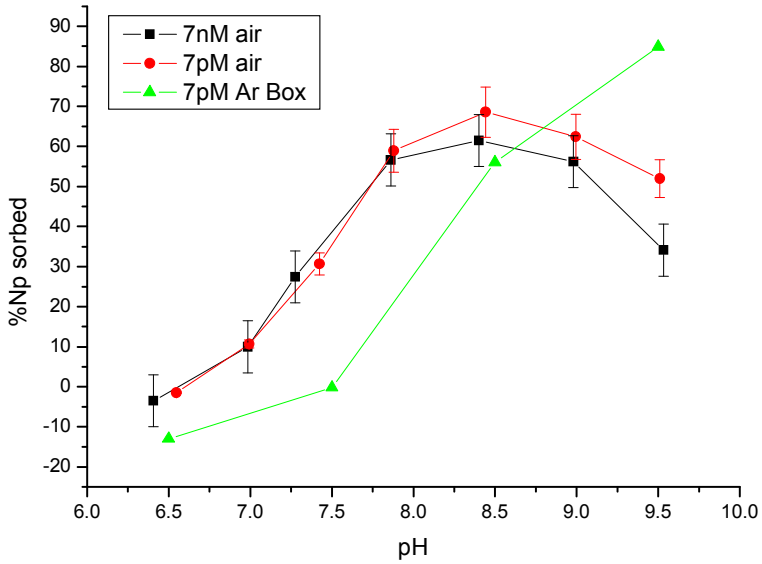

Fig. 4.10. Influence of CO_2 on the sorption of Np(V) in 0.1 M $NaClO_4$.

The batch experiments shown in Fig. 4.11. were performed in air at two different background electrolyte concentrations, i.e. 0.01 and 0.1 M $NaClO_4$. The solid to liquid ratio was 22 g/L to obtain a high Np uptake. In the presence of air, the sorption of Np(V) was independent from ionic strength, indicating inner-sphere sorption. This should be confirmed by EXAFS measurements.

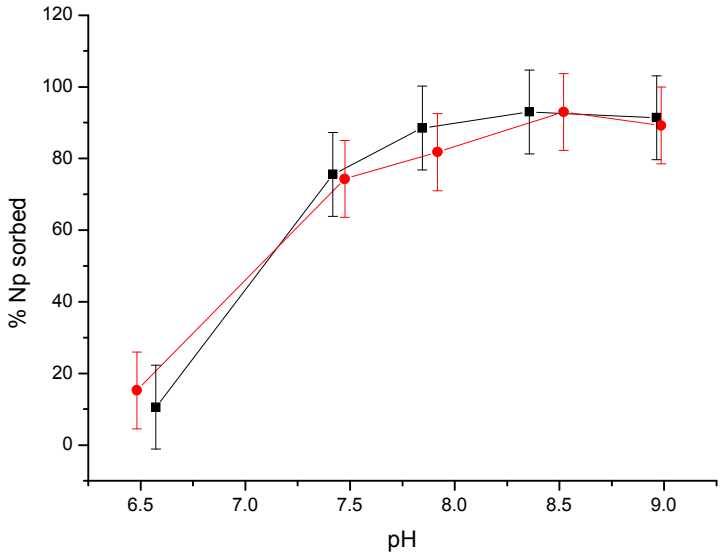

Fig. 4.11. Sorption of 7.0 pM Np(V) in equilibrium with air as function of pH at two electrolyte concentrations, [$NaClO_4$] = 0.1 M (black) and 0.01M (red).

The sorption of Np(V) in the presence of air at pH 8.5, 0.1 M $NaClO_4$, and 4 g/L was studied in the range of 10^{-13} – 10^{-4} M Np(V). According to the sorption isotherm shown in Fig. 4.12., the Freundlich plot (Fig. 4.13) of the Np(V) sorption onto gibbsite is nearly linear up to $2.8 \cdot 10^{-5}$ M Np. This obtained value fits very well with literature data for the solubility of Np [Neck 1994]. At this concentration, precipitation of Np(V) carbonates starts. In the linear range of the sorption isotherm, two zones with slightly different slopes have been observed, indicating the existence of weak and strong sorption sites of gibbsite. For the low concentration range a slope of 0.99939 was determined, whereas for the high concentration range a slope of 0.99684 could be fitted. These results are not shown.

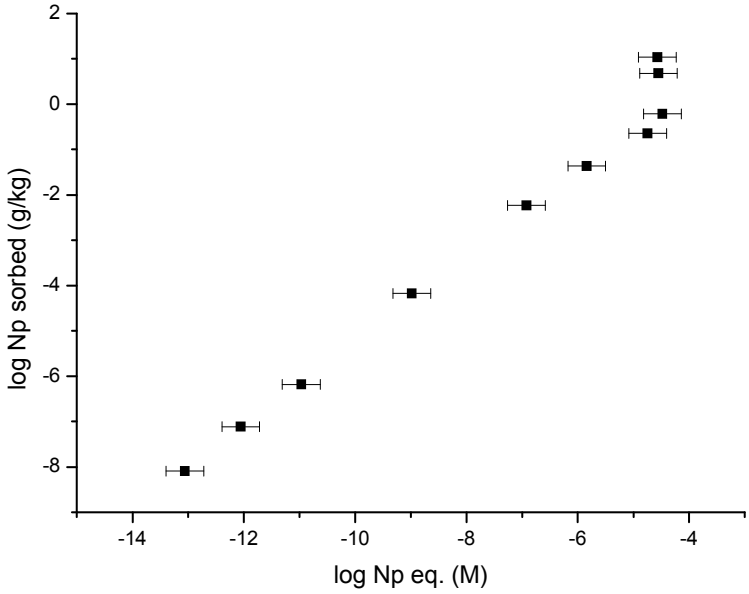

Fig. 4.12. Sorption isotherm of Np(V) onto gibbsite, pH 8.5, [$NaClO_4$]=0.1M, presence of air.

Excluding the last data points, which indicates precipitation of the $NaNpO_2CO_3$ [Neck 1994] above $[Np]_{eq} = 2.8 \cdot 10^{-5}$ M, a Freundlich fit with a correlation factor of 0.99917 was possible. As mentioned in section 2.4.1., Everett A. Jenne warns against segmenting the data for fitting [Jenne 1998], therefore the whole range was fitted by using one curve.

$$Log \frac{Np\,(g)}{gibbsite\,(kg)} = (3.9 \pm 0.14) + (0.91 \pm 0.14) \cdot Log\,[Np]_{eq} \qquad 4.1.$$

The obtained linearized equation 4.1., shows a similar slope to the slope obtained for γ-alumina [Dierking 2007 b], while the sorption is lower on gibbsite than on γ-alumina. A slope unequal to 1 points to nonlinear changes in the $\frac{Np\,(g)}{gibbsite\,(kg)}$ to $[Np]_{eq}$ ratio [Jenne 1998].

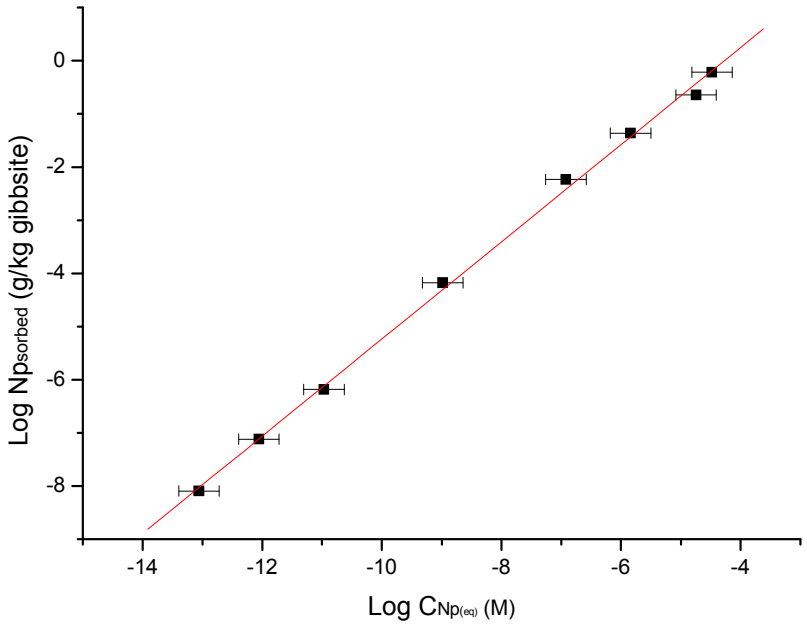

Fig. 4.13. Freundlich fit for the sorption isotherm of Np(V) onto gibbsite, pH 8.5, [$NaClO_4$] = 0.1M, presence of air.

4.2.3. EXAFS studies

The EXAFS measurements were performed at the INE Beamline at ANKA (see section 3.2.4.) 15 sweeps were made for each sample. EXAFS analysis was performed with the software packages EXAFSPAK [George 2000] and FEFF8.20 [Ankudinov 2002]. The results were published in the ANKA report 2007 [Vicente Vilas 2007].

The EXAFS samples were prepared from a 1.8 mM $^{237}Np(V)$ stock solution that was purified from traces of ^{239}Pu and ^{233}Pa. Gibbsite (Merck, 1.22 m^2/g) was suspended in MilliQ water (I = 0.1 M $NaClO_4$). The air samples (A.1, A.2) were equilibrated with air over two days, whereas the box samples (B.1, B.2) were equlibrated with an argon atmosphere. The pH was adjusted to the desired value with $HClO_4$ or NaOH. After adjusting the pH value for one week, Np was added; the total Np concentration was about 7.5 µM. During the contact time of two days, the pH was also readjusted. The solid and liquid phases were separated by centrifugation, and the Np uptake was determined by γ-spectrometry and liquid scintillation counting (LSC) in the supernatant. The wet pastes were then loaded into the sample holders. Table 4.3. summarizes the preparation conditions of the four samples.

Sample	Air / Box	pH	Beam Energy (GeV)	Np loading ppm
A.1	Air	8.5	2.5	70
A.2	Air	8.5	2.4	99
B.1	Box	10	2.5	218
B.2	Box	10	2.4	328

Table 4.3. Summary of the gibbsite wet-paste samples prepared at about 7.5 µM Np(V) and 0.1 M $NaClO_4$ for EXAFS measurements.

The neptunium in all samples is sorbed at the surface of gibbsite as Np(V). The k^3-weighted EXAFS data are shown in Fig.4.14. The two samples measured with 2.5 GeV beam energy, have better statistics than the two samples measured with 2.4 GeV beam energy. Sample B.1 shows a different EXAFS pattern, in particular in the k range 6 – 8.5 $Å^{-1}$, as compared with the other samples.

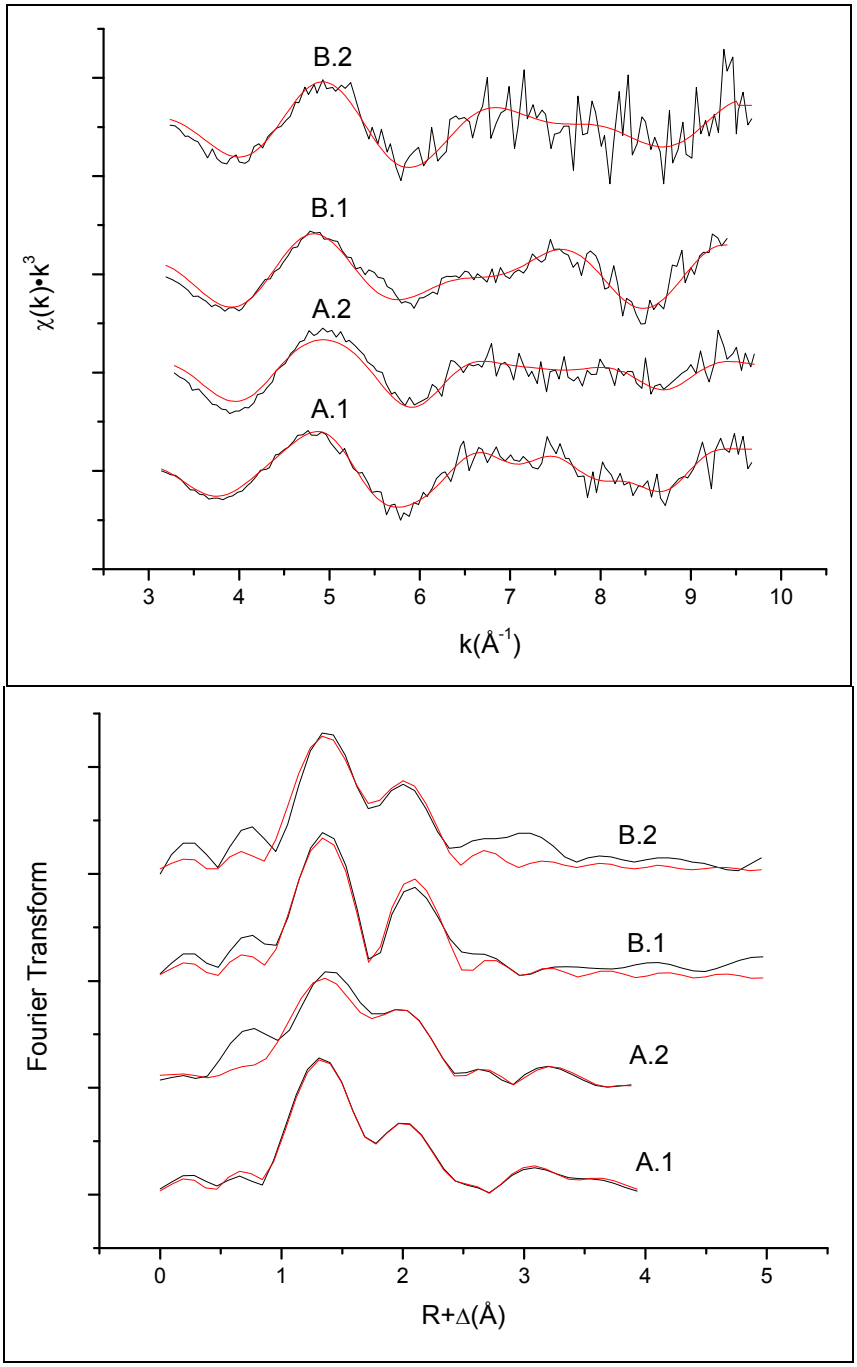

Fig.4.14. Np L_{III}-edge EXAFS data (above) and FT (down). Experimental data are in both cases shown in black and the calculated fit in red.

All spectra were analyzed for the first two coordination shells of Np(V), and for the A.1 sample, an additional Np-Al shell could be included. The Np-Oax bond distances are in the same range as the typical values for the NpO_2^+ published data [Reich 2000]. The Np-Oeq distance for the sample B.1 could not be confirmed. Further measurements with better statistics are required to improve the information about the Np(V) surface complexes onto gibbsite. Table 4.4. summarizes the obtained EXAFS data.

Sample	$2xO_{ax}$	$4xO_{eq}$	1xAl
A.1	1.82	2.45	3.26
A.2	1.82	2.45	-
B.1	1.82	2.54	-
B.2	1.81	2.44	-
$NpO_2(CO_3)^{-5}$ (aq) [Clark 1996]	1.86	2.53	-
NpO_2^+ [Reich 2000]	1.82	2.49	-

Table 4.4. Distances to Np neighbour in Å (± 0.02 Å).

4.2.4. Discussion

The batch experiments at different ionic strengths (Figure 4.11.) point to an inner-sphere sorption of neptunium on gibbsite, this result was also confirmed by the Np-O_{eq} distances (excluding the sample B.1) in the EXAFS measurements (Table 4.4.). These results are consistent with literature data for the sorption of Ni onto gibbsite [Yamaguchi 2002] and U onto gibbsite [Baumann 2005]. Furthermore the presence of ambient CO_2 affects the sorption (Figure 4.10.), probably maintaining the neptunyl ions in solution as carbonato complexes. The slightly different slopes in the isotherm at pH 8.5 under ambient conditions (Figure 4.12.) points to the existence of strong and weak sites in gibbsite. Similar results have been obtained for other model materials as γ-alumina [Dierking 2007 b].

4.3. Sorption of Np(V) onto hybrid clay-based materials: montmorillonite-melanoidin

The actinide concentrations in groundwaters are usually below the micro molar range, due to solubility limitations. The maximum solubility for neptunium considering the sodium concentrations in environmental conditions is below 10^{-5} M [Allard 1984]. Furthermore, natural aquatic systems contain other complexing agents both organic and inorganic (see table below).

	Rain waters	**Shallow groundwaters**	**Deep granitic groundwaters**	**Sea waters**
pH	**4 – 6**	**5 – 8.5**	**7 – 9**	**~8.1**
HCO_3^-	*<1*	*60 – 250*	*90 – 275*	*140*
SO_4^{-2}	*0.1 – 5*	*0.5 – 25*	*0.5 – 15*	*2650 – 2712*
HPO_4^{-2}	-	*0.01 – 0.1*	*0.01 – 0.2*	*<0.1*
NO_3^-	*0.1 – 4*	*0.1 – 5*	*0.01 – 0.05*	*<0.7*
F^-	*0 – 0.2*	*0.5 – 2*	*0.5 – 5*	*1.4*
Cl^-	*0.1 – 20*	*4 – 25*	*4 – 15*	*18980 – 19353*
HS^-	-	-	*<0.05*	-
Ca^{+2}	*0.5 – 5*	*5 – 50*	*10 – 40*	*380 – 399*
Mg^{+2}	*0.1 – 0.5*	*0.5 – 10*	*1 – 10*	*1272 – 1292*
Na^+	*0.3 – 20*	*2 – 25*	*10 – 100*	*10560 – 10766*
K^+	*0.1 – 4*	*0.5 – 5*	*1 – 5*	*380 – 399*
Fe (total)	-	*0 – 0.5*	*1 – 5*	*<0.02*
SiO_2	-	*3 – 30*	*3 – 14*	*0.01 – 7*

Table 4.5. Inorganic constituents in natural waters (mg/L) [Allard 1984].

Sorption of neptunium on the hybrid materials (HCM, see section 4.1.) was studied for the pH-range from 6 to 8.5 under ambient conditions (presence of CO_2), and at Np concentrations of 10^{-12} M (Figure 2). With increasing the pH, dissolution of organics from the HCM was observed, see Fig. 4.21., which was confirmed by UV/Vis absorption spectroscopy. Neptunium was also determined in the organic fraction >1kDa, which was separated by using ultrafiltration [Seibert 1999]. The presence of the melanoidins in the montmorillonite (STx-1 type) reduces the sorption of neptunium above pH 7 in comparison with the pure STx-1, due

to the release of organic material from the hybrid material into the aqueous phase, which is able to complex partially the present neptunium. Below pH 7, the sorption on the HCM is increased in comparison to pure montmorillonite due probably to complexing reactions with the partially negatively charged acidic groups in the organics..

4.3.1. Procedure

All sorption experiments were conducted in a batch at initial hybrid material concentrations of 4 g/L and neptunium concentrations of 10^{-12} M. The samples were pre-equilibrated at least 3 days; the equilibrium with CO_2 was accelerated by adding $NaHCO_3$ and Na_2CO_3 (Merck). The pH was daily controlled and if necessary readjusted with $HClO_4$, or NaOH (Merck). The contact time with Np was 3 days. After that, the final pH of the suspensions were measured and the phases were separated using a Beckmann Coulter Avanti J-30I High Performance Centrifuge (108800g, 1 hour).

For the determination of the organic substances in the supernatant of the samples, UV/vis-spectroscopy was used. $^{239}Np(V)$ stock solution was produced by irradiation of ^{238}U (see section 3.1.4.). The neptunium concentration in the supernatant was determined by using γ-spectroscopy (section 3.2.2.).

4.3.2. Release of organics

Since the organic bound to the STx-1 show the same STXM spectrum as the related melanoidin (see section 4.1.5.), an estimation of the bound melanoidin to the montmorillonite was possible. Furthermore, it was also possible to determine the amount of melanoidin release as a function of pH, by comparing the absorption of the sample solutions at 310 nm with the absorption of melanoidin standards. Those data will be used in the further discussion. Both melanoidins (i.e., THD and GHD) were dissolved in a $NaClO_4$ solution and also equilibrated with CO_2. The resulting melanoidin content of the two HCM is shown in Table 4.6.

Sample (160mg)	%C in HCM	%C in related melanoidin	Calculated melanoidin content (mg)
GHS	1.7	51.64	5.27
THS	1.3	53.32	3.9

Table 4.6. Calculated melanoidin content for the two HCM.

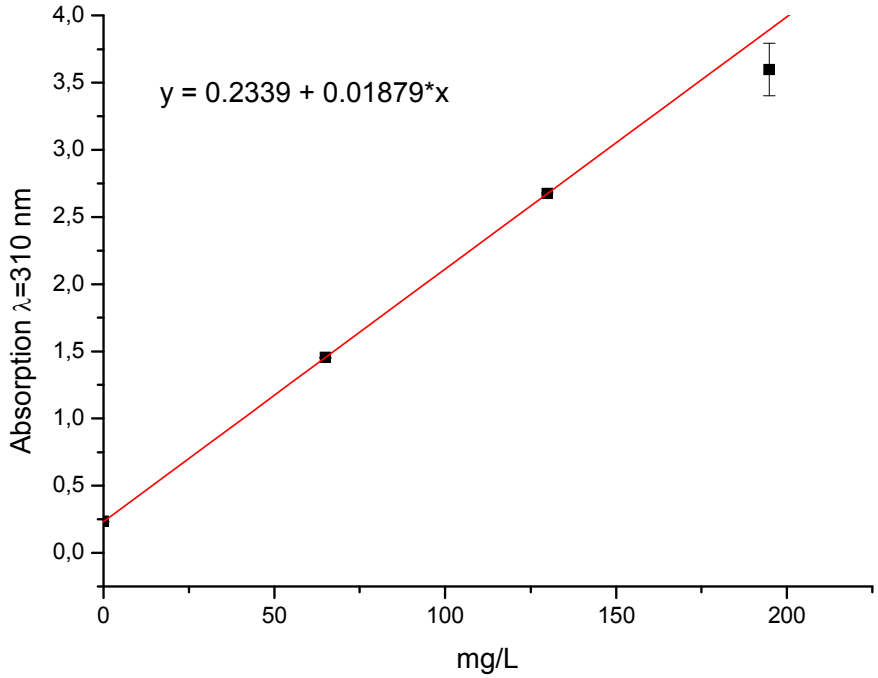

Fig. 4.15. Calibration curve for the determination of organics released from GHS.

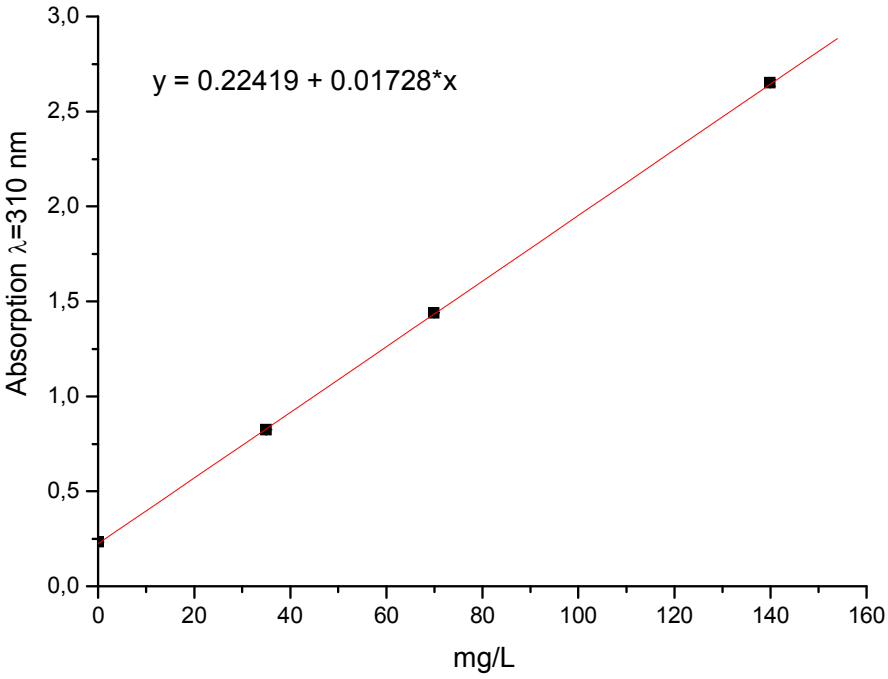

Fig. 4.16. Calibration curve for the determination of organics released from THS.

By plotting the melanoidins in solution, obtained with the equations shown above, against the pH, a linear correlation was obtained, see Fig. 4.17.

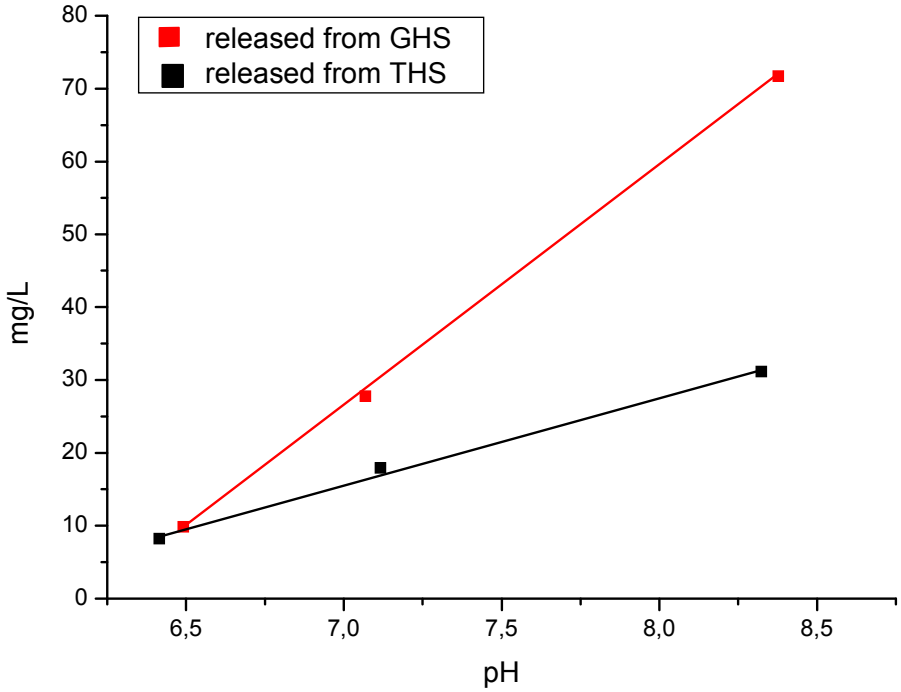

Fig. 4.17. Linear dependence between the pH and the organics release from the HCM.

4.3.3. Effect of the bound melanoidin on the sorption of Np(V)

In figure 4.18., 4.19. and 4.20. sorption coefficients of Np(V) ions on the hybrid materials and also on STx-1 montmorillonite as a function of pH are shown. In the absence of the melanoidins the sorption coefficients increase until pH about 8 presenting a plateau until pH 8.5 [Dierking 2008]. The presence of the melanoidins with a high content in carboxyl groups in the montmorillonite (GHS) enhances the sorption up to pH about 7.1, above this pH the presence of melanoidins results in a decrease of the sorption coefficient. These results are consistent with the literature data concerning the sorption of other actinides onto kaolinite [Banik 2007, Křepelová 2006 and Samadfam 2000]. The melanoidins with higher content in phenolic groups (THS) present a lower sorption capacity over the entire range of pH in comparison to the parental montmorillonite and the GHS. The formation of neptunium-organic and neptunium-carbonate complexes, is though to be the main factor involved in the sorption.

In our case the melanoidins were synthesised in the presence of the montmorillonite, and the hybrid material obtained may have suffered an alteration of the parental surface of the STx-1 montmorillonite. This alteration may be caused by blocking sorption sites of the montmorillonite surface or due to negative charge of the melanoidins bound to the montmorillonite.

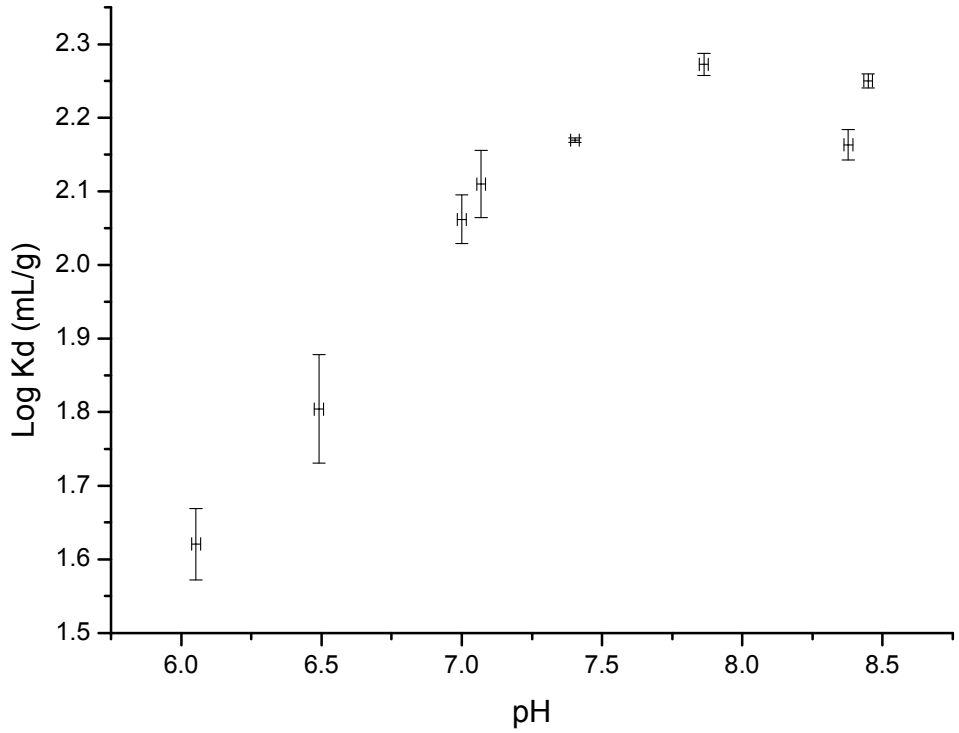

Fig. 4.18. Sorption coefficients for the sorption of Np(V) onto the GHS hybrid material.

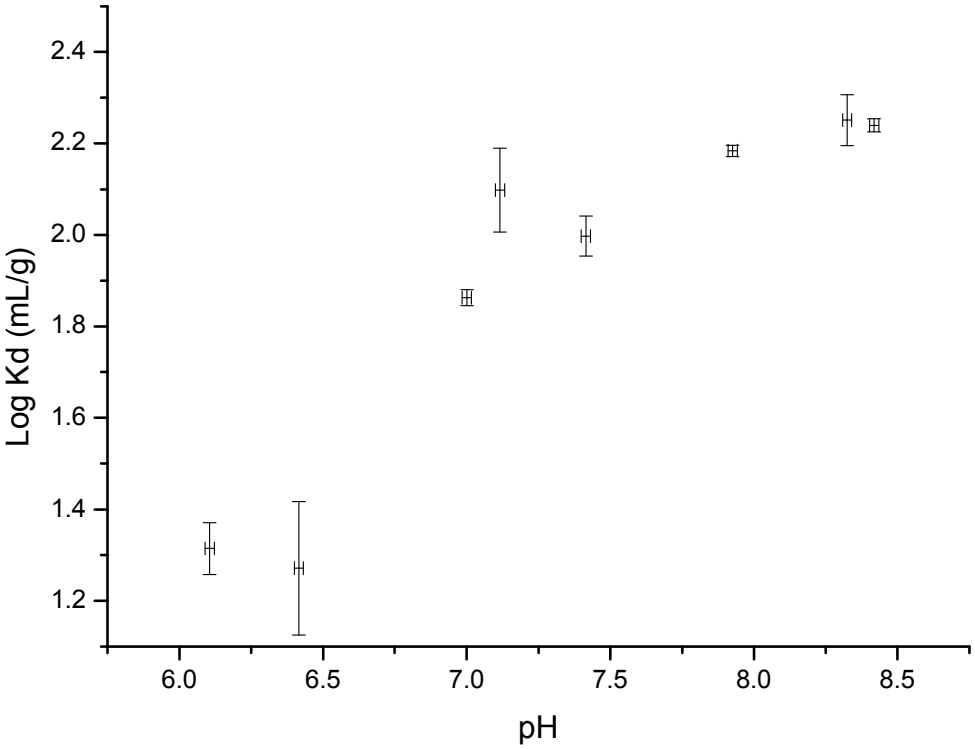

Fig. 4.19. Sorption coefficients for the sorption of Np(V) onto the THS hybrid material.

The differences between the sorption on GHS and on THS may be due to the lower content in carboxylic groups in the THS, which has higher phenolic group content. Carboxyl groups are known to be responsible for the complexation of neptunium (V) [Sachs 2005].

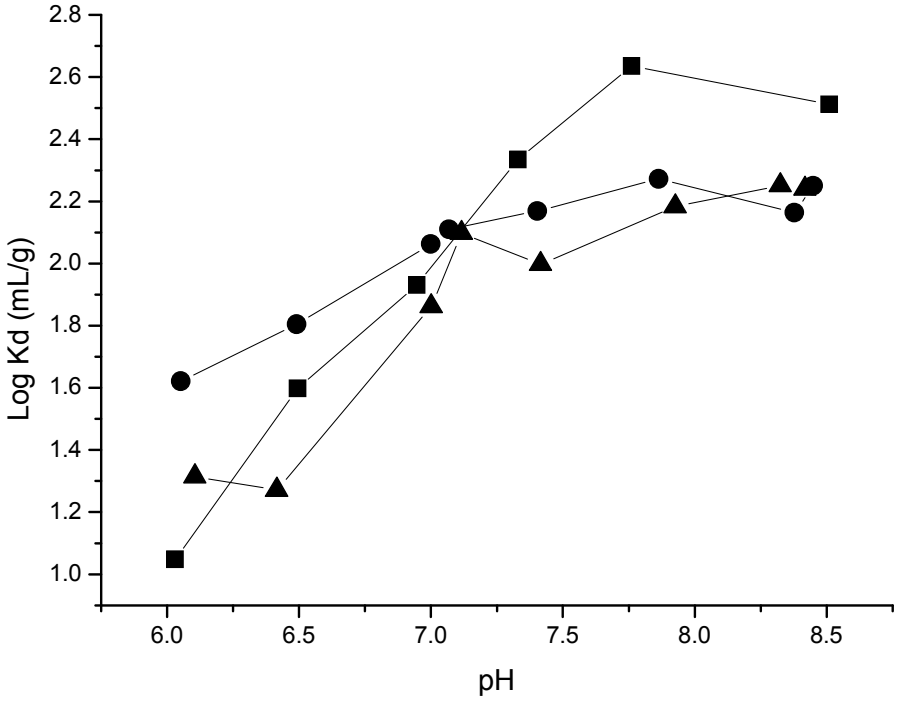

Fig. 4.20. Comparison between the sorption coefficients for the sorption of Np(V) onto the STx-1 (quadrangle), and the hybrid materials GHS (circle) and THS (triangle).

4.3.4. Complexation of Np(V)

After the phase separation, a fraction of the supernatant was ultra filtrated using 1kDa Microsep 1kOmega membrane filters (Pall Life Sciences, USA) in combination with centrifugation (Fritz Bayet OHG, Frankfurt M., Germany), at about 2500 rpm for 20 minutes (see section 3.2.6.). By comparing the total neptunium concentration and the neptunium concentration in the fraction <1kDa, where only the inorganic complexing agents are present, it is possible to determine the amount of complexed neptunium with the organic substances.

The results for GHS are shown in Fig. 4.22., those for THS in Fig. 4.23. The lower sorption of Np(V) on THS as compared to GHS was commented already above.

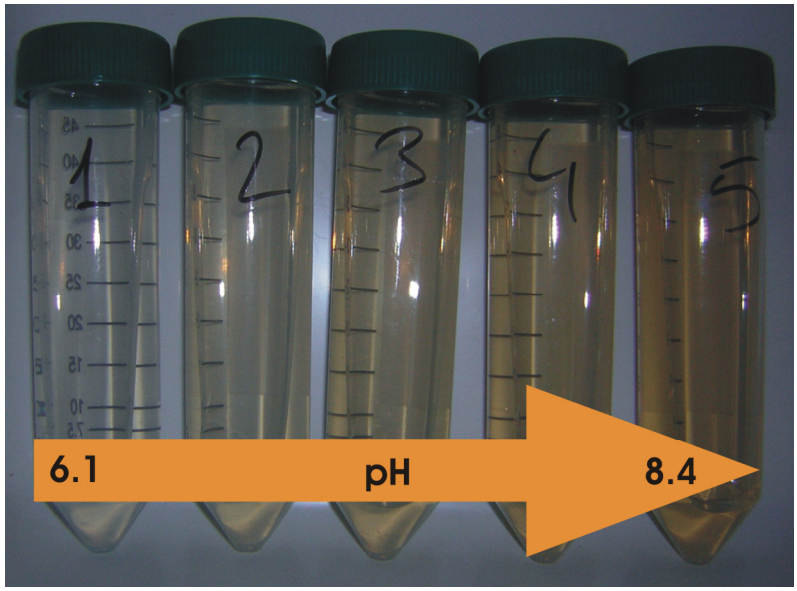

Fig. 4.21. Organic material release as a function of pH for THS.

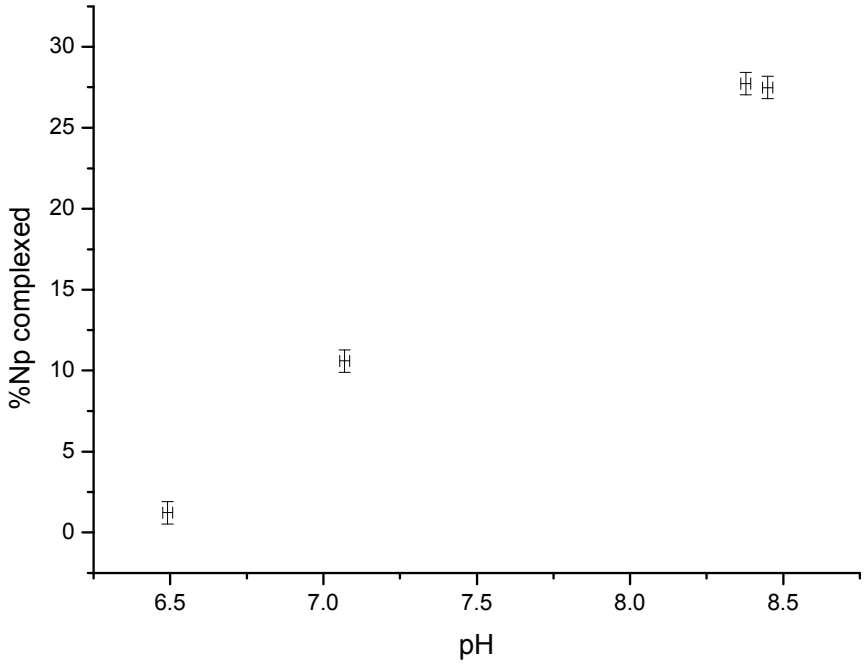

Fig. 4.22. Percentage of neptunium bound to the organic fraction for GHS as a function of pH.

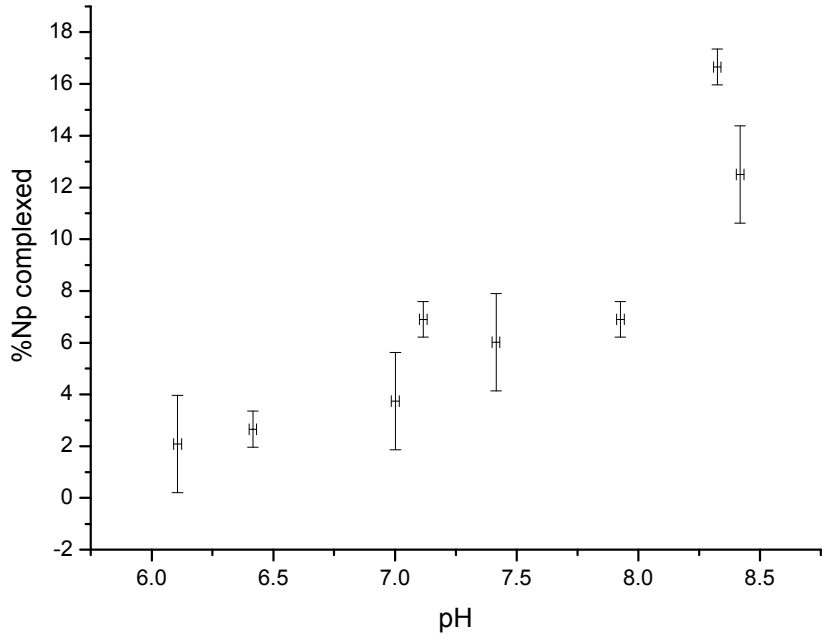

Fig. 4.23. Percentage of neptunium bound to the organic fraction for THS as a function of pH.

4.3.5. Testing the linear additive model for hybrid materials

The linear additive model was published by Zachara et al. in 1994 for the influence of humic substances on the sorption of Co^{+2} [Zachara 1994]. Basically, in this model, the components of the system act independently from each other. For this study, the equation proposed by Samadfam et al. [Samadfam 2000] was used:

$$Kd = \frac{Kd^{\,0} + (V/W)\cdot f_{HA}\cdot\beta\cdot[HA]}{1+(1-f_{HA})\cdot\beta\cdot[HA]} \qquad 4.1.$$

Kd – the sorption coefficient for the complex mixture

Kd^0 – the sorption coefficient for neptunium onto montmorillonite

β – the apparent stability constant for the complexation of neptunium by humic substances

[HA] – total concentration of humic (mineral bound and dissolved) eq/dm^3

W – total mass (in kg) of montmorillonite

V – suspension volume in dm^3

f_{HA} – sorbed fraction of humic on the mineral $f_{HA} = \chi_{HA}\cdot W/W_{HA}$, being χ_{HA} the mass fraction of humic and W_{HA} total mass of humic in kg (bound and dissolved). In our case calculated values using the linear dependence of the organic release from the HCM were used.

Seibert et al. have studied the complexation behaviour of neptunium with humic acid, and obtained a complexation constant log β = 5.0 ± 0.3 (meq/L) at neptunium concentrations below 10^{-11} mol/L, at pH 6, 7 and 8 [Seibert 2001]. Using those data for the complexation constants and the data for the sorption on STx-1 [Dierking 2008] in the linear additive model formula, the curve showed in fig. 4.18. was obtained.

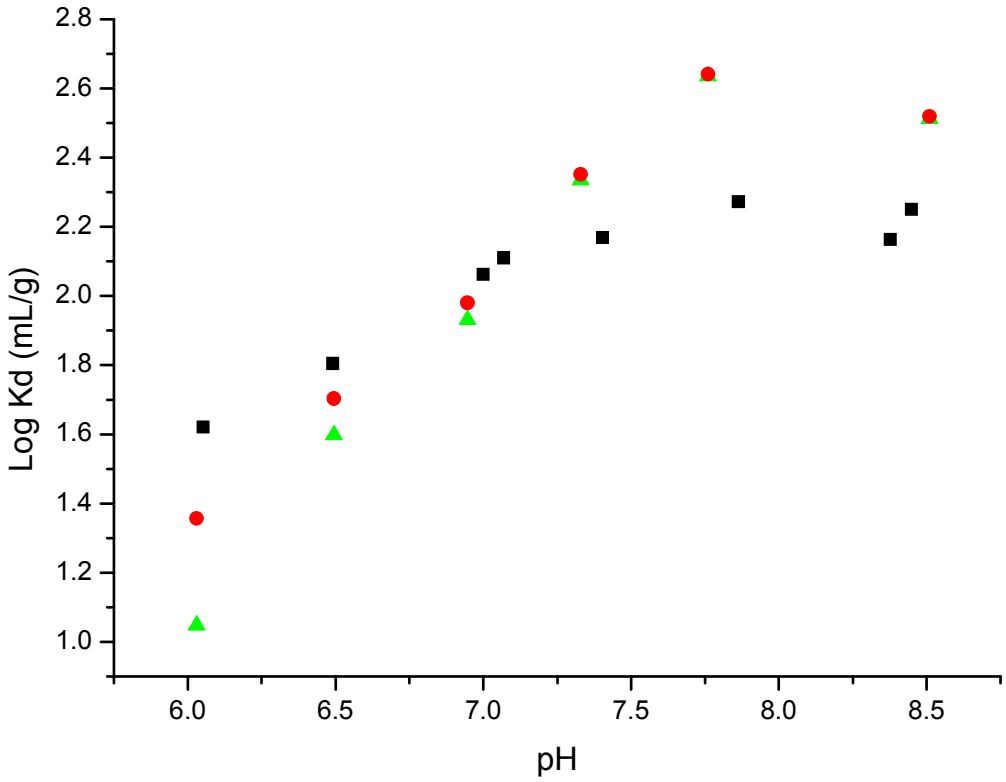

Fig. 4.24. Sorption coefficients obtained for GHS (black), STx-1 (green), and those calculated with the linear additive model (red).

The presence of closely bound organics to the mineral in the HCM produces the occurrence of more sorption sites for Np than the predicted by the Lineal Additive Model for the physical mixture of STx-1, melanoidins and Np at pH<7. On the other hand at pH>7 the release of organics and, therefore, of organic-Np-complexes from the HCM produces the mobilization of Np from the mineral surface. The Linear Additive Model is a very useful tool for the estimation of sorption coefficients in the ternary systems where the components are physically mixed, and a help to elucidate the trends in systems like the sorption on HCM, where two components are closely bound.

4.3.6. Discussion

The sorption of neptunium on hybrid clay materials was investigated. The presence of melanoidins in montmorillonite reduces the sorption of neptunium above pH 7 in comparison with pure montmorillonite, due to the release of organic material from the hybrid material into the aqueous phase. Below pH 7, the sorption on the HCM is increased. This behavior ressembles that of the sorption of actinide metal ions on kaolinite in the presence of Aldrich humic acid [Buda 2008]. The presence of closely bound organics to the mineral in the HCM produces the occurrence of more sorption sites for Np than the predicted by the Lineal Additive Model for the physical mixture of STx-1, melanoidins and Np at pH<7. On the other hand at pH>7 the release of organics and, therefore, of organic-Np-complexes from the HCM produces the mobilization of Np from the mineral surface. The Linear Additive Model is a very useful tool for the estimation of sorption coefficients in the ternary systems where the components are physically mixed, and a help to elucidate the trends in systems like the sorption on HCM, where two components are closely bound.

4.4. The influence of melanoidins on the sorption of Np(V) onto montmorillonite

Humic substances and their model substances, melanoidins, are supposed to be linked to the clay minerals over a "cation bridge", which may involve the displacement of a water molecule from the water shell of the cation by the humic acid [Theng 1975]. If this is so, the cations present in the system affect the linkage of the organic substances to the clay mineral. Experimental data presented by Theng and Scharpenseel, show that the affinity of humic acids for montmorillonite increases in the order $Na^+<K^+<Cs^+$ for samples saturated with mono-valent ions [Theng 1975]. In this work, the sorption of ^{14}C-M42 type melanoidins onto STx-1 montmorillonite in the presence of NpO_2^+ is discussed. The initial concentration range of the melanoidins in solution was 0 to 0.4 mg/mL, and the neptunium initial concentration was kept constant at 8μM, the pH was about 7.0. The sorption of the melanoidins was affected by the order in which the components were added and by the ionic strength. The sorption of Np being affected by the ionic strength, points to outer sphere sorption, whereas the presence of increasing amounts of melanoidins has little influence on the sorption.

4.4.1. Method

The M42 and ^{14}C-M42 type melanoidins were provided by the Research Center Dresden-Rossendorf (FZD). We used the ^{14}C-M42 batch R2/06A, which had a specific activity of 8.9 ± 0.6 MBq/g. The melanoidin was dissolved in a $NaClO_4$ (0.1 M and 0.01 M) solution equilibrated with CO_2 at pH about 7.0, obtaining a melanoidin stock concentration of 10.03 mg/mL in 0.1M $NaClO_4$ and 16.73 mg/mL in 0.01 M $NaClO_4$. The STx-1 suspension had a montmorillonite concentration of 22.78 g/L in 0.1 M $NaClO_4$ and 23.28 g/L in 0.01 M $NaClO_4$ and was also equilibrated with CO_2 and adjusted to pH about 7.0. The pH was daily controlled and if necessary readjusted with $HClO_4$, or NaOH (Merck). The ^{237}Np stock solution ([$NaClO_4$] = 0.1 M) was held at pH about 5 in order to prevent disproportionation.

Banik [Banik 2006] and Buda [Buda 2006] observed a dependence of the sorption on the order in which the reactants were added in ternary systems; therefore, two addition sequences were tested. In the first sample set, neptunium was first added to the montmorillonite suspension and after 72h, different amounts of the melanoidin stock solution were added in order to achieve the desired M42 concentrations. Two samples were prepared for each melanoidin concentration. After another 72h, samples were centrifuged using a Beckmann Coulter Avanti J-30I High Performance Centrifuge (81769g, 1 hour). In the second set, the order of addition was inversed.

4.4.2. Sorption Results

Although pH was supposed to be constant, some changes occurred during the manipulation and control of the samples. Samples were measured using different techniques. After the separation, the supernatant was measured using UV/Vis, LSC, and CE-ICP-MS. By using the linear additive model [Samadfam 2000], the trend of the distribution ratios Kd could be reproduced. For this purpose, the parameters published by M.H. Bradbury and B. Baeyens [Bradbury 2006] for the sorption of Np(V) onto SWy-1 montmorillonite were used. SWy-1 has higher iron content [Mermut 2001] than the STx-1, and its EXAFS results are therefore not suitable for comparison, but the sorption data are not affected by the iron content. Furthermore the obtained data were compared with literature results.

Melanoidin sorption

The concentration of melanoidins in the supernatant was determined by UV/Vis spectroscopy at 310 nm [Buda 2006]. Two samples where no Np was added acted as method standard by comparing their results with the results obtained by Theng and Scharpenseel [Theng 1975]. The order of addition and the ionic strength affect the sorption of the melanoidins on the STx-1 montmorillonite. In Figures 4.25. and 4.26., the determined amount of M42 in the supernatant is represented against the calculated sorbed amount, in order to facilitate the comparison with the results obtained by Theng and Scharpenseel [Theng 1975].

Figure 4.25. shows the data for the experiment done at ionic strength 0.1M. We can observe that the presence of neptunium blocks sorption sites for the melanoidins added afterwards. By firstly adding the M42, the sorption is increased in comparison to the samples without neptunium.

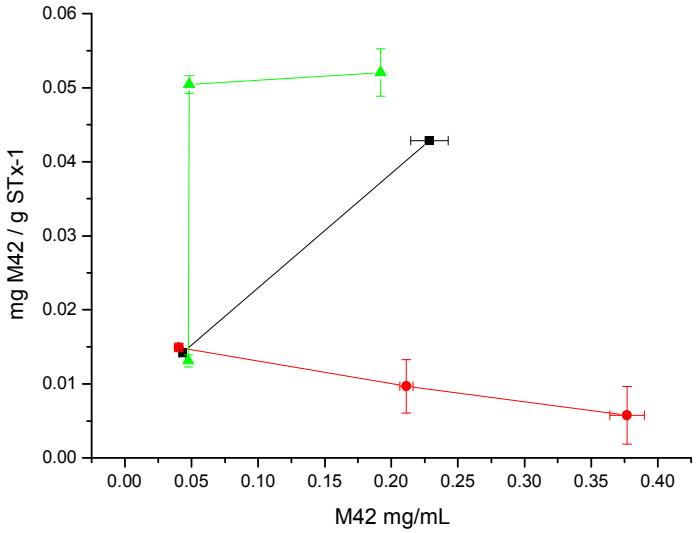

Fig. 4.25. Measured values for the sorption of M42 on STx-1 at ionic strength 0.1 M. The black quadrangles are the data obtained for the experiment without addition of Np, the red circles represent the data for the experiment where Np was added first, and the green triangles are the data for the experiment where M42 was added first, showing a very steep rise in the sorbed amount of melanoidins near 0.05 mg/mL M42.

Data obtained at ionic strength 0.01 M, see Figure 4.26., show a similar trend in the results obtained by adding neptunium first. The sorption decreases with increasing amount of melanoidins. When adding the M42 first, the sorption on montmorillonite decreases in the first fraction of the curve, increasing then sharply up to the value obtained without addition of neptunium.

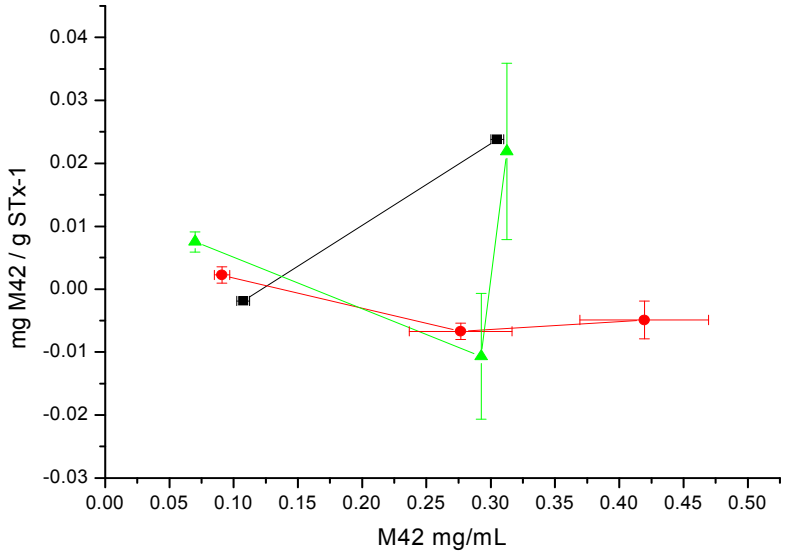

Fig 4.26. Measured values for the sorption of M42 on STx-1 at ionic strength 0.01 M, the black quadrangles are the data obtained for the experiment without addition of Np, the red circles represent the data for the experiment where Np was added first, and the green triangles are the data for the experiment where M42 was added first.

Unlike Na^+, K^+, and Cs^+, the presence of the NpO_2^+ cations before adding the melanoidins seems to reduce the sorption in both experiments (0.1 and 0.01 M).

Neptunium sorption

By using LSC, the concentration of ^{237}Np in the supernatant could be determined. Results were expressed as the logarithm of the Kd, and compared with the sorption on pure montmorillonite and the sorption modeled by using Visual MINTEQ ver. 2.53 [Gustafsson 2003]. The sorption in the neutral pH range seems to be nearly constant from pH = 6.5 to pH = 7, for higher pHs, a decrease in the log Kd appears, due to the formation of soluble carbonato complexes such as $NpO_2(CO_3)_3^{-5}$ [Clark 1995]. Literature data show that sorption of Np on polycarbonate centrifuge bottles is negligible [Bertetti 1998].

Investigations were conducted in the pH range where cation exchange and surface sorption compete. Therefore, a lower ionic strength facilitates the exchange at the interlayers of the montmorillonite and provides higher Kd values [Bertetti 1998]. Bertetti et al. studied the sorption of neptunium (V), $1 \cdot 10^{-6}$ M, onto SAz-1 montmorillonite, 4g/L, obtaining an approximate value of log Kd (mL/g) = 1.3 at ionic strength of [$NaNO_3$] = 0.1M [Bertetti 1998]. Figures 4.27. to 4.28. show the plots obtained with the experimental log Kd values in the presence of M42, showing in different plots the results obtained when adding Np first and those obtained when adding the M42 first. In the case of the experiments done at ionic

strength 0.1 M, the obtained value for the sorption on pure STx-1 of log Kd (mL/g) = 1.32 fits very well with the data published for SAz-1, although the cation exchange capacity of SAz-1 is higher (123 ± 3 meq/100 g) than the cation exchange capacity of STx-1 (89 ± 2 meq/100 g) [Bertetti 1998]. The surface charge changes among the three reference montmorillonites and it seems not to have as much influence on the sorption as the iron content, which is comparable between SAz-1 and STx-1 and higher in SWy-2.

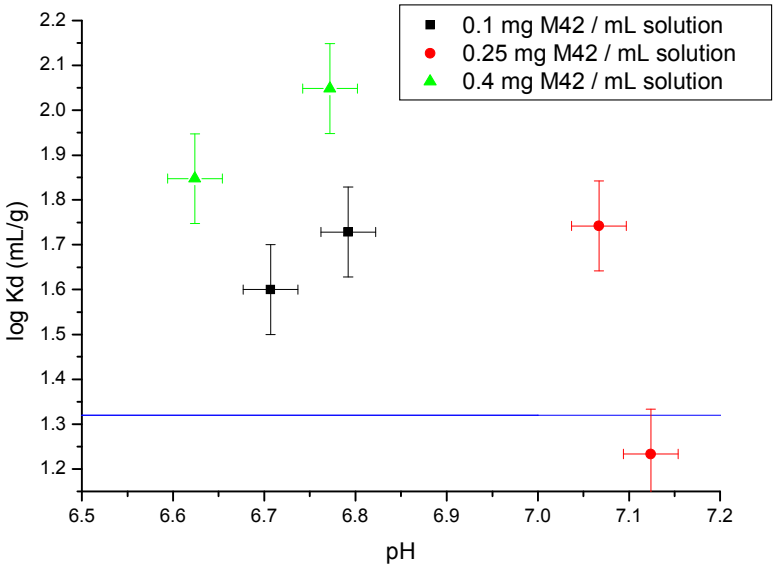

Fig. 4.27. Log Kd data for the experiment conducted under ionic strength [$NaClO_4$] = 0.1 M, where Np was added first, the blue line represents the sorption on pure STx-1.

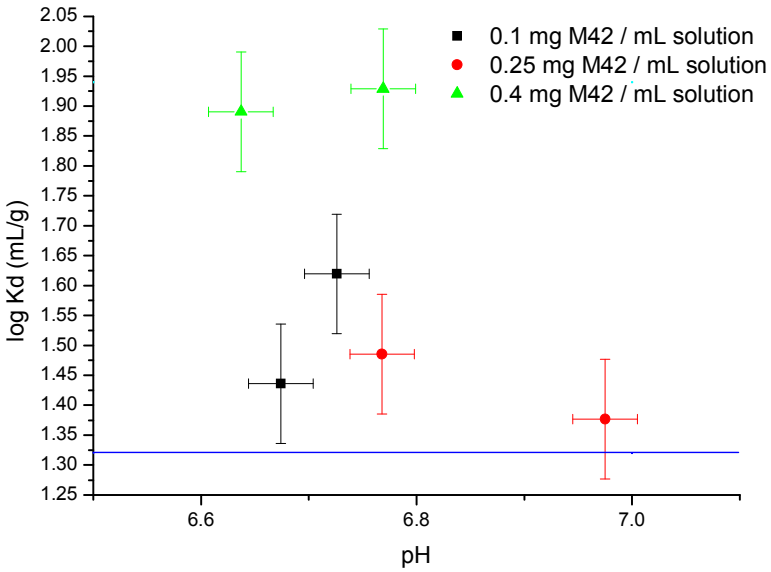

Fig.4.28. Log Kd data for the experiment conducted under ionic strength [$NaClO_4$] = 0.1 M, where the M42 melanoidins were added first, the blue line represents the sorption on pure STx-1.

For the experiments conducted under ionic strength of 0.1 M (Figures 4.27. and 4.28.), both series show a higher uptake of Np in the presence of the melanoidins in comparison with the sorption on pure montmorillonite. A suitable explanation is that being the interlayer space of the montmorillonite occupied by the sodium cations, the presence of the organic substances improves the sorption on the surface of montmorillonite due to the partially dissociated and therefore negatively charged carboxylic groups. The order of addition of the components has in this case little influence on the sorption.

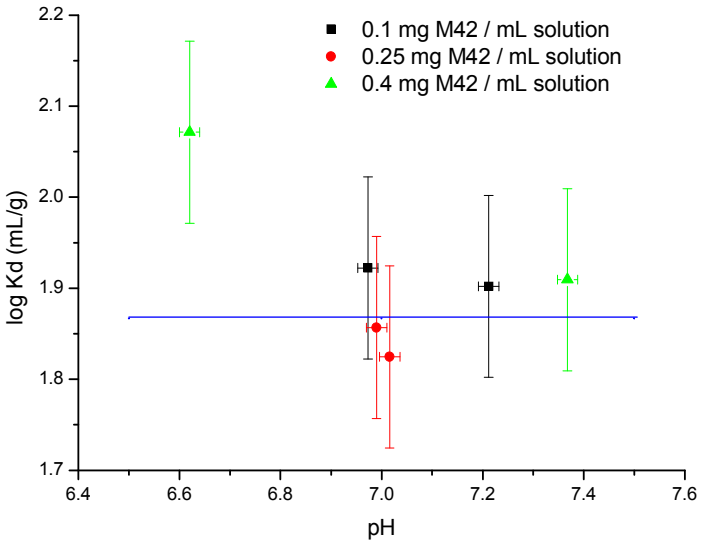

Fig. 4.29. Log Kd data for the experiment conducted under ionic strength [$NaClO_4$] = 0.01 M, where Np was added first, the blue line represents the sorption on pure STx-1.

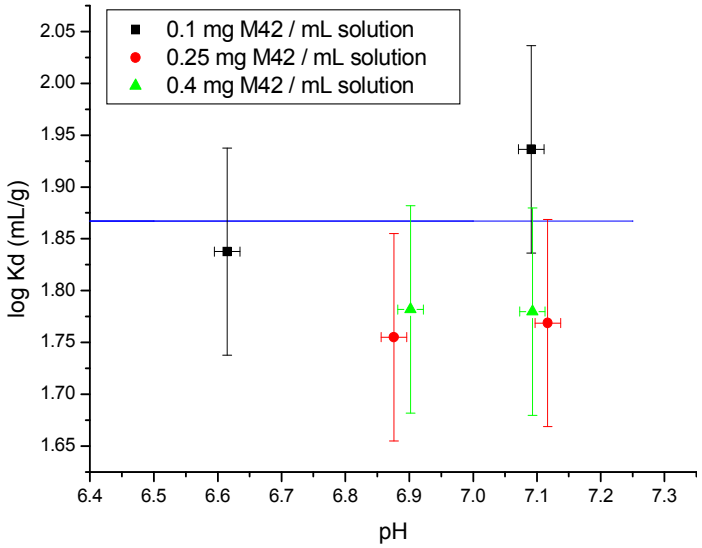

Fig. 4.30. Log Kd data for the experiment conducted under ionic strength [$NaClO_4$] = 0.01 M, where the M42 melanoidins were added first.

In the case of the experiments under ionic strength of 0.01 M (Figures 4.29. and 4.30.), both series show values comparable to the sorption on pure montmorillonite, which had a log Kd value of 1.867. In this case, the value calculated using the SWy-1 parameters [Bradbury 2006] and the Visual MINTEQ ver. 2.53 [Gustafsson 2003] of log Kd = 2.1 is higher than the obtained value but is in rough agreement with the experimental data. Since the exchange with the cations in the interlayer spaces has to be considered at low ionic strength, here the organic

material seems to have little influence on the sorption. Like in the experiments conducted under ionic strength of 0.1 M, the addition order has little influence on the sorption.

4.4.3. Speciation using the system CE-ICP-MS

A suitable method for the speciation in our samples after centrifugation is the separation using the capillary electrophoresis and the detection with the ICP-MS. For the separation of the actinides, the use of acetic acid 1M (pH about 2.4) as electrolyte has been reported [Kuczewski 2003] in contrast to the separation of lanthanides, where the use of a buffer solution acetic acid – acetate is the most suitable electrolyte [Kautenburger 2006]. The addition of 1M acetic acid to our melanoidins containing samples led to the formation of precipitates; therefore, a basic electrolyte (KH_2PO_4 3 mM and $Na_2B_4O_7$ 6 mM, pH~8.9) was added as reported by Pompe et al. for investigations on different humic substances [Pompe 1996]. The separation parameters were fixed at +/-30 kV, 6 bar Ar pressure at the nebulizer, furthermore make up solution with ~4.5 ppb of Rh 103 and 10% ethanol was continuously added using a syringe driver. We used the Scott type spray chamber.

Obviously, by adding this buffer, the speciation of the solution changes slightly, nevertheless qualitative information on the speciation changes in the samples is possible by comparing the data obtained for the different samples with the standards.

Differences in the standards, e.g., Np and Np with M42, searched for in the positive run (Figure 4.31.), are not remarkable. Hence, we can conclude that there is only one species present in the supernatant of the samples, independent of the presence of melanoidins and montmorillonite with the dominant species being NpO_2^+. The peak integrals show little differences in the positive run.

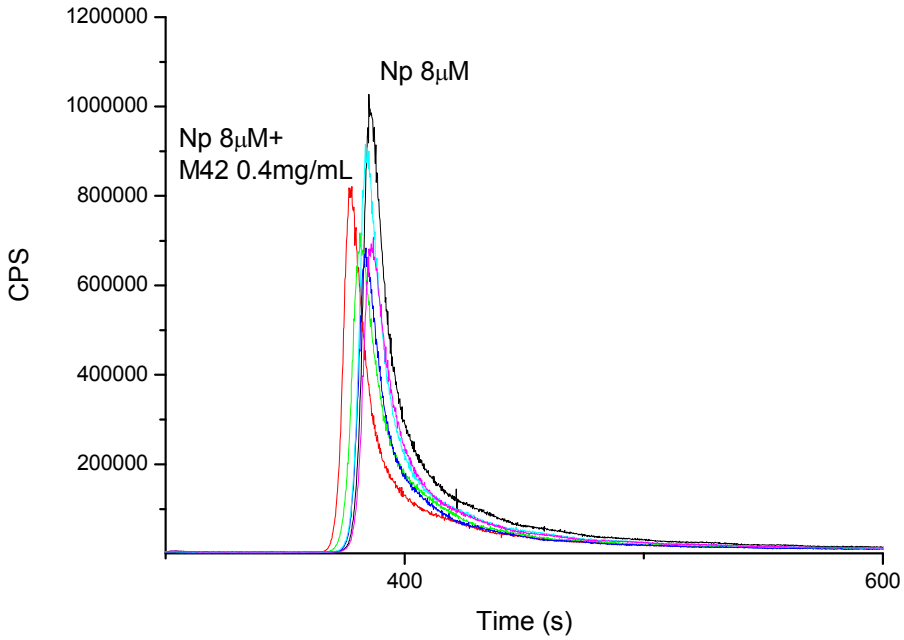

Fig. 4.31. Rhodium corrected data obtained with the Scott type spray chamber, for the samples under ionic strength 0.1 M and +30kV. The red curve represents the sample without addition of STx-1, and the black curve is the sample where only Np was present. The other curves represented show samples containing Np, STx-1 and M42.

Figure 4.32. shows the results for the experiments conducted at -30kV. By applying no pressure during the separation, no neptunium signal was observed, therefore, 400mbar pressure were applied to the capillary.

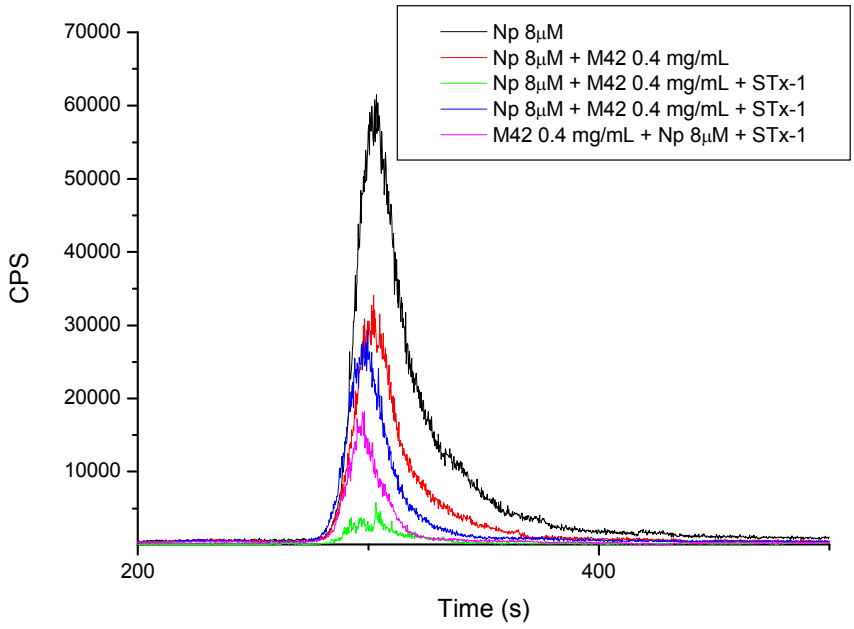

Fig. 4.32. Rhodium corrected data obtained with the Scott type spray chamber, for the samples under ionic strength 0.1 M and -30kV.

The electropherograms are consistent with the presence of one cationic species only, i.e. NpO_2^+. Figures 4.33. and 4.34. show the measurements done for the experiments conducted under ionic strength 0.01 M. Indication of a species with a lower charge to radius ratio was observed in the sample containing melanoidins and neptunium without montmorillonite (red curve in Figure 4.33.). Hence the presence of STx-1 montmorillonite produces a change in the speciation of the sample.

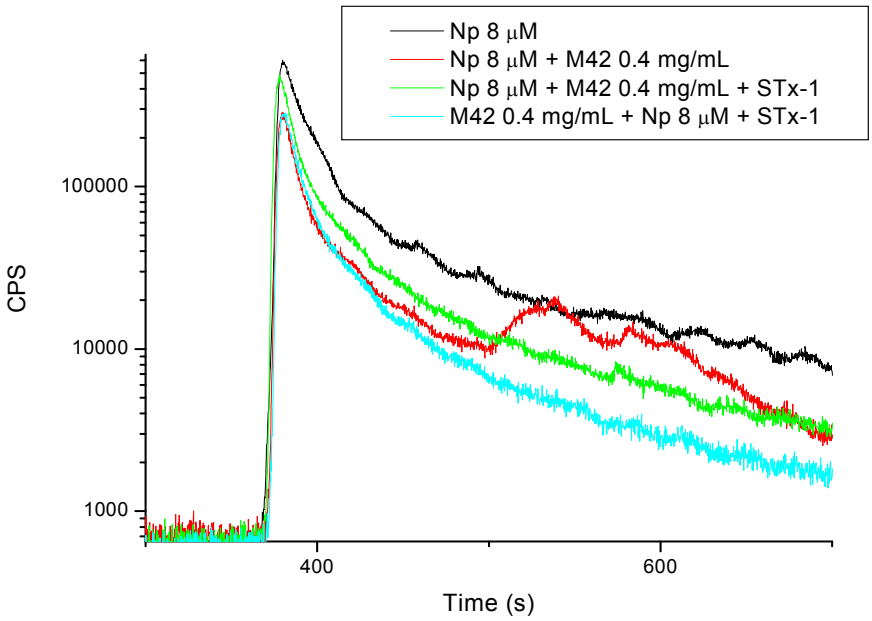

Fig. 4.33. Logarithmic representation of Rhodium corrected data obtained with the Scott type spray chamber, for the samples under ionic strength 0.01 M and +30kV. The red curve represents the sample containing M42 and Np without STx-1.

In the run conducted at -30kV, Figure 4.34., the occurrence of a little peak in the sample where only Np and M42 were present, indicates the presence of negatively charged M42-NpO_2^+ complexes.

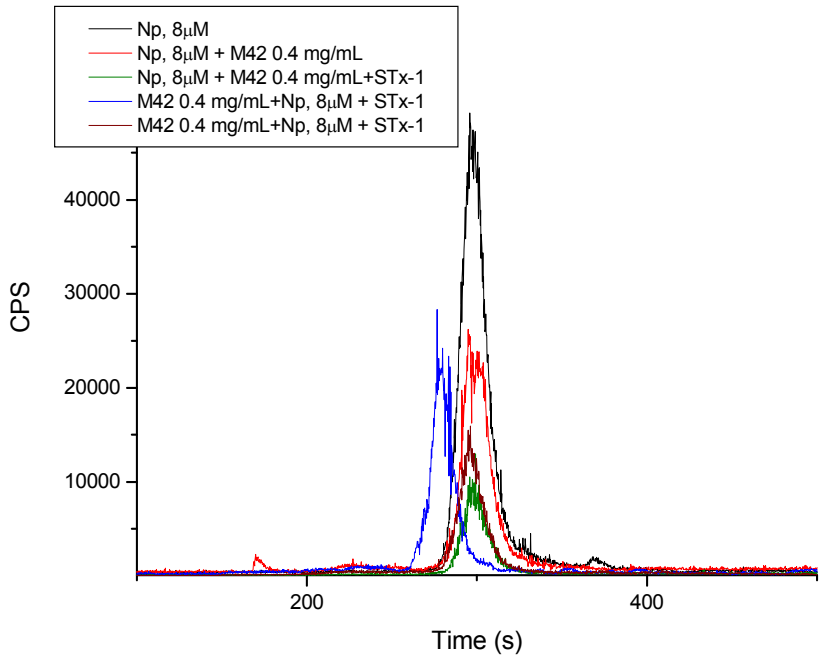

Fig. 4.34. Rhodium corrected data obtained with the Scott type spray chamber, for the samples under ionic strength 0.01M and -30kV. The red curve represents the sample without addition of STx-1, and the black curve is the sample where only Np was present.

4.4.4. Discussion

The presence of NpO_2^+ cations in solution seems to block sorption sites on the STx-1 for the melanoidins, as we can observe in the experiments where Np was added first in both 0.1 and 0.01 M ionic strength. Adding the M42 melanoidins first, improves drastically the sorption at 0.1 M ionic strength; whereas at ionic strength of 0.01 M the sorption firstly decreases and then rises to values comparable to the experiment done without addition of neptunium (see Figures 4.25. and 4.26.). In contrast, the sorption of neptunium was much affected by the ionic strength, and not so much by the addition order. Experiments conducted under high ionic strength ([$NaClO_4$] = 0.1 M), have shown that no cation exchange occurs, these results being consistent with literature data for the sorption of neptunium on SAz-1 montmorillonite. Moreover, the presence of M42 sorbed enhances the sorption of Np in comparison to pure STx-1 probably due to the presence of negatively charged carboxylic groups. Under low ionic strength ([$NaClO_4$] = 0.01 M), where cation exchange may occur, the presence of organic substances has little influence on the sorption.

Regarding the speciation in solution, CE-ICP-MS measurements in the supernatant were performed. Although the addition of a basic buffer has probably some influence on the speciation, a qualitative statement could be made. For the experiments conducted under 0.1 M

ionic strength, no remarkable differences in the solution speciation were observed. The dominant species in both experiments is the neptunyl cation. The experiments conducted under ionic strength 0.01 M, show two peaks corresponding to species with a lower charge to radius ratio in the positive run. In the negative run, a little peak occurring at smaller retention times than that for the NpO_2^+ cation, in the sample containing only Np and M42, indicates the presence of negatively charged M42-NpO_2^+ complexes.

In summary, a rather complex sorption behaviour of Np(V) on montmorillonite is observed depending i) on the ionic strength, ii) on the order in which the components are added and iii) on the amount of humic substances (melanoidins) in the aqueous phase.

Since neptunium will be responsible for the greatest amount of radiotoxicity one million years after discharge of the nuclear fuel from the reactor, it is very important to predict its behavior in the geosphere. Montmorillonite was selected as host mineral due to its contribution to the natural bentonites, which are widely considered to be part of the engineered barrier in the disposal, and melanoidins were investigated in order to understand the general complexing and sorption properties of humic substances. Moreover protein like compounds are supposed to play an important role in soils [Kleber 2007] and all the humin formation paths have to be considered since all paths may occur depending on the soil conditions.

Just a small part of the complex system, which is relevant for the safety assessment of radioactive waste in deep geological disposals, has been investigated within this work. Anyway, the way to a comprehensive and predictive research is open, and ongoing/future research will deliver the data needed for locating and managing the disposal. This data has to consider the sorption onto mixtures under more real conditions, e.g., pore water, and higher temperatures. After selection of the waste repository site, in situ experiments will be needed to improve the already obtained laboratory data.

Binary systems

Synthesis and characterization of the hybrid clay-based materials

The synthesis of hybrid clay-based materials starting from a reducing sugar, an amino acid, and montmorillonite has been achieved (section 4.1.). The organic material seems to penetrate partially into the interlayers of montmorillonite but stays also on the surface of the mineral, thus confirming former studies of Ziechmann [Ziechmann 1993]. This result was confirmed by the thermal analysis and comparison with literature data for the incorporation of fulvic acid in the interlaminar spaces of montmorillonite [Kodama 1969]. Ziechmann studied the formation of humic like material using hydroquinone in the presence of bentonite and proposed the formation of composites where the organic material was located partially between the layers of the mineral and partially on the surface, like a champagne bottle cork [Ziechmann 1993]. Presence of organic material on the surface could be confirmed by XPS and STXM. Treatment with H_2O_2 removes only the organic material located on the surface, making possible the agglomeration of the clay particles. The remainder of organics after treatment with H_2O_2 was confirmed by ^{29}Si solid-state NMR. Thus, we can conclude that the formation of the melanoidins takes place in a first stage between the layers of the montmorillonite, since the precursors of the melanoidins are able to penetrate into the

interlayers. The melanoidins spread out of the interlayers and fill the outer regions being fixed on the surface, with a champagne bottle cork structure [Ziechmann 1993].

The similarities in the morphology of the hybrid materials obtained starting from xylose and glutamic acid and the materials obtained starting from hydroquinone point to an occurrence of the resulting structure independent on the starting material, and therefore this kind of materials has to be expected to occur in soils.

Sorption of Np(V) onto gibbsite

The batch experiments at different ionic strengths point to an inner-sphere sorption of neptunium on gibbsite (section 4.2.). This result was also confirmed by the Np-O_{eq} distances (excluding the sample, neptunium sorption onto gibbsite in the absence of CO_2) in the EXAFS measurements. These results are consistent with literature data for the sorption of Ni onto gibbsite [Yamaguchi 2002] and uranium onto gibbsite [Baumann 2005]. Furthermore, the presence of ambient CO_2 affects the sorption, probably maintaining the neptunyl ions in solution as carbonato complex. The slightly different slopes in the isotherm at pH 8.5 under ambient conditions point to the existence of strong and weak sorption sites in gibbsite. Similar results have been obtained for other model materials such as γ-alumina [Dierking 2007 b].

Ternary systems

Sorption of Np(V) onto the hybrid clay-based materials

The sorption of neptunium on hybrid clay materials was investigated. The presence of melanoidins in montmorillonite reduces the sorption of neptunium above pH 7 in comparison with pure montmorillonite, due to the release of organic material from the hybrid material into the aqueous phase. Below pH 7, the sorption on the HCM is increased. This behavior ressembles that of the sorption of actinide metal ions on kaolinite in the presence of Aldrich humic acid [Buda 2008]. The presence of closely bound organics to the mineral in the HCM produces the occurrence of more sorption sites for Np than the predicted by the Lineal Additive Model for the physical mixture of STx-1, melanoidins and Np at pH<7. On the other hand at pH>7 the release of organics and, therefore, of organic-Np-complexes from the HCM produces the mobilization of Np from the mineral surface. The Linear Additive Model is a very useful tool for the estimation of sorption coefficients in the ternary systems where the components are physically mixed, and a help to elucidate the trends in systems like the sorption on HCM, where two components are closely bound.

The ternary system montmorillonite-Np-melanoidin

Investigations conducted on the ternary system (section 4.4.) were conducted under two ionic strengths high (0.1 M) and low (0.01 M). The presence of NpO_2^+ cations in solution seems to block sorption sites on the STx-1 for the melanoidins, as we can observe in the experiments where Np was added first at both 0.1 and 0.01 M ionic strength. Adding the M42 melanoidins first, improves drastically the sorption at 0.1 M ionic strength; whereas at ionic strength of 0.01M the sorption firstly decreases and then rises to values comparable to the experiment done without addition of neptunium. In contrast, the sorption of neptunium was much affected by the ionic strength, and not so much by the addition order. Experiments conducted under high ionic strength ($[NaClO_4]$ = 0.1 M), have shown that no cation exchange occurs, these results being consistent with literature data for the sorption of neptunium on SAz-1 montmorillonite. Moreover, the presence of M42 sorbed enhances the sorption of Np in comparison to pure STx-1 probably due to the presence of negatively charged carboxylic groups. Under low ionic strength ($[NaClO_4]$ = 0.01 M), where cation exchange may occur, the presence of organic substances has little influence on the sorption.

Regarding the speciation in solution, CE-ICP-MS measurements in the supernatant were performed. Although the addition of a basic buffer has probably some influence on the speciation, a qualitative statement could be made. For the experiments conducted under 0.1 M ionic strength, no remarkable differences in the solution speciation were observed. The dominant species in both experiments is the neptunyl cation. The experiments conducted under ionic strength 0.01 M, show two peaks corresponding to species with a lower charge to radius ratio in the positive run. In the negative run, a little peak occurring at smaller retention times than that for the NpO_2^+ cation, in the sample containing only Np and M42, indicates the presence of negatively charged M42-NpO_2^+ complexes.

In summary, a rather complex sorption behaviour of Np(V) on montmorillonite is observed depending i) on the ionic strength, ii) on the order in which the components are added and iii) on the amount of humic substances (melanoidins) in the aqueous phase.

6. Bibliography

Aiken 1985 — Aiken, G.R. *Humic substances in soil, sediment and water : geochemistry, isolation, and characterization.* New York, Wiley, 1985, 692p.

Albers 2001 — Albers, R. C., *Nature*, Volume 410, 2001, 759-761.

Allard 1984 — Allard, B., Olofsson, U., Torstenfelt, B. *Inorganica Chimica Acta*, Volume 94, 1984, 205-221.

Amadori 1931 — Amadori, M. *Rendiconti Atti Accademia Nazionale dei Lincei,* Volume 13, 1931, 72-73.

ANKA 2007 — *ANKA Instrumentation Book*, Heinrich, J. (editor) 2007, 85p.

Ankudinov 2002 — Ankudinov, A.L., Bouldin, C. E., Rehr, J. J., Sims, J. and Hung, H. *Physical Review B,* Volume 65, 2002, 104107-1-11.

Baeyens 1995 — Baeyens, B., and Bradbury, M.H. *NAGRA Technical Report 95-04. Part I,* 1995, 4-9.

Balan 2006 — Balan, E., Lazzeri, M., Morin, G., Mauri, F. *American Mineralogist,* Volume 91, 2006, 115-119.

Banik 2006 — Banik, N.L. PhD Thesis, University of Mainz, Germany, Germany, 2006.

Banik 2007 — Banik, N.L., Buda, R.A., Bürger, S., Kratz, J.V., Trautmann, N. *Radiochimica Acta*, Volume 95, 2007, 569-575.

Band 1979 — Band, I.M., Kharitonov, Yu. I., Trzhaskovskaya, M.B. *Atomic Data and Nuclear Data Tables*, Volume 23, 1979, 443-505.

Bates 1987 — Bates, R.L. & Jackson, J.A. (editors). *Glossary of Geology: American Geotechnical Institute*, Alexandria, 1987, 788p.

Baumann 2005 — Baumann, N., Brendler, V., Arnold, T., Geipel, G., Bernhard, G. *Journal of Colloid and Interface Science*, Volume 290, 2005, 318-324.

Bertetti 1998 — Bertetti, F.P., Pabalan, R.T. and Almendarez, M.G. "*Studies of Neptunium V Sorption on Quartz, Clinoptilolite, Montmorillonite, and α-Alumina"* in *Adsorption of Metals by Geomedia*. Ed. E. A. Jenne. Academic Press, London, 1998, 583p.

Boese 1997 — Boese, J., Osanna, A., Jacobsen, C. & Kirz J. *Journal of Electron Spectroscopy and Related Phenomena*, Volume 85, 1997, 9-15.

Borden 2001 — Borden, D. & Giese, R.F. *Clays and Clay Minerals*, Volume 4, 2001, 444-445.

Brandt 2003 — Brandt, K.B., Elbokl, T.A. and Detellier, C., *Journal of Materials Chemistry*, Volume 13, 2003, 2566–2572.

Bradbury 2006	Bradbury, M.H., and Baeyens, B. *Radiochimica Acta* 94, Volume 9-11, 2006, 619-625.
Briggs 1983	Briggs, D., and Seah, M.P. *Practical Surface Analysis by Auger and X-ray Photoelectron Spectroscopy*, New York, Wiley, 1983, 674p.
Buda 2006	Buda, R.A., PhD Thesis, University of Mainz, Germany, 2006.
Buda 2008	Buda, R.A., Banik, N.L., Kratz, J.V., Trautmann, N. *Radiochimica Acta*, accepted.
Bürger 2005	Bürger, S. PhD Thesis, University of Mainz, Germany, 2005.
Burney 1974	Burney, G.A., Harbour, R.M. Nuclear Science Series, National Academy of Science – National Research Council. Radiochemistry of Neptunium. 1974.
CANBERRA 2003	CANBERRA Germanium detectors specifications, 2003.
Chahi 1996	Chahi, A., Larque, Ph., Frere, Y., Gramain, Ph., Weber, F. *Soil Science*, Volume 161, 1996, 761-769.
Choppin 1983	Choppin, G.R., *Radiochimica Acta*, Volume 32, 1983, 43-53.
Choppin 1988	Choppin, G.R. *Radiochimica Acta*, Volume 44/45, 1988, 23-28.
Clark 1995	Clark, D.L., Hobart, D.E., Neu, M.P. *Chemical Reviews*, Volume 95, 1995, 25-48.
Clark 1996	Clark, D.L., Conradson, S.D., Ekberg, S.A., Hess, N.J., Neu, M.P., Palmer, P.D., Runde, W., Tait, C.D., *Journal of the American Chemical Society*, Volume 118, 1996, 2089-2090.
Cohen 1977	Cohen, B.L., *Reviews of Modern Physics,* Volume 49, 1977, 1-20.
Conradson 2000	Conradson, S.D. *Los Alamos Science,* Volume 26, 2000, 422-435.
Constanzo 2001	Constanzo, P.A. and Guggenheim, S. Guest Editors for the special issue *Clays and Clay Minerals*, Volume 4, 2001.
Darder 2005	Darder, M. and Ruiz-Hitzky, E. *Journal of Materials Chemistry,* Volume 15, 2005, 3913-3918.
Denecke 2005	Denecke, M.A., Dardenne, K., Marquardt, C.M. *Talanta*, Volume 65, 2005, 1008-1014.
Denecke 2006	Denecke, M.A. *Coordination Chemistry Reviews,* Volume 250, 2006, 730–754.
Diallo 2003	Diallo, M.S., Simpson, A., Gassman, P., Faulon, J.L., Johnson, J.H., Goddard, W.A., Hatcher, P.G. *Environmental Science & Technology,* Volume 37, 2003, 1783-1793.

Dierking 2007	Dierking, S., Amayri, S., Reich, Ta., Drebert, J., Reich, T. *ANKA Annual Report 2007*, 2007, 152-154.
Dierking 2007 b	Dierking, S., Vicente Vilas, V., Wu, T., Amayri, S., Reich, T. Poster at the Migration 2007, 26/31 August 2007, Munich (Germany).
Dierking 2008	Dierking, S. PhD Thesis, University of Mainz, Germany, in preparation.
Drever 1982	Drever, J.I. *The Geochemistry of Natural Waters*. Ed. Englewood Cliffs, N.J. Prentice Hall, 1982, 388p.
Duplessis 1977	Duplessis, J. and Guillaumont, R., *Journal of Radioanalytical and Nuclear Chemistry*, Volume 31, 1977, 293-302.
Eick 1964	Eick, H.A. and Mulford, R. *Journal Chemical Physics,* Volume 41, 1964, 1475-1478.
El-Naggar 2000	El-Naggar, H.A., Ezz El-Din, M.R., Sheha, R.R. *Journal of Radioanalytical and Nuclear Chemistry*, Volume 246, 2000, 493-504.
Enders 1938	Enders, C. and Theis, K. *Brennstoff-Chemie*, Volume 19, 1938, 360-365.
ENRESA 2004	ENRESA Publications, El Almacenamiento Geológico Profundo de los Residuos de Alta Actividad, 2004.
Evans 1959	Evans, L.T. and E.W. Russell, *European Journal of Soil Science*, Volume 10, 1959, 119-132.
Fairley 2005	Fairley, N. and Carrick, A. 2005. The Casa Cookbook – Part 1: Recipes for XPS Data Processing. Acolyte Science.
Feuerbacher 1978	Feuerbacher, B. *Photoemission and the Electronic properties of Surfaces*, New York, Wiley, 1978, 558p.
Francis 1992	Francis, J.T. and Hitchcock, A.P. *Journal Physical Chemistry,* Volume 96, 1992, 6598-6610.
Glaus 1995	Glaus, M.A., Hummel, W. and van Loon, L.R. *Environmental Science & Technology*, Volume 29, 1995, 1250-1253.
Glaus 2000	Glaus, M.A., Hummel, W. and van Loon, L.R. *Applied Geochemistry*, Volume 15, 2000, 953-973.
George 2000	George, G. N., Pickering, I.J. Stanford Synchrotron Radiation Laboratory (SSRL), 2000.
Gomper 2001	Gomper, K. *Radioaktivität und Kernenergie*, Forschungszentrum Karlsruhe, 2001, 153-167.
Gray 1975	Gray, A.L. *The Analyst*, Volume 100, 1975, 289-299.

Greenland 1956	Greenland, D.J. *European Journal of Soil Science*, Volume 7, 1956, 319-329.
Guggenheim 2001	Guggenheim S., Koster van Groost, A.F. *Clays and Clay Minerals*, Volume 49, 2001, 433-443.
Gustafsson 2001	Gustafsson, J.P. *Journal of Colloid and Interface Science*, Volume 244, 2001, 102-112.
Gustafsson 2003	Gustafsson, J.P., Pechová, P. and Berggren, D. *Environmental Science & Technology*, Volume 37, 2003, 2767-2774.
Günzl 2000	Günzl, A. PhD Thesis, Technical University Munich, Germany, 2000.
Helmholtz 1879	Helmholtz, H.Z. *Annalen der Physik und Chemie*, Volume 7, 1879, 337-382.
Hendricks 1940	Hendricks, S.B. and Alexander, L.T. *Agronomy Journal*, Volume 32, 1940, 455-458.
Holleman 1995	Holleman-Wiberg. *Lehrbuch der Anorganischen Chemie.* Wiberg, Nils. Berlin – New York, Walter de Gruyter: 1995, 2033p.
Holm 1987	Holm, E., Årkrog, A., Ballestra, S., *Journal of Radioanalytical and Nuclear Chemistry*, Articles, Volume 115, 1987, 5-11.
Hummel 1997	Hummel, W. *Binding Models for Humic Substances* in *Modelling in Aquatic Chemistry* Ed. I. Grenthe and I. Puigdomenech. OECD Publications, 1997, 724p.
Hummel 2000	Hummel, W., Glaus, M.A. and van Loon, L.R. *Applied Geochemistry*, Volume 15, 2000, 975-1001.
IAEA 1995	IAEA, Principles of Radioactive Waste Management, Safety Series No. 111-F, Vienna 1995.
Jacobsen 1991	Jacobsen, C., Williams, S., Anderson, E., Browne, M.T., Buckley, C.J., Kern, D., Kirz, J., Rivers, M., Zhang, X. *Optics Communications*, Volume 86, 1991, 351-364.
Jenne 1998	Jenne E.A. "*Adsorption of Metals by Geomedia: Data Analysis, Modeling, Controlling Factors and Related Issues"* in *Adsorption of Metals by Geomedia*. Ed. E. A. Jenne. Academic Press, London, 1998, 583p.
Jermolayev 2005	Jermolajev, A., Kasbohm, J. R., Amayri, S., Reich, T. *Annual Report, Institute of Nuclear Chemistry, Mainz* (Germany) 2005, C5.
Jorgenson 1981	Jorgenson, J.W., Lukacs, K.D. *Analytical Chemistry*. Volume 53, 1981, 1298-1302.

Katz 1986	Katz, Seaborg and Morss. *The Chemistry of the Actinide Elements*, Vol.1 and 2 Second Edition Chapmann and Hall: 1986.
Kautenburger 2006	Kautenburger, R., Nowotka, K., Beck, H.P. *Analytical and Bioanalytical Chemistry,* Volume 384, 2006, 1416-1422.
Kaznacheyev 2002	Kaznacheyev, K., Osanna, A., Jacobsen, C., Plashkevych, O., Vahtras, O., Ågren, H., Carravetta, V., Hitchcock, A.P. *Journal Physical Chemistry A,* Volume 106, 2002, 3153-3168.
Kim 1986	Kim, J.I. *Handbook on the Physics and Chemistry of the Actinides*, Editors A.J. Freeman and C. Keller, Elsevier, 1986.
Kim 1989	Kim, J.I., Buckau, G., Bryant, E., Klenze, R. *Radiochimica Acta*, Volume 48, 1989, 135.
Kim 1996	Kim, J. I. and Czerwinski, K. R. *Radiochimica Acta*, Volume 73, 1996, 5-10.
Kleber 2007	Kleber, M., Sollins, P., Sutton, R. *Biogeochemistry*, Volume 85, 2007, 9-24.
Klenze 1998	Klenze, R., Fanghänel, Th. *Nachricten Forschungzentrum Karlsruhe*, Jahrg. 30, 2/98, 83-96.
Kodama 1969	Kodama, H., and Schnitzer, M. *Proceedings of the International Clay Conference, Tokyo,* 1969, 765-774.
Komori 1998	Komori, Y., Sugahara, Y., Kuroda, K. *Journal of Materials Research*, Volume 13, 1998, 930-934.
Komori 1999	Komori, Y., Sugahara, Y., Kuroda, K. *Chemistry of Materials*, Volume 11, 1999, 3-6.
Křepelová 2006	Křepelová, A., Sachs, S., Bernhard, G. *Radiochimica Acta*, Volume 94, 2006, 825-833.
Kuczewski 2003	Kuczewski, B., Marquardt, C.M., Seibert, A., Geckeis, H., Kratz, J.V. and Trautmann, N. *Analytical Chemistry*, Volume 75, 2003, 6769 – 6774.
Laboriau 1996	Labouriau, A., Kim, Y.W. and Earl, W.L. *Physical Review B,* Volume 54, 1996, 9952-9959.
Lecomte 2002	Lecomte, M., Lacquement, J., *Clefs CEA,* Volume 46, 2002, 13-17.
Ledl 1990	Ledl, F., Schleicher, E. *Angewandte Chemie, International Edition English*, Volume 29, 1990, 565-706.
Lees 1950	Lees, H. *Biochemical Journal*, Volume 46, 1950, 450-451.

Lemire 2001	Lemire, R.J., Fuger, J., Nitsche, H., Potter, P., Rand, M.H., Rydberg, J., Spahiu, K., Sullivan, J.C., Ullman, W.J., Vitorge, P. and Wanner, H. *Chemical Thermodynamics of Neptunium and Plutonium, 4,* 2001, 872 p.
Lieser 1988	Lieser, K.H., Mühlenweg, U., *Radiochimica Acta*, Volume 43, 1988, 27-35.
van Loon 2005	van Loon, G.W. and Duffy, S.J., *Environmental Chemistry A Global Perspective*, Oxford University Press, 2005, 532 p.
Lundén 1997	Lundén, I., Andersson, K., Skarnemark, G. *Aquatic Geochemistry*, Volume 2, 1997, 245-358.
Madic 2002	Madic, C., Lecomte, M., Baron, P., Boullis, B. *Comptes Rendus Physique*, Volume 3, 2002, 797-811.
Maillard 1912	Maillard L.C. *Les Comptes rendus de l'Académie des sciences*, Volume 154, 1912, 66-68.
Mangold 2007	Mangold, S. Oral presentation at the course "Synchrotron X-ray and IR methods in the Geosciences" 26/27 November 2007. Karlsruhe (Germany).
McMillan 1940	McMillan, E. and Abelson, *Physical Review*, Volume 57, 1940, 1185-1186.
Mermut 2001	Mermut, A.R. & Faz Cano, A. *Clays and Clay Minerals*, Volume 4, 2001, 381-386.
Michaelis 1909	Michaelis, L. *Biochemische Zeitschrift*, Volume 16, 1909, 81.
Moulin 1995	Moulin, V., Moulin, C. *Applied Geochemistry*, Volume 10, 1995, 573-580.
Neck 1994	Neck, V., Runde, W., Kim, J. I., Kanellakopulos, B. *Radiochimica Acta*, Volume 65, 1994, 29-37.
Neck 2001	Neck, V., Kim, J.I., Seidel, B.S., Marquardt, C.M., Dardenne, K., Jensen, M.P., Hauser, W., *Radiochimica Acta*, Volume 89, 2001, 439-446.
Neck 2006	Neck, V., *Geochimica et Cosmochimica Acta*, Volume 70, 2006, 4551-4555.
Neck 2001 b	Neck, V. and Kim, J.I., *Radiochimica Acta*, Volume 89, 2001, 1-16.
Newville 2004	Newville, M. *Fundamentals of XAFS*. 2004, 41p.
Occelli 2000	Occelli, M.L., Auroux, A., and Ray, G.J. *Microporous and Mesoporous Materials,* Volume 39, 2000, 43-56
Oda 1997	Oda, R.P. and Landers, J.P. Introduction to Capillary Electrophoresis in Handbook of Capillary Electrophoresis. Ed. J.P. Landers. CRC Press. 1997. 894p.
Omel'yanenko 2007	Omel'yanenko, B.I., Livshits, T.S., Yudintsev, S.V. and Nikonov, B.S. *Geology of Ore Deposits*, Volume 49, 2007, 173-193.

Peerani 2006 Peerani, P. *ESARDA Bulletin*, 35, 2006, 64-67.

Pikaev 2001 Pikaev, A.K., Gogolev, A.V., Shilov, V.P. *High Energy Chemistry*, Volume 35, 213-218.

Pompe 1996 Pompe, S., Bubner, M., Denecke, M.A., Reich, T., Brachmann, A., Geipel, G., Nicolai, R., Heise, K.H., Nitsche, H. *Radiochimica Acta*, Volume 74, 1996, 135-140.

Pompe 1998 Pompe, S., Brachmann, A., Bubner, M., Geipel, G., Heise, K.-H., Bernhard, G., Nitsche, H. *Radiochimica Acta*, Volume 82, 1998, 89-95.

POSIVA 2004 Posiva Working Report, Natural Clays as Backfilling Materials in Different Backfilling Concepts, Keto, P. (editor), 2004, 63 p.

POSIVA 2006 Posiva Reports, Expected Evolution of a Spent Nuclear Fuel Repository at Olkiluoto, Pastina, B., Hellä, P. (editors), 2006, 412 p.

Ravel 2005 Ravel, B and Newville, M. *Journal of Synchrotron Radiation*, Volume 12, 2005, 537-541.

Rai 1985 Rai, D., and Ryan, J.L., *Inorganic Chemistry*, Volume 24, 1985, 247-251.

Rai 1999 Rai, D., Hess, N. J., Felmy, A. R., Moore, D. A., Yui, M., *Radiochimica Acta*, Volume 84, 1999, 159–169.

Rao 2004 Rao, L., Srinivasan, T.G., Garnov, A.YU., Zanonato, P., di Bernardo, P., Bismondo, A., *Geochimica et Cosmochimica Acta,* Volume 68, 2004, 4821-4830.

Rao 2006 Rao, L., Srinivasan, T.G., Garnov, A.YU., Zanonato, P., di Bernardo, P., Bismondo, A., *Geochimica et Cosmochimica Acta,* 70, Volume 17, 2006, 4556-4562.

Reed 1961 Reed, T.B. *Journal of Applied Physics*, Volume 32, 1961, 821-824.

Reich 2000 Reich, T., Bernhard, G., Geipel, G., Funke, H., Hennig, C., Rossberg, A., Matz, W., Schell, N. and Nitsche, H. *Radiochimica Acta,* Volume 88, 2000, 633-637.

Reich 2007 Reich, T., Reich, T.Ye., Amayri, S., Drebert, J., Banik, N.L., Buda, R.A., Kratz, J.V. and Trautmann N. Proceedings of the 13th International Conference on X-ray Absorption Fine Structure-XAFS13 held in Stanford, California, USA, 9-14 July 2006. *AIP Conference Proceedings* 882.

Ross 1991 Ross, B.S., Chambers, D.M., Hieftje, G.M. *Mikrochimica Acta*, Volume 104, 1991, 287-297.

Rubert de la Rosa 2007	Rubert de la Rosa, S., Vicente Vilas, V., Kratz, J.V. Poster at the Euroclay2007. 22/27 July 2007. Aveiro (Portugal).
Sabodina 2006	Sabodina, M.N., Kalmykov, S.N., Artem'eva, K.A., Zakharova, E.V. and Sapozhnikov, Yu.A. *Radiochemistry*, Volume 48, 2006, 488-492.
Samadfam 2000	Samadfam, M., Jintoku, T., Sato, S., Ohashi, H., Mitsugashira, T., Hara, M., Suzuki, Y. *Radiochimica Acta*, Volume 88, 2000, 717-721.
Sachs 2003	Sachs, S., Heise, K.H. and Bernhard, G. *Wissenschaftliche Berichte Research Center Karlsruhe*, FZKA6800, 2003, 51-64.
Sachs 2004	Sachs, S. and Bernhard, G. *FZR – IRC Annual Report* 2004, 49.
Sachs 2005 a	Sachs, S., Schmeide, K., Reich, T., Brendler, V., Heise, K.H., and Bernhard, G. *Radiochimica Acta*, Volume 93, 2005, 17-25.
Sachs 2005 b	Sachs, S. and Bernhard, G. *Radiochimica Acta*, Volume 93, 2005, 141-145.
Schaumlöffel 1998	Schaumlöffel, D. and Prange, A. 1998. German Patent, 198 41 288.6.
Schäfer 2005	Schäfer, T., Buckau, G., Artinger, R., Kim, J.I., Geyer, S., Wolf, M., Bleam, W.F., Wirick, S., Jacobsen, C. *Organic Geochemistry*. Volume 36, 2005, 567-582.
Schnitzer 1967	Schnitzer, M. and Kodama, H. *Soil Science Society of America Journal*, Volume 31, 1967, 632-636.
Schmeide 2005 a	Schmeide, K., Reich, T., Sachs, S., Brendler, V., Heise, K.H., Bernhard, G. *Radiochimica Acta*, Volume 93, 2005, 187-196.
Schmeide 2005 b	Schmeide, K., Geipel, G., Bernhard, G. *Wissenschaftliche Berichte Research Center Karlsruhe*, FZKA7070, 2005, 19-31.
Schleidt 2006	Schleidt, S., PhD Thesis, University of Mainz, Germany, 2006.
Schroth 1997	Schroth, B.K. & Sposito, G. *Clays and Clay Minerals*, Volume 45, 1997, 85-91.
Schulthess 1996	Schulthess, C.P. and Dey, D.K. *Environmental Science & Technology*, Volume 60, 1996, 433-442.
Seibert 1999	Seibert, U.A., PhD Thesis University of Mainz, Germany, 1999.
Seibert 2001	Seibert, A., Mansel, A., Marquardt, C.M., Keller, H., Kratz, J.V. and Trautmann, N. *Radiochimica Acta*, Volume 89, 2001, 505-510.
Solomon 1968	Solomon, D.H., Loft, B.C. and Swift, J.D. *Clay Minerals*, Volume 7, 1968, 399-408.

Stevenson 1982	Stevenson, F.J. *Humus Chemistry; Genesis, Composition, Reactions*, New York, Wiley-Interscience, 1982, 443 p.
Taguchi 1986	Taguchi, K. and Sampei, Y. *Organic Geochemistry*, Volume 10, 1986, 1081-1089.
Theng 1974	Theng, B.K.G., *The Chemistry of Clay-Organic Reactions*, London, Adam Hilger, 1974, 325 p.
Theng 1975	Theng, B.K.G. and Scharpenseel, H.W., *Proceedings of the International Clay Conference*, Mexico City, 1975, 643-653.
Theng 1979	Theng, B.K.G., *Formation and Properties of Clay-Polymer Complexes, Developments in Soil Science 9*, Elsevier Scientific Publishing Company, Amsterdam, Oxford, New York 1979, 362 p.
Theng 2006	Theng, B.K.G., oral presentation at the 18th World Congress of Soil Science in Philadelphia (USA), 2006.
Tipping 1992	Tipping, E., Hurley, M.A. *Geochimica et Cosmochimica Acta,* Volume 56, 1992, 3627-3641.
Tipping 1994	Tipping, E. *Computers & Geosciences,* Volume 20, 1994, 973-1023.
Tipping 1998	Tipping, E. *Aquatic Geochemistry*, Volume 4, 1998, 3-48.
Tommaseo 2002	Tommaseo, C.E. PhD Thesis, University of Mainz, Germany, 2002.
Tremblay 2006	Tremblay, L. and Brenner, R. *Geochimica et Cosmochimica Acta*, Volume 70, 2006, 133-146.
Turner 1998	Turner, D.R., Pabalan, R.T., Bertetti; F.P. *Clays Clay Minerals,* Volume 46, 1998, 256-269.
Vernon-Parry 2000	Vernon-Parry, K.D. *III-Vs Review*, Volume 13, 2000, 40-44(5).
Viani 2002	Viani, A., Gualtieri, A., Artioli, G. *American Mineralogist,* Volume 87, 2002, 966-975.
Vicente Vilas 2007	Vicente Vilas, V., Dierking, S., Amayri, S., Reich, Ta., Drebert, J., Kratz, J.V., Reich, T. *ANKA Annual Report 2007*, 2007, 179-181.
Vitorge 2003	Vitorge, P., Capdevila, H., *Radiochimica Acta*, Volume 91, 2003, 623-631.
Wagner 1979	Wagner, C.D., Riggs, W.M., Davis, L.E., Moulder, J.F., Mullenberg, G.E. 1979. X-Ray Photoelectron Spectroscopy, Perkin-Elmer Corporation, Physical Electron Division.
Waksmman 1932	Waksman, S.A. *Humus.* Baltimore, Williams and Wilkins Co., 1932.

Weijuan 2003	Weijuan, L., Zuyi, T. *Journal of Colloid and Interface Science*, Volume 267, 2003, 25-31.
Yamaguchi 2002	Yamaguchi, N.U., Scheinost, A.C. and Sparks, D.L. *Clays and Clay Minerals*, Volume 50, 2002, 784-790.
Yariv 1990	Yariv, Sh. *Journal of Thermal Analysis*, Volume 36, 1990, 1953-1961.
Yoshida 2006	Yoshida, Z., Kimura, T., Johnson, S.G. and Krsul, J.R. *Neptunium* in *The Chemistry of the Actinide and Transactinide Elements*. Morss, L.R.; Edelstein, N.M.; Fuger, J.; Katz, J.J. (Eds.) 3rd ed., 2006, 3664 p.
Yuov 2004	Yuov, A.B. and Fedoseev, A.M., *Radiochemistry*, Volume 46, 2004, 121-124.
Zachara 1994	Zachara, J.M., Resch, C.T. and Smith, S.C. *Geochimica et Cosmochimica Acta*, Volume 58, 1994, 553-566.
Ziechmann 1993	Ziechmann, W. *Humic Substances*. Mannheim, Wissenschaftsverlag, 1993.

List of figures

List of tables